the department of OCEANOGRAPHY

Technical Reports
Nos 378, 379, 380, 381 and 382

A COMPILATION OF ARTICLES REPORTING
RESEARCH SPONSORED BY
THE OFFICE OF NAVAL RESEARCH

Office of Naval Research

Contract N-00014-75-C-0502
Project NR 083 012

Reference M80-20
JUL 1980

seattle, washington 98195

UNIVERSITY OF WASHINGTON
DEPARTMENT OF OCEANOGRAPHY
Seattle, Washington 98195

(10)

(21) [Includes Rept. nos.:]

Technical Reports
[TR- 378, TR- 379, TR- 380, TR- 381 and TR- 382.]

(6)

A COMPILATION OF ARTICLES REPORTING RESEARCH

SPONSORED BY

THE OFFICE OF NAVAL RESEARCH

[Technical Rept.]

[(11), Dec 80]

(15)

[(12) 94]

Office of ~~Naval Research~~
Contract [N00014-75-C-0502]
Project NR 083 012

[(14) TR-379,]
Reference M 80-20
~~July 1980~~

G. C. Anderson
George C. Anderson
Associate Chairman for Research

370280

ARTICLES REPORTING RESEARCH SPONSORED BY THE OFFICE OF NAVAL RESEARCH

TECHNICAL REPORT NO. 378

The Depth Variability of Meridional Gradients of Temperature, Salinity and Sound Velocity in the Western North Pacific, G. I. Roden

TECHNICAL REPORT NO. 379

On the Subtropical Frontal Zone North of Hawaii During Winter, G. I. Roden

TECHNICAL REPORT NO. 380

Upper Ocean Workshop, Summary Report, M. C. Gregg

TECHNICAL REPORT NO. 381

Signatures of Mixing from the Bermuda Slope, the Sargasso Sea and the Gulf Stream, M. C. Gregg and T. B. Sanford

TECHNICAL REPORT NO. 382

On the Variability of Surface Temperature Fronts in the Western Pacific, as Detected by Satellite, G. R. Roden

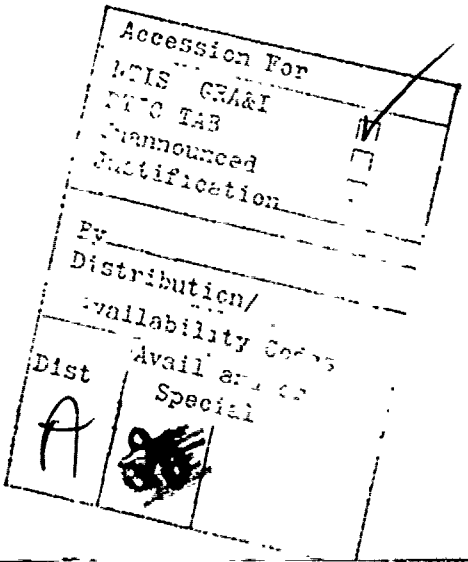

Reprinted from JOURNAL OF PHYSICAL OCEANOGRAPHY, Vol. 9, No. 4, July 1979
American Meteorological Society
Printed in U. S. A.

The Depth Variability of Meridional Gradients of Temperature, Salinity and Sound Velocity in the Western North Pacific[1]

GUNNAR I. RODEN

Department of Oceanography, University of Washington, Seattle 98195

(Manuscript received 21 August 1978, in final form 12 January 1979)

ABSTRACT

In the western North Pacific, meridional gradients of temperature, salinity and sound velocity show considerable variation with depth. Gradients of frontal intensity (more than three times the rms value) occur in the upper 600 m of the ocean. Fronts in the surface layer are spaced at irregular intervals. Many deep fronts have no surface manifestation and are spaced at intervals between 300 and 600 km. A spectral analysis of the meridional gradients as functions of depth and longitude was carried out for the wavenumber range between 0 and 13.4 cycles per 1000 km (c.p. 1000 km). The shape of the power density spectra strongly depends on depth. In the upper 150 m the shape is irregular. Between 300 and 600 m, the spectra show a well-defined peak between 1.5 and 3.3 c.p. 1000 km and a sharp decrease in power beyond 10 c.p. 1000 km. While the shape of the power density spectra shows little variation with longitude, there is a substantial decrease in the total power when crossing the Emperor seamount chain. Meridional gradients at the sea surface are coherent with those in the upper 150 m and incoherent with those below. Meridional gradients at 300 m have a good coherence with those at greater depths. The coherence between meridional temperature and salinity gradients increases with increasing depth. The depth dependence of the spectra and coherence is attributed to different processes of gradient formation in the upper and lower layers of the sea. A comparison of the wavenumber spectra of the meridional gradients with the wavenumber spectra of zonal gradients derived from Bernstein and White's (1977) and Wilson and Dugan's (1978) data shows that in each case the dominant spectral peak occurs between about 1.5 and 3 c.p. 1000 km, indicating the prevalence of features with zonal and meridional wavelengths in the 300–600 km range.

1. Introduction

The western Pacific is noted for numerous fronts (Uda, 1938; Roden, 1975), eddies (Bernstein and White, 1974, 1977) and Rossby-type long waves (Kawai, 1972; Cheney 1977; Roden, 1977), which occur together and give rise to a complicated thermohaline structure. In March and April 1971, the R.V. *Thomas G. Thompson* made three long meridional sections in the area (Fig. 1). The extraordinary complexity of the thermohaline structure is revealed in Fig. 2, which shows a sound velocity section along longitude 168°E, between latitudes 43° and 20°40′N. The 2500 km long section is based on 37 km horizontal and 3 m vertical sampling intervals. Frontal features, associated with strong meridional gradients, appear in black (for the purpose of this paper, meridional gradients exceeding three times the rms value over the section will be regarded as fronts). Fronts are found to occur not only in the upper wind stirred layer, but also at greater depths. Many of the deep fronts have no surface manifestation. In the upper 150 m, fronts are spaced at irregular intervals, while those below have a tendency to occur at regular intervals apart. This difference between surface and deep fronts points to different dynamic processes of formation. In the upper layer, fronts separate water masses of different origin and form primarily in response to differential *horizontal* advective and surface exchange processes, which vary considerably from one geographical region to another. In the deep layer, where vertical stratification is dominant, fronts form primarily in response to differential *vertical* advective processes. When the vertical velocity is influenced by wave motion, regularly spaced fronts can be expected. Similar conditions are known to exist in the atmosphere, where the dynamics of lower and upper tropospheric fronts are fundamentally different (Palmén and Newton, 1969; Shapiro, 1970).

In order to describe the complicated structure shown in Fig. 2, it is convenient to regard the meridional gradients as stochastic variables and analyze them by spectral analysis methods. The

[1] Contribution No. 1065 from the Department of Oceanography, University of Washington.

0022-3670/79/040756-12$07.00

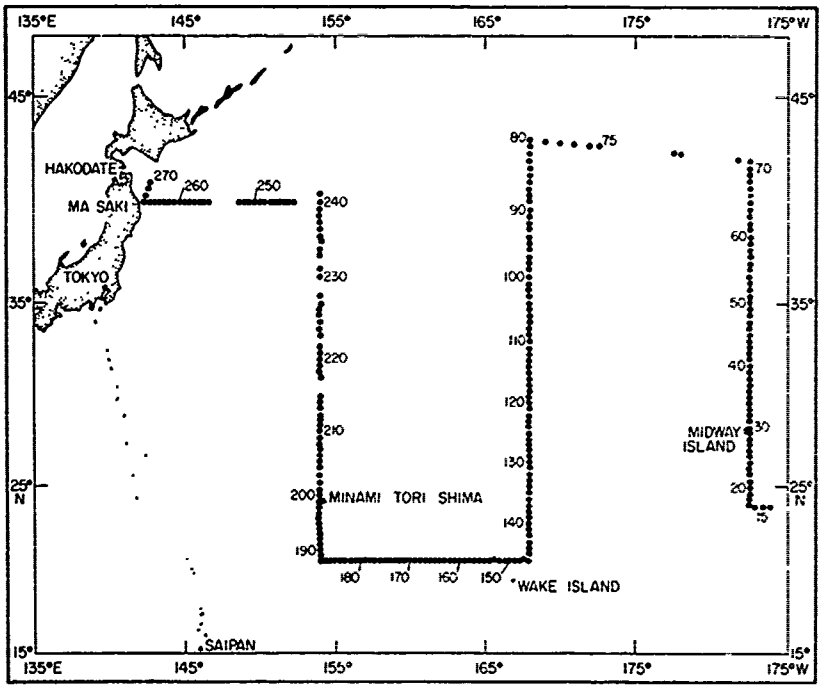

FIG. 1. Stations occupied during the 58th voyage of the R.V. *Thomas G., Thompson*, 19 March–3 May 1971.

following questions become relevant then: 1) What are the typical rms and extreme values of the meridional gradients at different depths? 2) How does the spectral density of the meridional gradients change with meridional wavenumber and are there any preferred wavenumbers at which the spectral density is concentrated? 3) How do the spectral densities change with depth and longitude? 4) For a given variable, what is the depth coherence of its meridional gradients? 5) For a given depth, how are the meridional gradients of different variables, such as temperature and salinity, related?

2. Data

The following analysis is based on STD data collected during the 58th cruise of the R.V. *Thomas G. Thompson* in March and April 1971 (Roden, 1972). Temperatures and salinities were measured directly, to an accuracy of 0.01°C and 0.03‰, respectively. Sound velocity was computed from Wilson's equation (Tolstoy and Clay, 1966) using STD temperatures and salinities as input. The thermohaline gradients were computed by the central difference approximation for six depths: 0, 150, 300, 450 and 600 m. The Tukey method was used to compute the wavenumber spectra. The computations were carried out for the wavenumber range between 0 and 13.4 cycles per 1000 km (c.p. 1000 km), with a resolution of 0.6 c.p. 1000 km. This allows one to detect dominant wavelengths from 75 to about 800 km.

Zonal wavenumber spectra published by Bernstein and White (1977) and Wilson and Dugan (1978) were utilized for comparison. The conversion from the original temperature spectra to temperature gradient spectra was achieved by multiplying the original spectra by the zonal wave-number squared.

3. Observed meridional gradients and their rms and extreme values

The observed meridional gradients of temperature, salinity and sound velocity along longitude 168°E are shown in Fig. 3. The outstanding feature is the change of the character of the gradients with depth. At the sea surface, the meridional gradient associated with the subarctic front (near 42°N) dominates over all others and the spacing between the peaks is irregular. At 300 m and below, the amplitudes of the positive and negative gradients are more equal and the peaks are spaced at rather regular intervals, which suggests wave motion. The distance between crests varies between 400 and 500 km, which indicates that Rossby-type waves could be involved (Longuet-Higgins, 1965; Philander, 1978). At present, the above argument must be regarded as tentative, because it is impossible to prove the exact origin of the quasi-

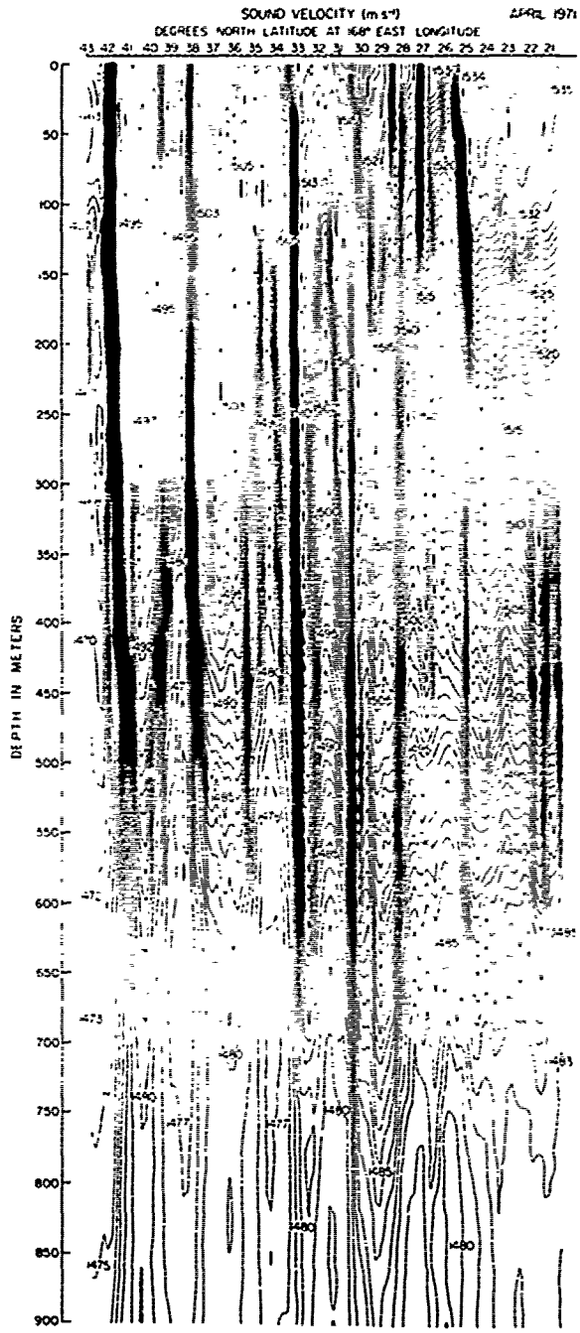

FIG. 2. Meridional sound velocity section along longitude 168°E, obtained between 3 and 11 April 1971. The contour interval is 1 m s^{-1}. Frontal features associated with strong meridional gradients appear in black.

regularly spaced oscillations from the limited data at hand.

The rms and extreme amplitudes of the meridional gradients are listed in Table 1 as functions of longitude and depth. It is seen that the strongest meridional gradients occur frequently at subsurface depths rather than at the sea surface and that the rms and extreme amplitudes are substantially larger at longitudes 154°E and 168°E than at longitude 177°20'W. The major topographic feature in the region is the Emperor seamount chain near 170°E, which rises up to 4500 m from the surrounding sea floor and comes to within 800 m of the sea surface in places. West of the Emperor seamount chain, rms amplitudes of the meridional gradients reach 2.2°C (100 km)$^{-1}$ for temperature, 0.3‰ (100 km)$^{-1}$ for salinity and 7.9 m s^{-1} (100 km)$^{-1}$ for sound velocity. East of this chain, the corresponding values for 1.3°C (100 km)$^{-1}$, 0.1‰ (100 km)$^{-1}$ and 4.2 m s^{-1} (100 km)$^{-1}$, respectively. Extreme amplitudes of the meridional gradients west of the chain are 8.2°C (100 km)$^{-1}$ for temperature, 1.4‰ (100 km)$^{-1}$ for salinity and 29.7 m s^{-1} (100 km)$^{-1}$ for sound velocity. East of the chain, the extreme amplitudes are about half of the above mentioned. The large eastward decrease of the amplitude of the temperature perturbations across the Emperor seamount chain was noted also by Bernstein and White (1977).

4. Spectra of meridional gradients

The power density spectra for the meridional gradients of temperature, salinity and sound velocity at 168°E are shown in Fig. 4 for the meridional wavenumber range from 0.6 to 13.4 c.p. 1000 km. The arrows indicate the 80% confidence limits. The shape of the power density spectra depends strongly upon depth. In the upper 150 m, where meridional gradients are formed mainly by differential horizontal advective and surface exchange processes, the spectra are irregular in shape and do not show any significant peaks. Between 300 and 600 m, where meridional gradients are largely formed by differential vertical advective processes, the spectra show a well-defined peak at a wavenumber of 2.43 c.p. 1000 km, which corresponds to a dominant wavelength of 411 km. The meridional wavenumbers corresponding to the half peak-power densities are 1.5 and 3.3 c.p. 1000 km, approximately, indicating that wavelengths between 300 and 666 km are fairly common also. Beyond meridional wavenumbers of 10 c.p. 1000 km, the power density becomes very low, which suggests a cutoff for waves of length of less than about 100 km. The peak power density decreases with depth rapidly between 300 and 600 m. For meridional gradients of temperature and sound velocity, the decrease is 25% between 300 and 450 m and 70% between 300 and 600 m. For meridional gradients of salinity, the corresponding values are 53 and 83%, respectively. The different attenuation rates for temperature and salinity are not fully understood at present.

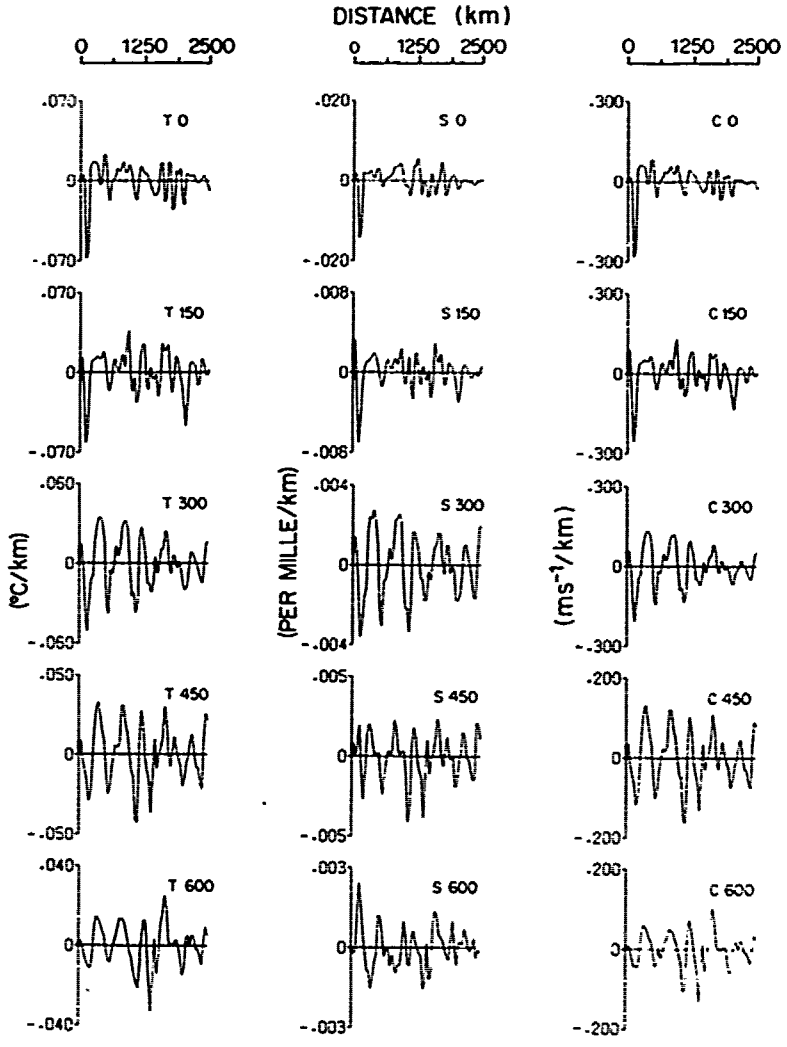

FIG. 3. Meridional gradients of temperature, salinity and sound velocity along longitude 168°E obtained in early April 1971. North is to the left.

5. Longitudinal variation of the spectra of meridional gradients

The above description has dealt exclusively with meridional wave-number spectra at longitude 168°E. It is of interest to know how representative these results are at other longitudes and, in particular, whether differences occur in the spectra west and east of the Emperor seamount chain. In Fig. 5 are shown the spectra of meridional gradients of temperature, salinity, sound velocity and density as a function of longitude. The arrows indicate the 80% confidence limits.

At all longitudes, the spectra show a broad peak in the wavenumber range between about 1.5 and 4.5 c.p. 1000 km and a sharp decrease in spectral density beyond 10 c.p. 1000 km, indicating a prevalence of waves with lengths between 222 and 666 km and a scarcity of those with lengths of less than 100 km. There is a sharp drop of the spectral density levels between 168°E and 177°20'W, with the levels west of the Emperor seamount chain (near 170°E) exceeding those to the east of the chain by a factor of 2–4.

A closer examination of the spectra shows that the highest peaks occur at a wavenumber of 3.64 c.p. 1000 km at longitude 154°E, at 2.43 c.p. 1000 km at longitude 168°E and at 3.04 c.p. 1000 km at longitude 177°20'W. The corresponding wavelengths are 274, 411 and 329 km, respectively. It is not possible to assess the significance of these differences in wavelengths, because of the shortness of the available records. If real, the differences would indicate a decrease in wavelength away from 168°E, the longitude closest to the Emperor seamount chain.

TABLE 1. rms and extreme amplitudes of meridional temperature gradients [°C(100 km)$^{-1}$] meridional salinity gradients [‰(100 km)$^{-1}$] and meridional sound velocity gradients [m s^{-1}(100 km)$^{-1}$] in the western Pacific.

Variable	Depth (m)	Longitude 154°00'E rms	154°00'E extreme	168°00'E rms	168°00'E extreme	177°20'W rms	177°20'W extreme
Temperature gradient	0	1.52	5.3	1.51	6.8	0.97	2.6
	150	1.93	8.2	1.83	6.3	1.33	4.9
	300	2.16	6.9	1.95	5.2	0.92	2.4
	450	1.82	5.4	1.76	4.3	0.83	2.4
	600	1.14	2.9	1.05	3.3	0.60	1.2
Salinity gradient	0	0.13	0.4	0.31	1.4	0.13	0.3
	150	0.15	0.7	0.17	0.7	0.13	0.4
	300	0.18	0.6	0.16	0.4	0.10	0.2
	450	0.14	0.5	0.14	0.4	0.08	0.3
	600	0.10	0.3	0.08	0.2	0.04	0.1
Sound velocity gradient	0	4.58	18.0	5.91	28.4	3.09	7.3
	150	6.59	29.7	6.46	25.8	4.24	14.4
	300	7.95	24.7	7.30	20.9	3.33	7.9
	450	6.95	20.6	6.80	16.5	3.21	9.1
	600	4.50	11.4	4.17	13.1	2.43	5.0

6. Depth coherence of meridional gradients

An important problem in the analysis of oceanic fronts is the depth coherence of horizontal gradients of temperature, salinity and sound velocity. The coherence between the meridional gradients at the sea surface and those at subsurface depths is shown in Fig. 6 for the wavenumber range between 0 and 13.4 c.p. 1000 km. The dashed line indicates the 95% confidence limit. The meridional gradients at 0 and 150 m are coherent over the entire wavenumber range, indicating that frontogenetic processes in the upper mixed layer are similar. As the depth increases, the coherence with the surface signature drops. At 300 m and below, significant coherence is found only in a narrow wavenumber range centered around 2.43 c.p. 1000 km. Even there, no more than 40 to 60% of the variance of the meridional gradients is related to the variance at the sea surface. This suggests that frontogenetic processes in the layer above and below the pycnocline are different.

The above is relevant for remote sensing from space. Satellite imagery of the sea surface temperature gradients and salinity gradients can be used only to detect upper layer temperature and salinity fronts. The horizontal thermohaline structure below pycnocline depth cannot be inferred from infrared and colorimetric measurements from space.

In contrast to the poor coherence between surface and deep meridional gradients, the gradients below pycnocline depth are strongly related to each other. This is shown in Fig. 7, where the meridional sound velocity gradients at 300 m are related to those at other depths. In the depth range between 150 and 600 m there is statistically significant coherence at all wavenumbers between 0 and 13.4 c.p. 1000 km. The phase (not shown) does not vary by more than 10° from zero, indicating that the fluctuations are in phase over the depth range investigated.

7. Coherence between meridional gradients of temperature and salinity

The coherence between meridional gradients of temperature and salinity is shown in Fig. 8 for different depths. There is statistically significant coherence at all depths and over the entire wavenumber range. The coherence is better at subsurface depths than at the sea surface. This is not surprising, because temperatures and salinity at the sea surface are influenced by the largely independent processes of radiative heat transfer and rainfall, which affect one variable but not the other. At greater depths, where the influence of surface processes is not felt, temperature and salinity can be regarded as passive variables, carried along by particle motion. Here a close correspondence can be expected among temperature, salinity and velocity gradients (Kirwan, 1975).

8. Notes on zonal thermohaline gradients in the western Pacific

The discussion so far has dealt with meridional thermohaline and sound velocity gradients in the western Pacific and the question arises as to the character of the zonal gradients. Unfortunately,

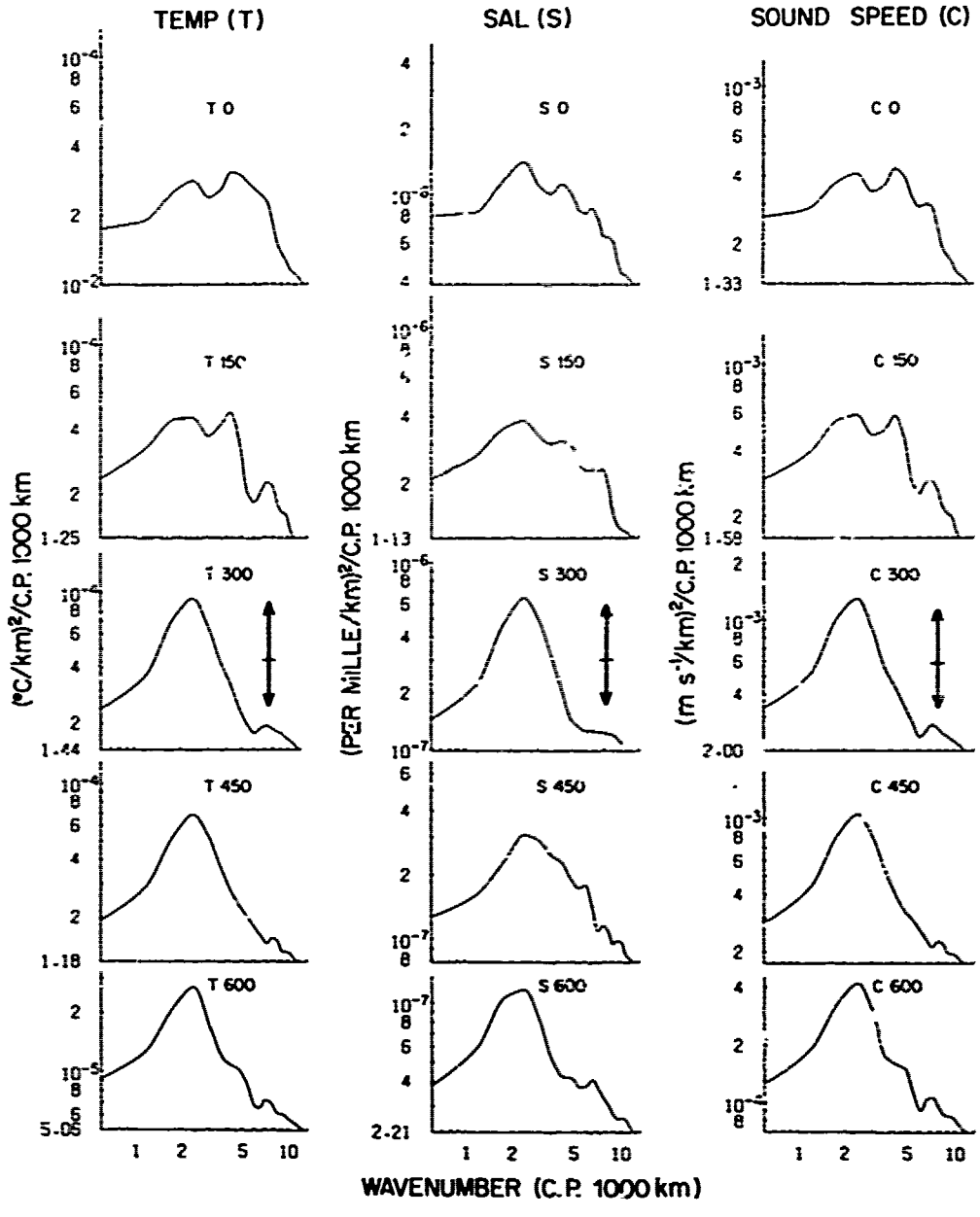

FIG. 4. Power density spectra of meridional gradients of temperature, salinity and sound velocity along longitude 168°E. Arrows indicate the 80% confidence limits.

few sections with a station spacing of 50 km or closer exist. The results given below are of a tentative nature, therefore.

The power density spectra for the zonal gradients of temperature, salinity, sound velocity and density at latitude 20°40'N are shown in Fig. 9 for the zonal wavenumber range between 0.6 and 13.4 c.p. 1000 km. The arrows indicate the 80% confidence limits. The spectra indicate two peaks: one at a wavenumber of about 1.5 c.p. 1000 km, corresponding to a wavelength of approximately 666 km, and the other at a wavenumber of 6.8 c.p. 1000 km, corresponding to a wavelength of about 150 km. Beyond 10 c.p. 1000 km, the spectral densities decrease rapidly with increasing zonal wavenumber.

In Fig. 10 (left) is shown the zonal wavenumber spectrum derived from Wilson and Dugan's (1978) observations. The spectrum represents the zonal gradient of the 12°C isotherm depth at latitudes 30°30'–32°N and is based on a multi-ship coordinated

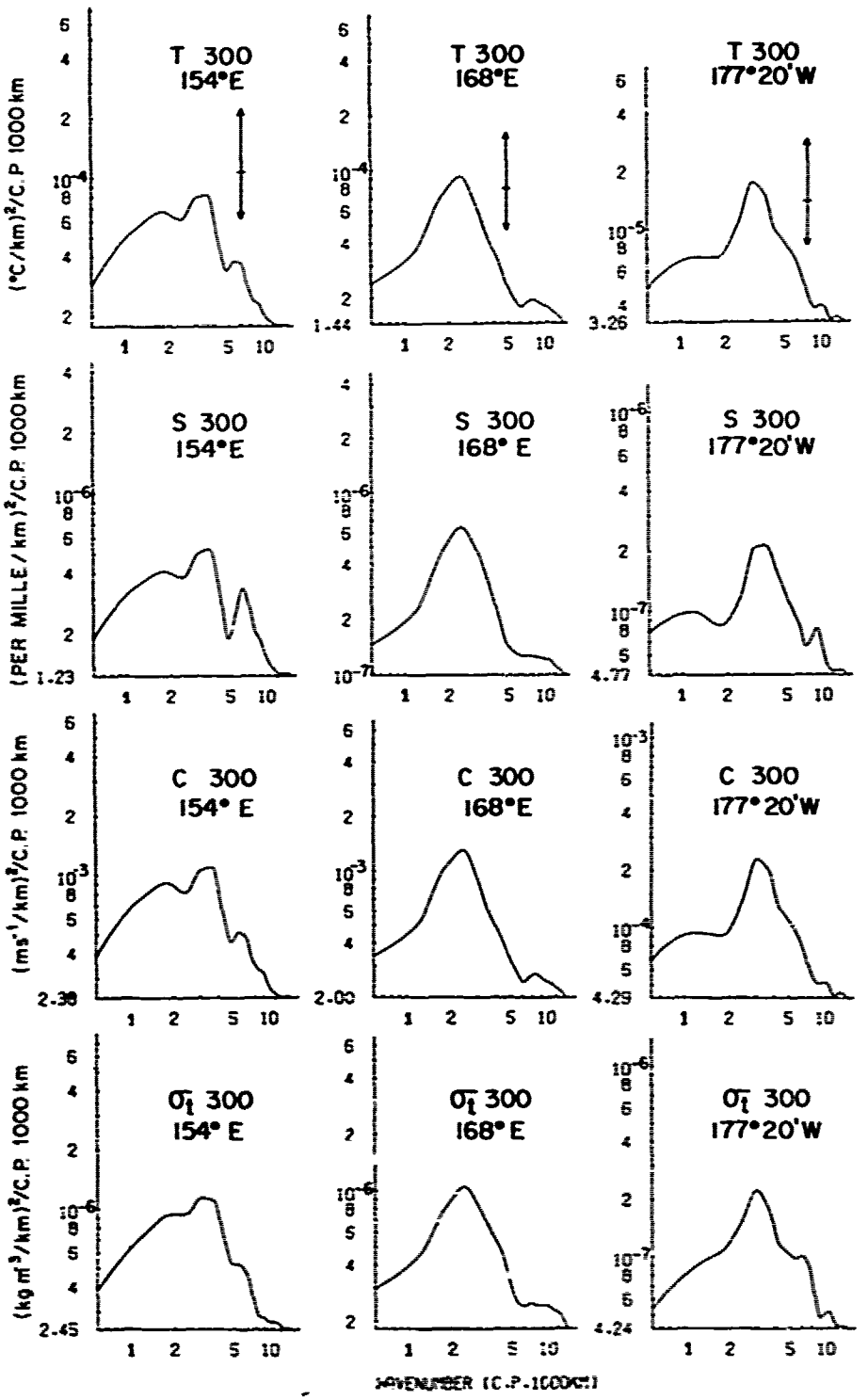

FIG. 5. Power density spectra of meridional gradients of temperature, salinity, sound velocity and density at 300 m, at longitudes 154°E, 168°E and 177°20'W. Arrows indicate the 80% confidence limits.

west-to-east expendable bathythermograph (XBT) survey. The spectrum shows a statistically significant peak at a wavenumber of 2 c.p. 1000 km. The wavenumbers corresponding to the half peak power are 1.8 and 3.5 c.p. 1000 km, respectively. This indicates that wavelengths between 285 and 555 km are common and that the most frequently encountered wavelength is 500 km. There is a sharp

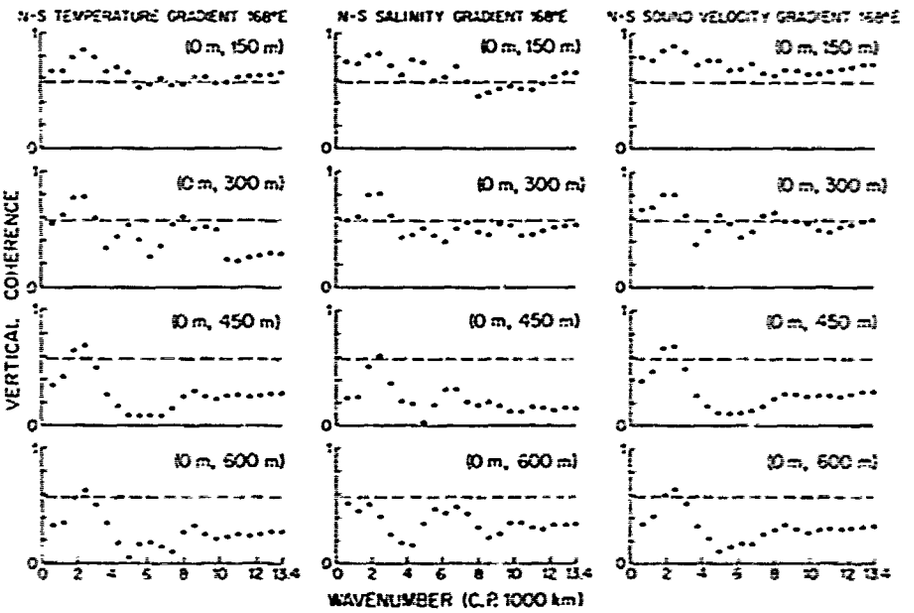

FIG. 6. Coherence between the meridional gradients at the sea surface and those at other depths along longitude 168°E. The dashed line indicates the 95% confidence limit.

decrease in power spectral density beyond 10 c.p. 1000 km, just as in the case discussed above.

In Fig. 10 (right) is shown the spectrum of the zonal temperature gradient at 300 m, derived from Bernstein and White's (1977) data. It is based on ship-of-opportunity XBT data between 35 and 38°N during the year 1975. The spectrum shows a statistically significant peak at 2 c.p. 1000 km, in agreement with Wilson and Dugan's (1978) findings. At wavenumbers beyond 4 c.p. 1000 km (dashed) the

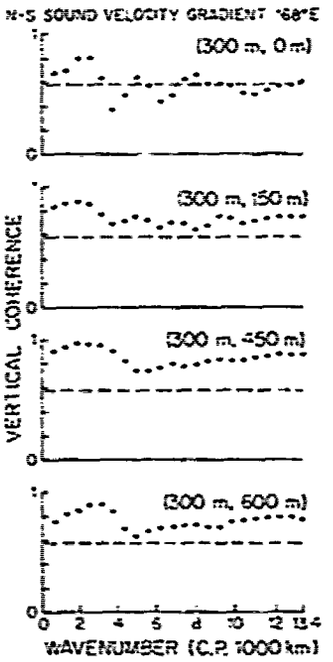

FIG. 7. Coherence between meridional sound velocity gradients at 300 m with those at other depths along longitude 168°E. The dashed line indicates the 95% confidence limit.

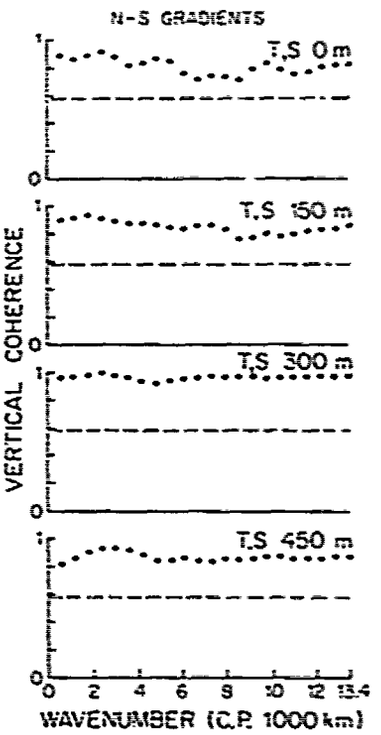

FIG. 8. Coherence between meridional gradients of temperature and salinity along lontitude 168°E. The dashed line indicates the 95% confidence limit.

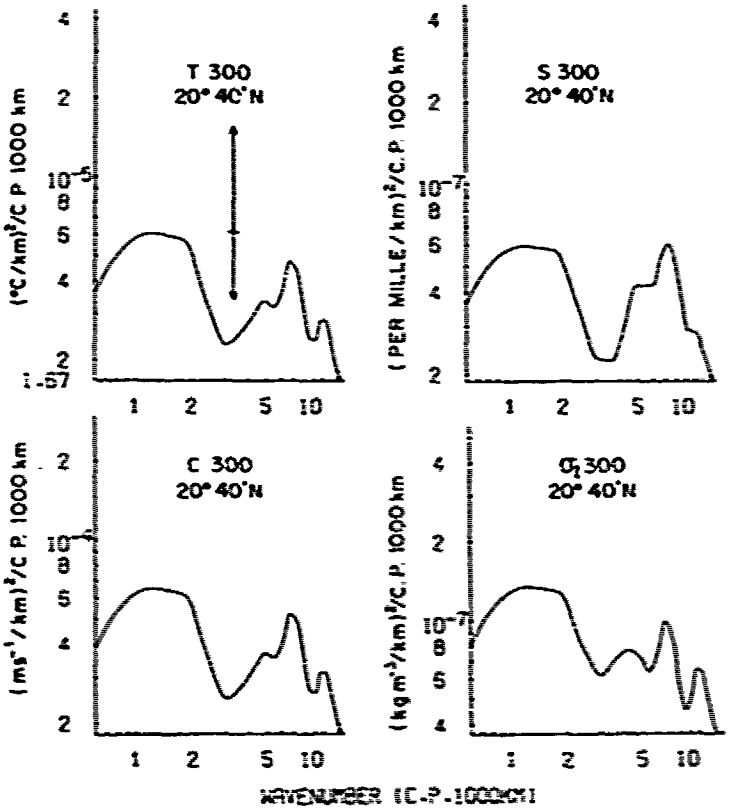

FIG. 9. Power density spectra of zonal gradients of temperature, salinity, sound velocity and density at 300 m, at latitude 20°40'N. The arrow indicates the 80% confidence limit.

power density does not decrease with increasing wavenumber. This behavior of the spectrum at high wavenumbers is atypical of the gradient spectra investigated so far and may result from instrumental limitations.

9. Oscillations of dynamic height in the western Pacific

The spectra of thermohaline and sound velocity gradients below pycnocline depth suggest the pres-

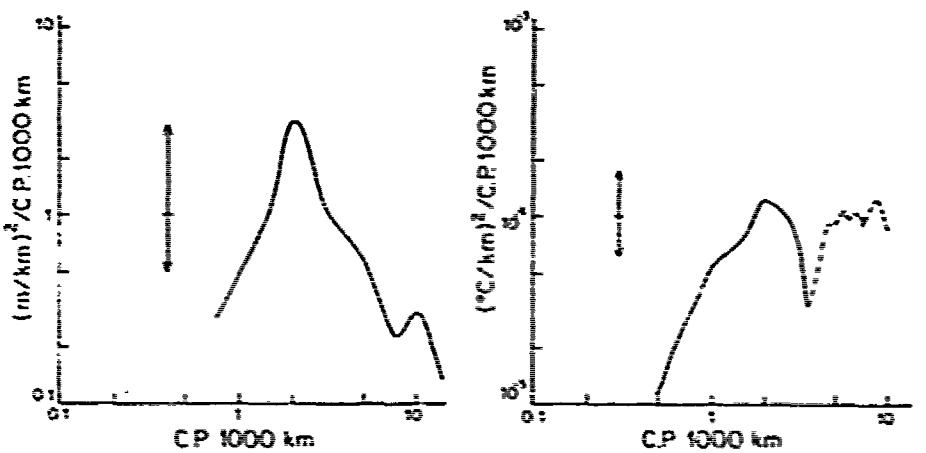

FIG. 10. Power density spectrum of the zonal gradient of the depth of the 12°C isotherm, based on Wilson and Dugan's (1978) data (left), and power density spectrum of the zonal temperature gradient at 300 m, based on Bernstein and White's (1977) data (right). The arrows indicate the 95% confidence limits.

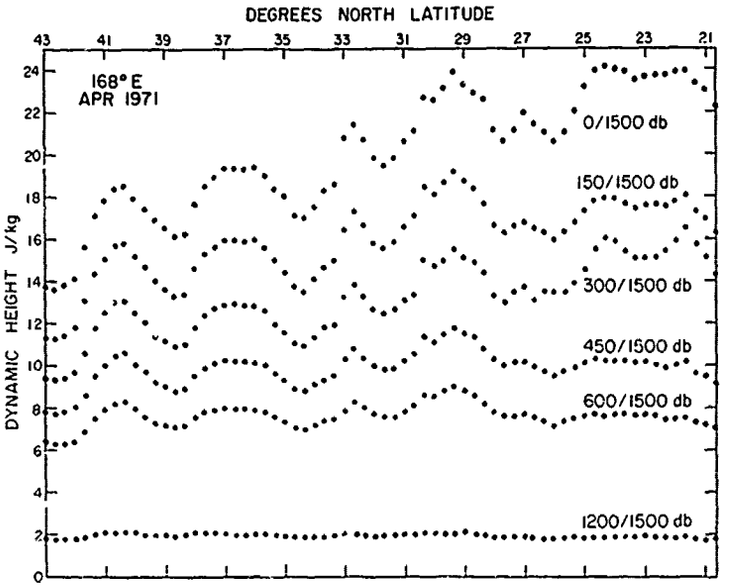

FIG. 11. Oscillations of dynamic heights, relative to 1500 db, along longitude 168°E in early April 1971.

ence of oscillations of 300–600 km wavelength. It is of interest to know whether similar oscillations occur in dynamic height.

In Fig. 11 are shown the dynamic heights relative to 1500 db along longitude 168°E. Oscillations of approximately 400 km length are prominent in the upper 600 m. Maximum amplitudes are close to 5 J kg^{-1}, equivalent to about 50 cm in sea surface elevation. The amplitudes appear to attenuate exponentially with depth: one-half the amplitude is encountered at 300 m and one-quarter at 600 m. Similar attenuation rates were observed in the central Pacific (Roden, 1977).

The power density spectrum for the 0/1500 db dynamic heights is shown in Fig. 12. A single prominent peak centered at 2.14 c.p. 1000 km stands out. The spectrum of the dynamic height gradient can be derived from the above by multiplying through by the wavenumber squared. When this is done, the peak shifts to 2.4 c.p. 1000 km, indicating a dominant wavelength of about 400 km. This is the same as found for the meridional thermohaline gradients below pycnocline depth.

8. Conclusions and discussion

The following conclusions can be drawn from an analysis of thermohaline and sound velocity gradients in the western North Pacific:

1) Strong meridional gradients, some of which attain frontal intensity (exceeding three times the rms gradient) are not limited to the surface layer, but occur at depths to 600 m. Many of the deep fronts have no surface manifestation, making detection from space difficult.

2) Fronts in the upper layer are spaced irregularly, while those between 300 and 600 m are spaced at quasi-regular intervals. This suggests that the dynamic processes of gradient formation differ for the upper and lower layers of the sea.

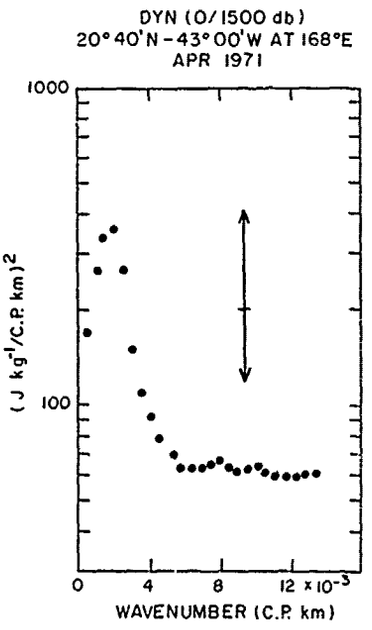

FIG. 12. Power density spectrum of the 0/1500 dynamic heights along longitude 168°E. The arrow indicates the 80% confidence limit.

3) The rms and extreme meridional gradients west of the Emperor seamount chain are considerably larger than to the east of it.

4) The shape of the power density spectra of meridional gradients depends strongly upon depth. In the upper 150 m, the shape is irregular. Between 300 and 600 m a well-defined peak is observed. The peak is broad and indicates that oscillations with a wavelength between 300 and 600 km are common. Beyond 10 c.p. 1000 km, the power density becomes very low, which suggests a cutoff wavelength of about 100 km.

5) The power density spectra of the meridional gradients show some dependence on longitude. The power levels west of the Emperor seamount chain are substantially higher than those to the east. Whether the differences in wavelengths associated with the spectral peaks (274 km at 154°E, 411 km at 168°E and 329 km at 177°20'W) are significant, cannot be determined from the limited data on hand.

6) Meridional gradients at the sea surface are coherent with those in the upper 150 m and incoherent with those below. Meridional gradients at 300 m have a good coherence with those at greater depths. This indicates that the surface and deep fronts are largely unrelated and must be detected by different means.

7) Meridional gradients of temperature and salinity are coherent in the wavenumber range between 0 and 13.4 c.p. 1000 km. The coherence is better at subsurface depths than at the sea surface. The less good coherence at the sea surface results from radiative heat transfer and precipitation processes which act largely independent of each other.

8) The power density spectra of the zonal temperature gradients at 300 m show a broad peak at wavenumbers between 1 and 3 c.p. 1000 km. The information at hand is insufficient to determine whether latitudinal differences exist. It is of interest to note that the zonal and meridional wavenumber ranges associated with the peaks in the zonal and meridional spectra are approximately the same. This indicates that in midlatitudes of the western Pacific the dominant east-west and north-south wavelengths are about equal.

Several unanswered questions remain. It is not known definitely whether the observed features are due to Rossby-type waves or eddies. The observed wavelengths (300–600 km, typically) and the cutoff wavelength of about 100 km are compatible with existing theories of Rossby waves (Longuet-Higgins, 1975; Lighthill, 1967; Philander, 1978); but do not rule out other processes, such as eddy formation by flow over complicated bottom topography. It is not known whether the spectra and coherences change with season, and whether the wavenumbers associated with the spectral peaks are the same during the stormy and calmer seasons. The change of the spectra and coherences with distance from major topographic features, such as the Emperor seamount chain, requires further study.

Answers to the above problems depend to a large degree on an effective sampling program. Some of the problems involved are discussed by Woods (1977). In the future, remote sensing by satellites holds promise. Frontal features above pycnocline depth can be detected by microwave and infrared techniques (Legeckis, 1975). Frontal features below pycnocline depth can be detected, in principle, by satellite radar altimetry, though the method has yet to be applied. This method will work at deep baroclinic fronts, across which there is a large sea surface slope. The slope can be detected from radar altimetry and a knowledge of the shape of the earth's geoid (Leitao *et al.*, 1978).

Acknowledgments. I am indebted to C. A. Barnes, L. H. Larsen and M. Rattray for advice. K. Bhatia carried out the programming. The scientific and operational crew of the R.V. *Thomas G. Thompson*, Captain Robert Schelling commanding, are to be commended for outstanding performance. The research reported herein was supported by the Office of Naval Research under Contract N-00014-75-C-0502, Project NR 083-012.

REFERENCES

Bernstein, R. L., and W. B. White, 1974: Time and length scales of baroclinic eddies in the central North Pacific Ocean. *J. Phys. Oceanogr.*, 4, 613–624.

——, and ——, 1977: Zonal variability in the distribution of eddy energy in the mid-latitude North Pacific Ocean. *J. Phys. Oceanogr.*, 7, 123–126.

Cheney, R. E., 1977: Synoptic observations of the oceanic frontal system of Japan. *J. Geophys. Res.*, 82, 5459–5468.

Kawai, H., 1972: Hydrography of the Kuroship Extension. *Kuroshio. Physical Aspects of the Japan Current*, H. Stommel and K. Yoshida, Eds., University of Washington Press, 235–341.

Kirwan, A. D., 1975: Oceanic velocity gradients. *J. Phys. Oceanogr.*, 5, 729–735.

Legeckis, R., 1975. Application of synchronous meterological satellite date to the study of time dependent sea surface temperature change along the boundary of the Gulf Stream. *Geophys. Res. Lett.*, 2, 435–538.

Leitao, C. D., N. E. Huang, and C. G. Parra, 1978: Remote sensing of Gulf Stream using GEOS-3 radar altimeter. NASA Tech Pap. 1209, 31 pp.

Lighthill, M. J., 1967: On waves generated in dispersive systems by travelling forcing effects, with application to the dynamics of rotating fluids. *J. Fluid Mech.*, 27, 725–752.

Longuet-Higgins, M. S., 1965: The response of a stratified ocean to stationary or moving wind systems. *Deep-Sea Res.*, 12, 923–973.

Palmén, E., and C. W. Newton, 1969: *Atmospheric Circulation Systems.* Academic Press, 602 pp.

Philander, S. G., 1978: Forced oceanic waves. *Rev. Geophys. Space Phys.*, 16, 15–43.

Roden, G. I., 1972: Temperature and salinity fronts at the

boundaries of the subarctic-subtropical transition zone in the western Pacific. *J. Geophys. Res.*, **77**, 7175–7187.

——, 1975: On North Pacific temperature, salinity, sound velocity and density fronts, and their relation to the wind and energy flux fields. *J. Phys. Oceanogr.*, **5**, 557–571.

——, 1977: On long wave disturbances of dynamic height in the North Pacific. *J. Phys. Oceanogr.*, **7**, 41–49.

Shapiro, M. A., 1970: On the applicability of the geostrophic approximation to upper level frontal scale motions. *J. Atmos. Sci.*, **27**, 408–720.

Tolstoy, I., and C. S. Clay, 1966: *Ocean Acoustics*. McGraw-Hill, 293 pp.

Uda, M., 1938: Researches on "siome" or current rip in the seas and oceans. *Japan Geophys. Mag.*, **11**, 307–372.

Wilson, W. S., and J. P. Dugan, 1978: Mesoscale thermal variability in the vicinity of the Kuroshio Extension. *J. Phys. Oceanogr.*, **8**, 537–540.

Woods, J. D., 1977: Information theory related to experiments in the upper ocean. *Modelling and Prediction of the Upper Layers of the Ocean*, Pergamon Press, 263–283.

Reprinted from JOURNAL OF PHYSICAL OCEANOGRAPHY, Vol. 10, No. 3, March 1980
American Meteorological Society
Printed in U. S. A.

On the Subtropical Frontal Zone North of Hawaii During Winter

GUNNAR I. RODEN

On the Subtropical Frontal Zone North of Hawaii During Winter[1]

GUNNAR I. RODEN

Department of Oceanography, University of Washington, Seattle 98195

(Manuscript received 9 April 1979, in final form 13 September 1979)

ABSTRACT

Oceanic fronts in the subtropical frontal zone north of Hawaii are investigated and related to atmospheric forcing. Particular attention is paid to the winter of 1974 when a detailed study was made of the thermohaline structure aboard the R. V. *Thomas G. Thompson*. In that winter, well-defined fronts occurred at 34, 31 and 28°N. In the upper 100 m, these fronts are nearly vertical and are characterized by temperature, salinity and sound velocity gradients of up to 2°C (27 km)$^{-1}$, 0.3‰ (27 km)$^{-1}$ and 12 m s^{-1} (27 km)$^{-1}$, respectively. Horizontal density gradients across the northern two fronts are small because of compensating horizontal temperature and salinity gradients. A thin layer of increased stability is encountered between 100 and 125 m. Below this layer, there are prominent lateral intrusions of cool and low-salinity subsurface water under warmer and higher salinity surface water, at latitudes north of 31°N and longitudes east of 155°W. The 0/1500 db dynamic height topography bears no similarity to the configurations of the surface isotherms and isohalines, indicating that surface thermohaline fronts are not determined by the baroclinic flow field. Instead, agreement is found between the subtropical frontal zone and the Ekman confluence zone on long time scales. A warm and saline anticyclonic eddy with large thermohaline gradients around its periphery is found near 29°30'N, 158°W. The mean baroclinic flow in the subtropical frontal zone is ~0.04 m s^{-1} and does not vary with season. Perturbations from the mean flow are up to 0.4 m s^{-1} and vary strongly with season. Aspects of frontogenesis in the subtropical frontal zone are investigated. In the upper layer, wind-induced differential horizontal advection of the Ekman type leads to concentration of horizontal thermohaline gradients. In the lower layer, differential vertical advection is primarily responsible for the concentration of such gradients.

1. Introduction

The central North Pacific is characterized by two main water masses. To the north of latitude 42°N there is a cool and low-salinity water mass of subarctic origin, characterized by winter temperatures < 8°C, salinities < 33.8‰ and a pronounced halocline at ~150 m. To the south of latitude 32°N, there is a warm and high-salinity water mass of subtropical origin, called North Pacific Central Water by Sverdrup *et al.* (1942) which is characterized by winter temperatures > 18°C, salinities > 34.8‰ and a well-developed halocline near 100 m. In between lies the *subarctic-subtropical transition* zone, in which both water masses are present and the halocline is weak. The change of temperature and salinity with latitude is not uniform, however, but occurs rather abruptly along the northern and southern boundaries of this zone (McGary and Stroup, 1958; Roden, 1977a). The region of rapid southward temperature and salinity increase along the southern boundary of the transition zone will be be called *subtropical frontal zone*. A closer examination of the thermohaline structure inside this zone reveals that it is often complex, with several fronts (a front will be regarded here as the magnitude of a gradient with a tendency toward discontinuity) present simultaneously. No general agreement exists what the different fronts inside the subtropical frontal zone should be called. McGary (1956) and Seckel (1968) found that climatologically the North Pacific Central Water is bounded by a front in which 34.8‰ isohaline and the 18°C winter isotherm are embedded. For descriptive purposes, this climatological front will be called here the *subtropical front*.

The formation of the subarctic-subtropical transition zone depends on the establishment of primary thermohaline gradients through large-scale geographical variations of radiative heat flux, sensible heat flux, evaporation and precipitation (Roden, 1975). Concentration of these primary gradients into the subtropical frontal zone results primarily from convergence and deformation of the Ekman flow set up by a geographically nonuniform wind stress (Kirwan, 1975; Mooers, 1978).

The *large-scale* wind field in the central North Pacific is dominated by the westerlies and the trade winds. This results in eastward stresses in the north, westward stresses in the south and a broad region of

[1] Contribution No. 1138 from the Department of Oceanography, University of Washington.

0022-3670/80/030342-21$09.25

weak stresses in between. The strongest wind stress gradients are observed at the edges of these two major wind systems.

The above configuration of the wind stress field leads to the following dynamically important features: 1) a zone of strong surface convergence of Ekman transports at the southern edge of the westerlies; 2) a zone of strong surface convergence of Ekman transports at the northern edge of the tradewinds, and 3) in the region between the major wind systems, a zone of confluence of poleward and equatorward Ekman transports (the term confluence is here understood to mean the phenomenon of streaming together that results from the presence of a deformation field. In the confluence zone there is a line of juncture between flows which will be termed the confluence line). It is noteworthy that surface convergence implies vertical motion to satisfy the continuity equation, while surface confluence does not.

No general agreement exists on the geographical terminology of the above features in the Ekman flow field, because the position of the features varies with time. For the purposes of the following discussion, the convergence zone associated with the boundary of the westerlies will be called the *northern Ekman convergence zone*, that associated with the tradewind boundary the *southern Ekman convergence zone* and the zone of merging poleward and equatorward flows the *Ekman confluence zone*.

All three zones are frontogenetic in a horizontally stratified fluid. The relationship between thermohaline fronts and the Ekman convergence and confluence zones is not simple, however, because it depends on the degree of existing horizontal temperature and salinity stratification and on the duration and intensity of convergence and confluence. The following points will clarify this relationship further. First, a given favorable configuration of the Ekman flow field will lead to strong frontogenesis in some geographical areas and weak frontogenesis in others, depending on the magnitude of the initial horizontal thermohaline gradients. Second, a given favorable configuration of the Ekman flow field must persist over a certain length of time, before measurable frontogenesis occurs [for flow on 100 km scales, the time scale appears to be one week (Roden and Paskausky, 1978)]. Third, thermohaline fronts do not disappear instantly after Ekman convergence and confluence cease, but take time to decay (the exact dissipation time is not known). "Fossil" fronts as well as "live" fronts coexist on synoptic time scales and complicate the interpretation of synoptic field observations.

The discussion so far has dealt with Ekman-type frontogenesis. Upper layer fronts can be generated also through deformation and convergence in the geostrophic flow field and, in case of strong and spatially variable flow, this has been observed (Uda, 1938). The effectiveness of these processes in creating and maintaining thermohaline fronts in the central North Pacific is not known in any detail. The large-scale geostrophic flow in this part of the ocean is weak and is characterized by an anticyclonic gyre (Wyrtki, 1974; Reid and Arthur, 1975). The region north of Hawaii lies in the eastern half of this gyre, where the flow has a southward component. Geostrophic convergence, which is proportional to the northward flow component, does not contribute toward frontogenesis here. Geostrophic deformation, which depends mainly on the mixed second derivative of pressure, is favorable for frontogenesis in regions where the isobars approach each other in the downstream direction. Seckel (1968) observed fronts in the confluence zone of the north equatorial current with the gyre circulation of the central Pacific.

While convergence and confluence in the flow field are the main processes concentrating thermal and haline gradients in the upper layer of the ocean, horizontal gradients in the interior of the ocean are more effectively concentrated by differential vertical advection (Newton, 1978). Differential vertical advection arises from both the areal variability of the vertical thermohaline stratification and of the vertical velocity. The latter varies in response to wave disturbances (Newton, 1978) and torques produced by irregular bottom topography and wind stress vorticity (Rattray and Dworski, 1978).

The different modes of upper and lower layer frontogenesis must be kept in mind when interpreting vertical thermohaline sections in which surface fronts appear to be sheared off from the fronts below pycnocline depth. A difficulty arises with the nomenclature of such disjoint fronts. Both can occur in the same geographical area, but they do not arise necessarily from the same processes and hence it is arguable whether they should carry the same name. The position taken here is to name them separately, if there is reason to believe that the processes are fundamentally different.

The objective of the present paper is to focus on the subtropical frontal zone north of Hawaii, to describe the observed horizontal and vertical thermohaline structure, and to relate the observed frontal features to the baroclinic and Ekman flow fields. Emphasis will be placed on the winter of 1974, for which there exists an extensive data set.

2. Field measurements and data reduction

To investigate the detailed thermohaline structure of the subtropical frontal zone, the R.V. *Thomas G. Thompson* occupied 261 stations between 8 January and 10 February 1974. The station pattern is shown in Fig. 1 and consists of five meridional crossings of

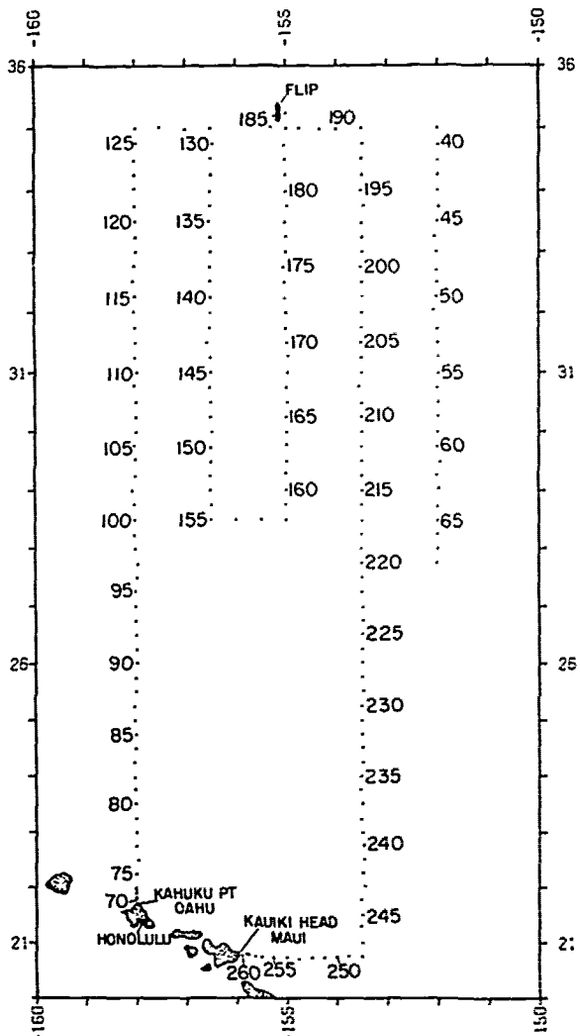

FIG. 1. Stations occupied during the 86th voyage of the R. V. *Thomas G. Thompson*, 8 January–10 February 1974.

the frontal zone. Stations were taken at intervals of 27 km (15 n mi) to resolve the complex thermohaline features. The chief instrument employed on the cruise was the Plessey model 9040 conductivity-temperature-depth probe, commonly known as the CTD. The instrument has a temperature precision of 0.01°C, a conductivity precision of 0.003 s m^{-1}, and a depth precision of 0.25% of the full-scale depth. The instrument was deployed between 0 and 1500 m and was calibrated in the field against Rosette sampler information. Salinities were computed from the CTD output by methods outlined by Roden and Irish (1975). Sound velocity was computed from Wilson's equation (Tolstoy and Clay, 1966) and the Väisälä frequency (Väisälä, 1925) was computed from the vertical density gradient and the compressibility term (Eckart, 1960). The CTD output was in digital form, with a scan every 2–3 m. The digitized data were passed through a linear interpolation scheme to yield values at exactly 3 m intervals. These equally spaced data form the basis of all subsequent calculations. This permits one to resolve vertical length scales > 6 m.

3. Horizontal structure of the subtropical frontal zone in winter

The details of the subtropical frontal zone depend upon the scale of analysis. With a coarse resolution grid employed by McGary (1956) and McGary and Stroup (1958), it is possible to outline the main characteristics of this zone. This is shown in Fig. 2, where the North Pacific Central Water has been shaded. The northern boundary of this water appears between 31 and 33°N and a well-defined salinity front and a weaker temperature front are found in its vicinity. Typical salinity gradients in the frontal area vary between 0.2 and 0.5‰ (100 km)$^{-1}$, while temperature gradients seldom exceed 2°C (100 km)$^{-1}$. The latter finding is in good agreement with sea surface temperature maps derived from satellite observations (National Environmental Satellite Service, 1977–1979), which is based on a similar coarse resolution grid (100 km by 100 km), and with results from air-drops of expendable bathythermographs (Barnett, 1976).

When the resolution is increased, the subtropical frontal zone attains a more complicated character. This is shown in Figs. 3 and 4, which illustrate the temperature, salinity and density distributions at 0 and 150 m, respectively. Fronts occur not only along the northern boundary of the North Pacific Central Water, but at other locations as well. To avoid ambiguity, the front along the northern boundary of this water mass will be called the subtropical front, as before, while the other fronts will be identified by separate names.

At the sea surface, the subtropical front appears between latitudes 31 and 32°N. It has a meandering shape, is about 50 km wide and is characterized by salinity differences of 0.2‰ and temperature differences of 0.5°C across. These differences balance each other in such a way that the resulting density differences across the front are small. The temperature difference necessary to balance a given salinity difference completely is listed in Table 1. The table was constructed by making use of the equation of state and of the coefficients of thermal expansion and haline contraction. Because these coefficients depend strongly on temperature and weakly on salinity, the results are shown as a function of temperature. It is seen that to balance a given salinity difference, a much smaller temperature difference is required at high than at low temperatures. For the subtropical front, of interest here, a temperature

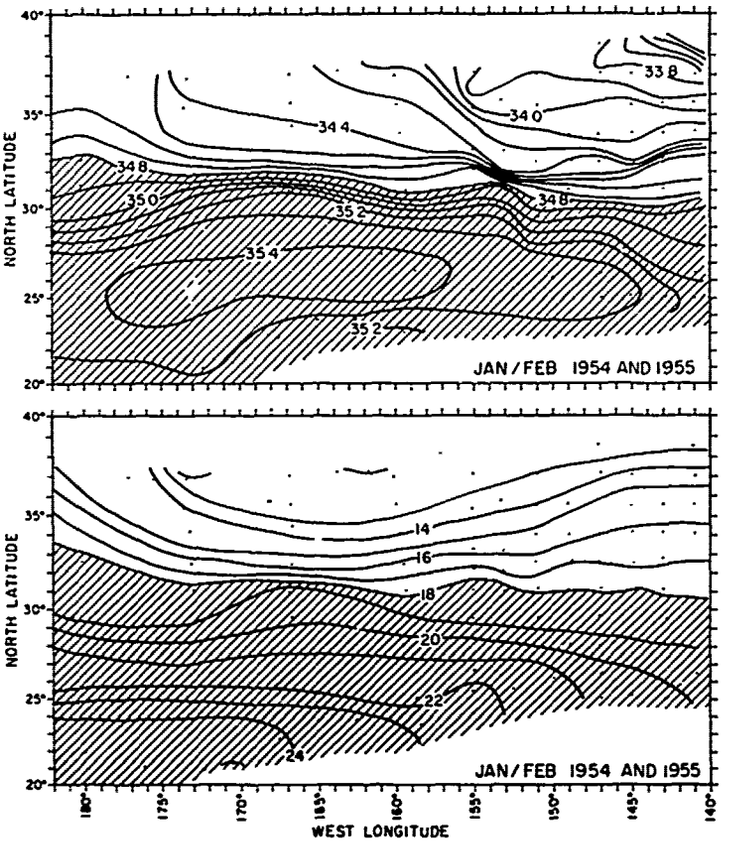

FIG. 2. Salinity and temperature distribution at the sea surface during the winters of 1954 and 1955. Dots indicate station positions (McGary, 1956; McGary and Stroup, 1958). Shading indicates North Pacific Central Water.

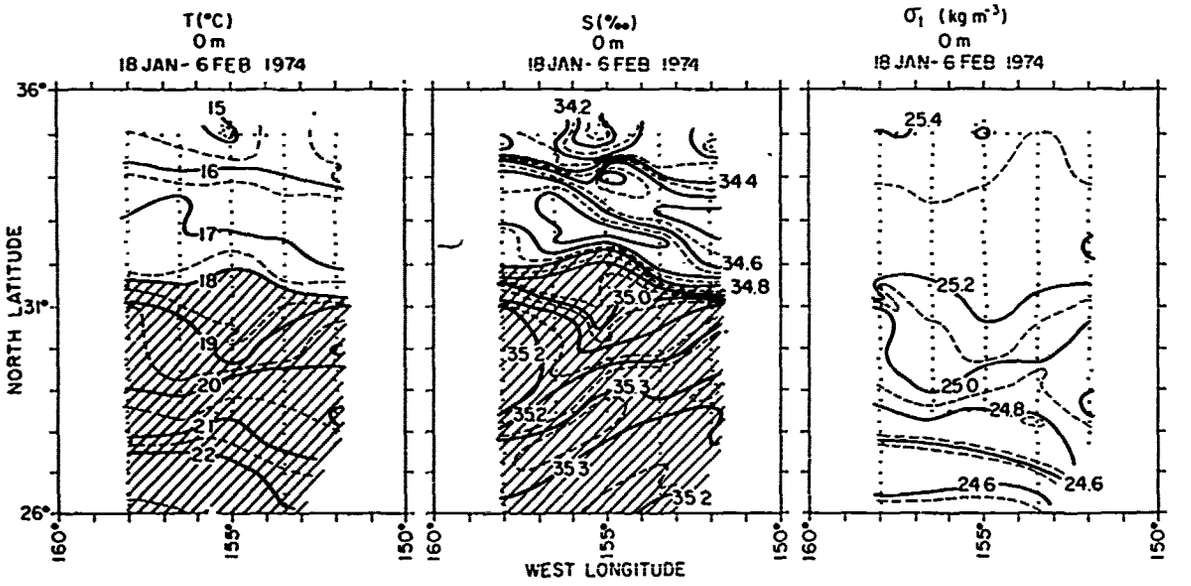

FIG. 3. Temperature, salinity and density distribution at the sea surface during the winter of 1974. Dots indicate station positions. Shading indicates North Pacific Central Water.

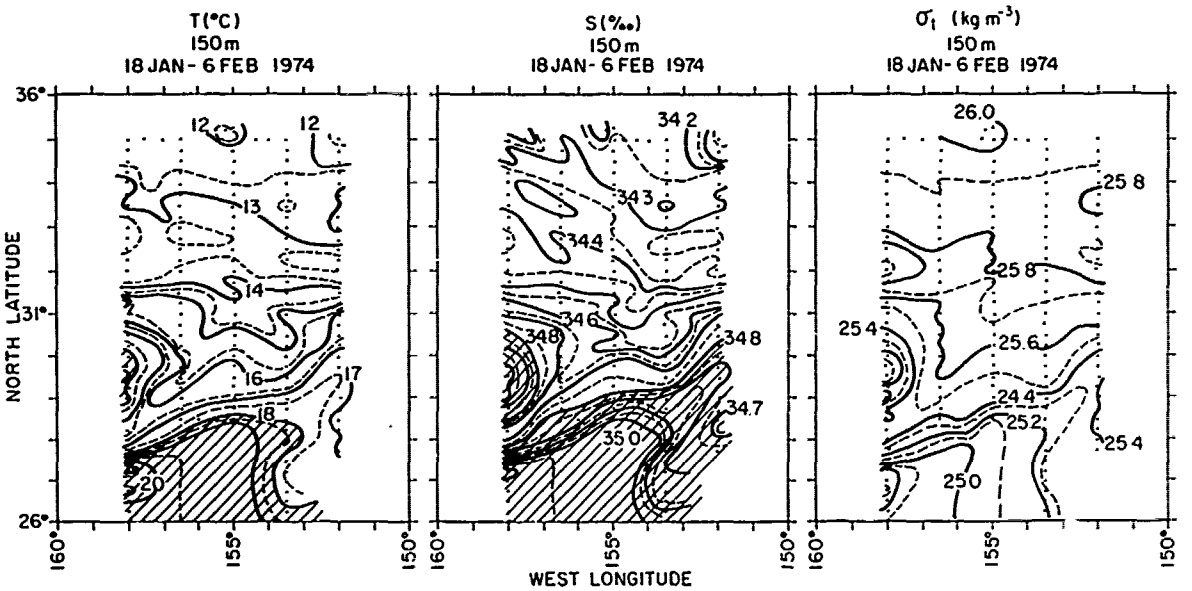

FIG. 4. As in Fig. 3 except at 150 m.

difference of 0.6°C is required to balance a salinity difference of 0.2‰ such that the density difference vanishes.

A surface front similar to the subtropical one occurs near 34°N. This front, which will be called the *34°N front*, is ~50 km wide and is almost totally density compensated.

At 150 m, conditions differ markedly from those at the sea surface. The boundary of the North Pacific Central Water lies further southward, extending in a WSW-ENE direction between latitudes 27, and 29°N. The accompanying front is characterized by temperature gradients of 1.5°C (27 km)$^{-1}$ and salinity gradients of 0.2‰ (27 km)$^{-1}$ which, unlike those encountered at the sea surface, are not density compensating. In addition, the thermohaline structure at 150 m reveals a conspicuous eddy of North Pacific Central Water centered at 29°30'N, 158°W. The boundaries of this eddy are marked by strong temperature, salinity and density gradients. Eddies of this type are comon in the subtropical frontal zone of the Atlantic (Voorhis *et al.*, 1976; Leetmaa and Voorhis, 1978) but their frequency of occurrence in the subtropical frontal zone of the Pacific has not been investigated so far.

TABLE 1. Temperature difference (ΔT) required to balance a salinity difference (ΔS) of given magnitude such that the resulting density difference vanishes. The ratio of the coefficients of haline contraction to thermal expansion is indicated by r. The table is valid for ocean water near 35‰ salinity.

		ΔT (°C)				
T (°C)	r	ΔS = 0.2‰	ΔS = 0.4‰	ΔS = 0.6‰	ΔS = 0.8‰	ΔS = 1‰
0	−13.52	2.70	5.40	8.11	10.81	13.52
2	−9.60	1.92	3.84	5.76	7.68	9.60
4	−7.46	1.49	2.98	4.47	5.79	7.46
6	−6.11	1.22	2.44	3.66	4.88	6.11
8	−5.20	1.04	2.08	3.12	4.16	5.20
10	−4.55	0.91	1.82	2.73	3.64	4.55
12	−4.04	0.80	1.61	2.42	3.23	4.04
14	−3.67	0.73	1.46	2.20	2.93	3.67
16	−3.36	0.67	1.34	2.01	2.68	3.36
18	−3.10	0.62	1.24	1.86	2.68	3.10
20	−2.88	0.57	1.15	1.72	2.30	2.88
22	−2.70	0.54	1.08	1.62	2.16	2.70
24	−2.55	0.51	1.02	1.53	2.04	2.55
26	−2.41	0.48	0.96	1.45	1.93	2.41
28	−2.30	0.46	0.92	1.38	1.84	2.30
30	−2.19	0.43	0.87	1.31	1.75	2.19

The baroclinic flow at 0 and 150 m, relative to 1500 m, is shown in Fig. 5. At the sea surface, there is little resemblance between the patterns of baroclinic flow and of the thermohaline fronts. Neither the 34°N front nor the subtropical front are accompanied by strong baroclinic flow. On the other hand, close agreement exists between the baroclinic flow and the frontal patterns at 150 m. Here, currents up to 0.5 m s^{-1} are observed along the edge of the North Pacific Central Water and along the rim of the anticyclonic warm core eddy at 29°30'N, 158°W.

The lack of agreement between surface fronts and surface baroclinic flow is not surprising. First, baroclinic flow will be minimal when the horizontal temperature and salinity gradients are density compensating such as at the 34°N front. Ekman dynamics, rather than baroclinic flow dynamics, can then be expected to control the generation of surface fronts

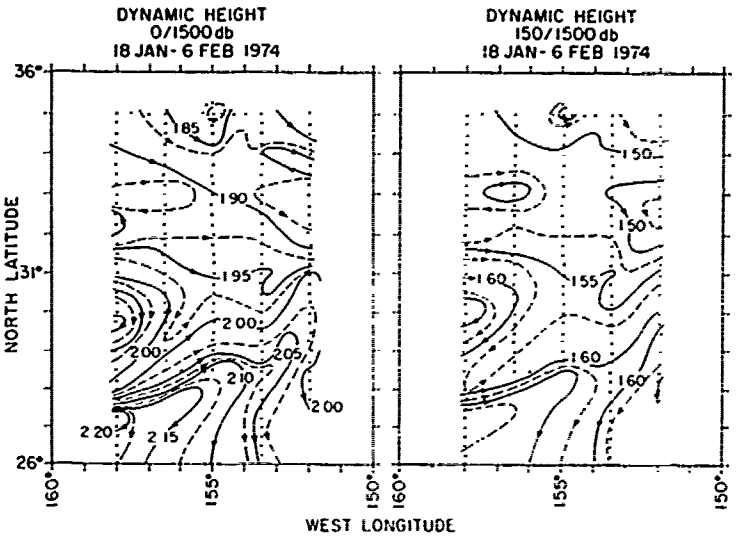

FIG. 5. Dynamic topography relative to 1500 db during the winter of 1974. Dots indicate station positions. Arrows indicate the direction of baroclinic flow.

(Newton, 1978). Second, surface baroclinic flow is not determined by the thermohaline gradients at the surface or in the upper mixed layer, but in the entire underlying water column. When the horizontal thermohaline structure of the surface layer differs from that in the deeper layers, the region of strongest baroclinic flow will be displaced from the surface manifestation of the front.

4. Vertical Structure of the Subtropical Frontal Zone in Winter

The following discussion is based on vertical sampling at 3 m intervals and horizontal sampling at 27 km intervals. This allows one to resolve vertical features > 6 m and horizontal features > 54 km.

a. Hydrostatic stability

Hydrostatic stability is an important parameter in frontal dynamics, because it determines the depth to which surface momentum, heat and salt fluxes can penetrate by processes of convection and stirring. Direct meteorological forcing of fronts is generally limited to depths between the sea surface and the underlying high stability layer. In the subtropical frontal zone, hydrostatic stabilities are generally low, because vertical temperature and salinity gradients point in the same direction, leading to a diminished vertical density gradient. The hydrostatic stability expressed in terms of the Väisälä frequency is

$$N^2 = -g\left(\frac{1}{\rho}\frac{\partial \rho}{\partial z} + \frac{g}{c^2}\right),$$

where ρ is density, g the acceleration of gravity and c the sound velocity. The ratio of the sound velocity term to the density gradient term during the winter season varies between 0.5 in the pycnocline to 1 in the upper layer. Instabilities with resultant convection will occur when the vertical density gradient is less than $-g\rho c^{-2}$ or about -4×10^{-3} kg m^{-4}.

Meridional sections of hydrostatic stability, expressed in terms of the Väisälä frequency are shown in Fig. 6 for five different longitudes. The layer in which the Väisälä frequency ≥ 0.01 s^{-1} is shaded. This layer of increased stability is only 10–20 m thick, and occurs at an average depth of ~125 m. Numerous irregular perturbations with amplitudes up to 50 m are superimposed. The origin of the perturbations is not known, though oscillations set up by stationary and traveling storms have been implicated in some cases (Philander, 1978).

b. Temperature and salinity

The meridional distributions of temperature and salinity in the upper 900 m of the subtropical frontal zone are shown in Figs. 7–9. The basic vertical structure consists of three layers: a warm and saline top layer ~100 m deep, a layer of rapid temperature and salinity decrease between 100 and 500 m, and a deep layer in which the temperatures slowly decrease and the salinities slowly increase with depth. The basic structure is perturbed by fronts, lateral intrusions, oscillations in the thermocline and halocline and, in some areas, by isolated water parcels of various size.

Several fronts occur in the subtropical frontal zone. In the north, a well developed front is ob-

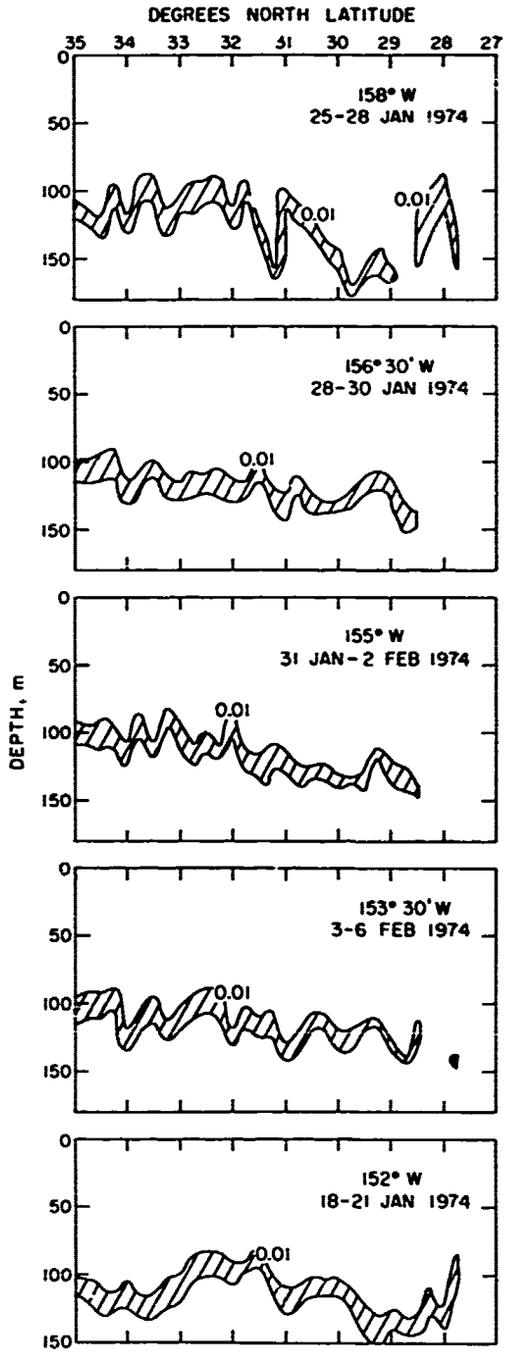

FIG. 6. Meridional sections of the Väisälä frequency (s^{-1}) during the winter of 1974. The layer of high stability is shaded.

served near latitude 34°N. It is most pronounced in the upper 100 m, occurs on all meridional sections, is about 50 km wide, and is characterized by salinity gradients of 0.2‰ (27 km)$^{-1}$ and temperature gradients of 0.5°C (27 km)$^{-1}$. This 34°N front is almost vertical above the high stability layer (125 m) and is more than 360 km north of the North Pacific Central Water boundary. The shallowness of this front, its vertical orientation and the fact that it is far from the boundary of a source region make it plausible to assume that it is primarily formed by convergence and deformation in the Ekman flow field.

The poleward boundary of the North Pacific Central Water occurs between latitudes 31 and 32°N and is accompanied by several fronts in the vicinity. The front in which the 34.8‰ isohaline and the 18°C isotherm are embedded includes the boundary and will be regarded as the subtropical front. This front is well defined in all meridional sections and is 30–50 km wide. It is characterized by salinity gradients of 0.2–0.3‰ (27 km)$^{-1}$ and temperature gradients of 0.5–1.0°C (27 km)$^{-1}$, which are almost constant in the upper 100 m. The other fronts in the vicinity of this water mass boundary are less intense and have typical horizontal gradients of 0.1‰ (27 km)$^{-1}$ and 0.2°C (27 km)$^{-1}$, respectively.

The origin of the multiple fronts near the northern edge of the North Pacific Central Water can be speculated on only at present. It is possible that these result from the intricate dynamics inside the frontal zone (Mooers, 1978). It is equally possible that some of these fronts are decaying remnants of previous positions of the subtropical front. The subtropical front is likely to move some distance from its mean position under the influence of wind forcing. When the winds cease, the front does not disappear instantly, but takes time to decay.

The thermohaline structure below the upper layer is complicated. There are indications of lateral intrusions of cool and low-salinity subsurface water under warmer and higher salinity surface water at longitudes of 152–155°W. These intrusions result from differential motion of the upper and lower layers. The upper layer, dominated by Ekman flow, moves northward (Fig. 15), while the lower layer, dominated by baroclinic flow, moves to the eastward and southward (Fig. 5). Numerous isolated patches of salinity different from ambient occur below the leading edge of the 34°N front and in the region of the lateral intrusions. At some locations, such as 34°N, 156°30'W, sinking of high-salinity water at the front is indicated clearly. The dynamical processes leading to such patchiness and sinking are not well known. Gregg (1975) observed that lateral intrusions are effective in creating small-scale structure, while Turner (1973), Garrett and Horne (1978) and Bowman and Okubo (1978) have suggested that double diffusion and cabbeling (instabilities created by mixing together waters of different temperatures and salinities, but of the same density) can also create such structure.

A curious feature is the pronounced temperature and salinity front, which occurs between 125 and

300 m at 27°45'N, 158°W. It involves the boundary of the North Pacific Central Water, is ~50 km wide, and is characterized by temperature differences of 3°C and salinity differences of 0.4‰ across. At first sight, one may be tempted to connect this front to the upper layer subtropical front, because it involves the same water mass boundary. A closer examination of the vertical thermohaline structure at different iongi-

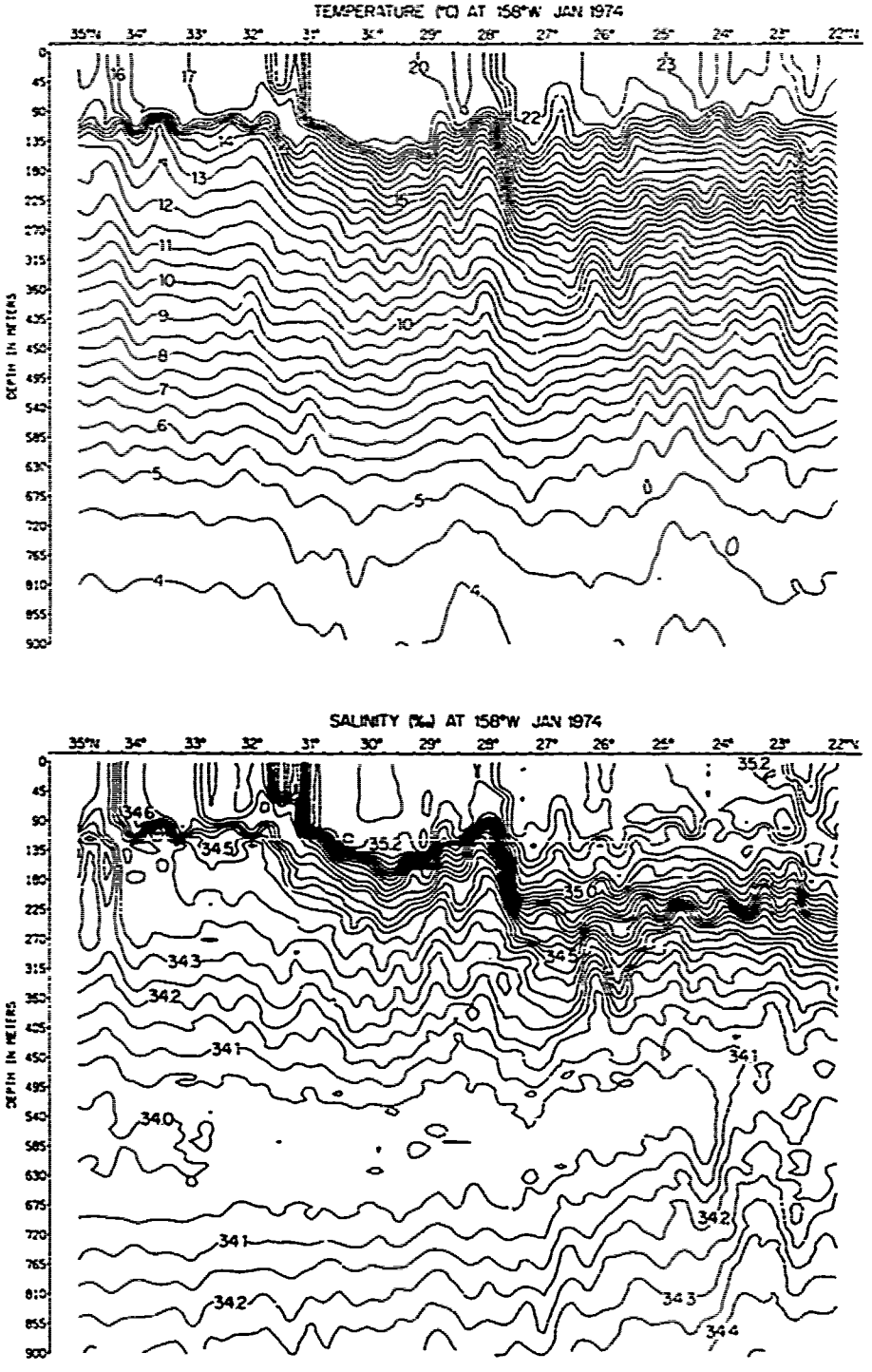

FIG. 7. Meridional sections of temperature (top) and salinity (bottom) along longitude 158°W, during the winter of 1974.

tudes reveals, however, that this front, unlike the surface front, is not present at all longitudes, and thus must have been created by different processes. A possible, but not proven, process could be differential vertical motion induced by the Musicians Seamount Chain, which is located nearby.

Between 200 and 600 m, there are numerous oscillations in the main thermocline and the main halocline. These oscillations are of both short and long wavelengths and can be expected to have a broad wavenumber spectrum (Roden, 1979). No detailed analysis of the oscillations will be attempted in this paper. Attention is drawn, however, to the unusual wave activity in the 300–600 m depth interval at longitude 155°W, latitudes 32–34°N. The waves have an amplitude of ~20 m, a wavelength of ~60

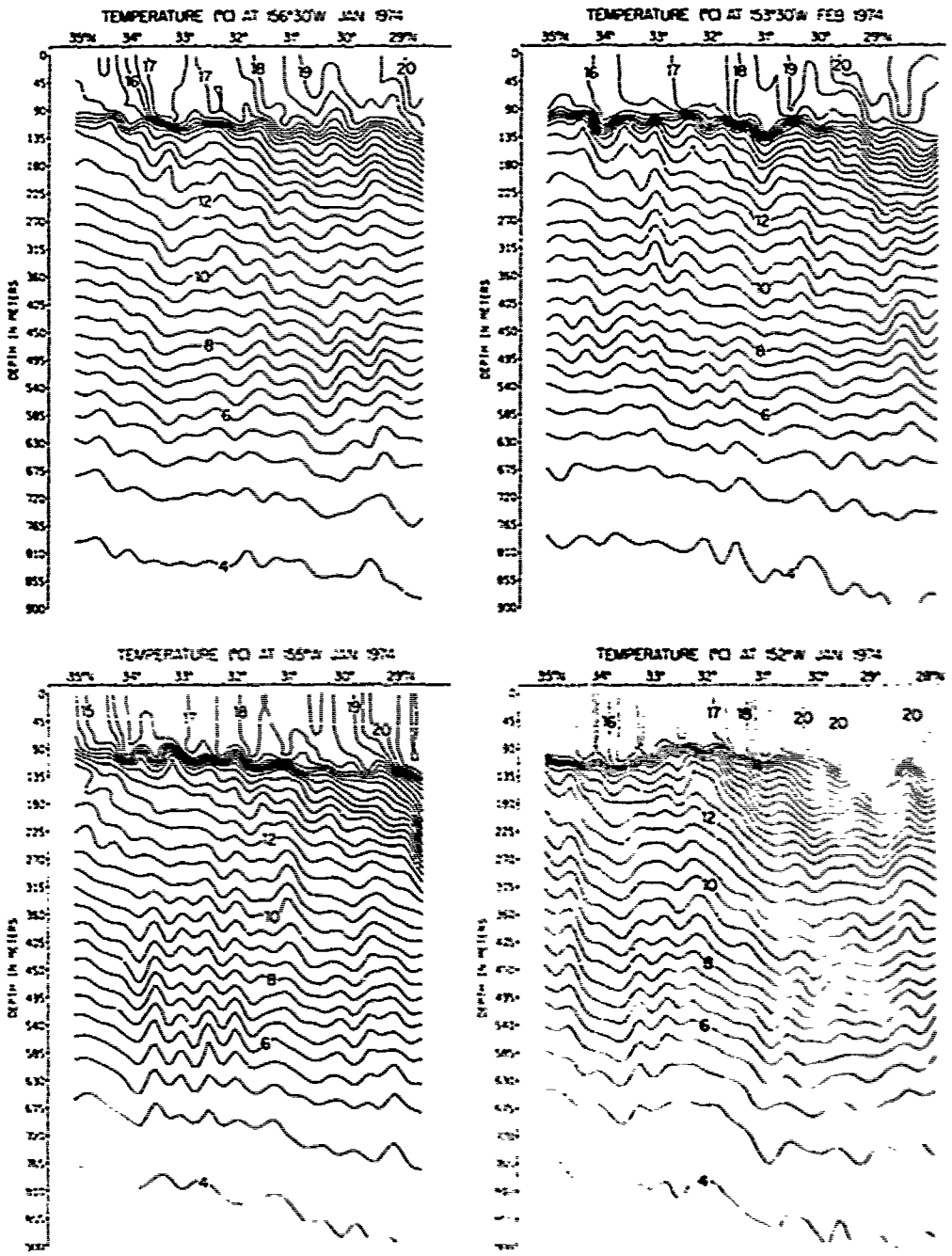

FIG. 8. Meridional sections of temperature at longitudes 156°30'W, 155°W, 153°30'W and 152°W, during the winter of 1974.

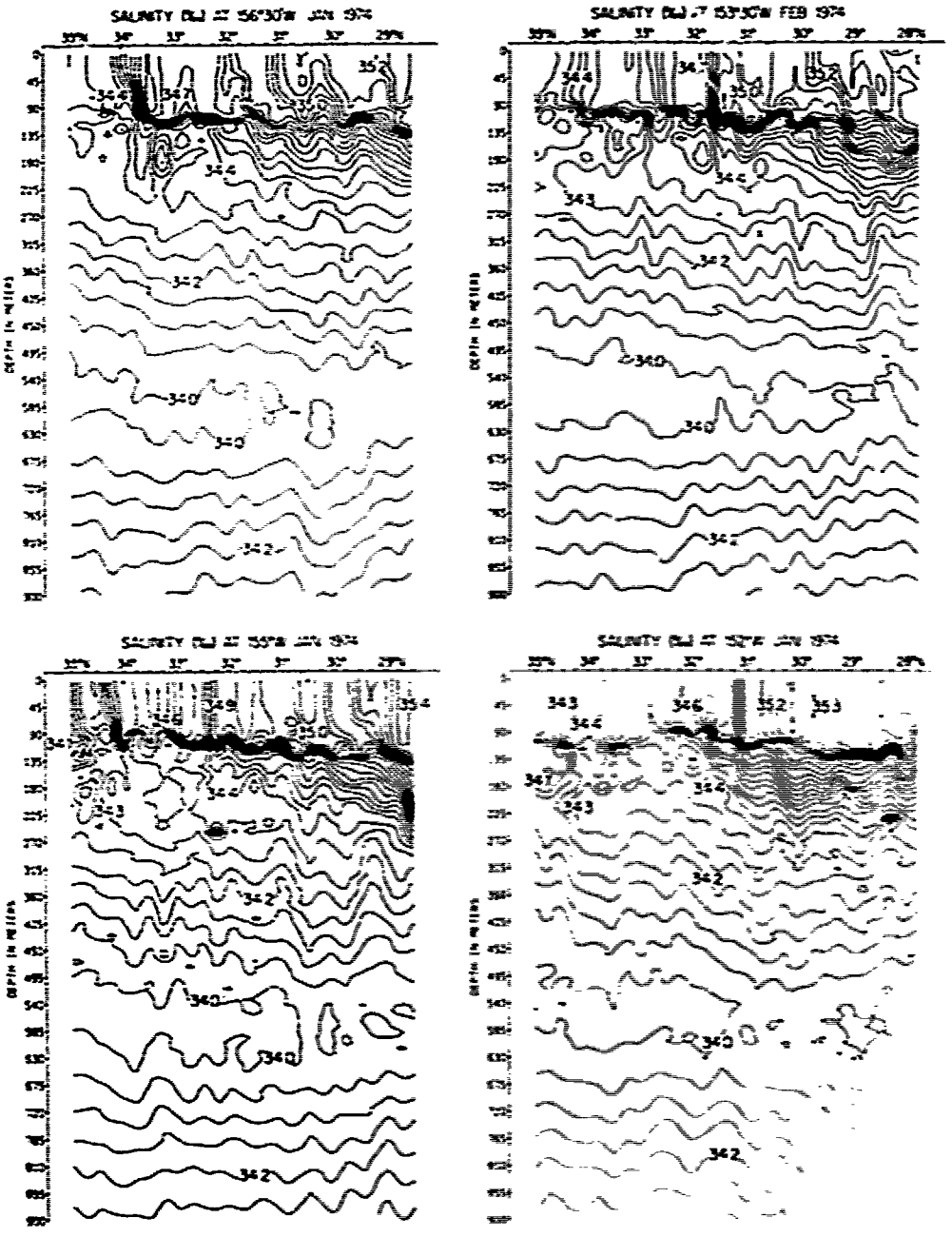

FIG. 9. As in Fig. 5 except for salinity.

km and are larger than those elsewhere. It is noteworthy that the latitude range in which they occur corresponds to the zone between the subtropical and 34°N fronts in the upper layers. Whether this is a significant association or not cannot be ascertained at present.

The deep salinity minimum, characterized by salinities of about 34‰ and temperatures close to 6°C, occurs near 550 m. This intermediate water is formed near the surface in higher latitudes (perhaps near the subarctic front in winter), sinks and subsequently spreads along density surfaces between σ_t = 26.7 and 26.8 kg m^{-3} (Reid, 1965; Kuksa, 1977). The core of water with salinities ≥ 34‰ extends to the vicinity of the subtropical front; south of it, the salinities in the core increase slightly.

c. *Sound velocity*

The meridional distribution of sound velocity in the upper 900 m of the subtropical frontal zone is shown in Fig. 10 (top). The basic vertical structure

consists of three layers: a surface layer ~100 m deep, in which the sound velocity is almost uniform with depth; a well-developed sonocline (layer of rapid sound velocity decrease) between 100 and 600 m; and the deep sound velocity minimum between 600 and 900 m. Considerable meridional variability is superimposed on the basic vertical structure. In the upper layer, there are three fronts: the 34°N front, the subtropical front at 31°N, and a front at 28°N. Of these, the subtropical front is

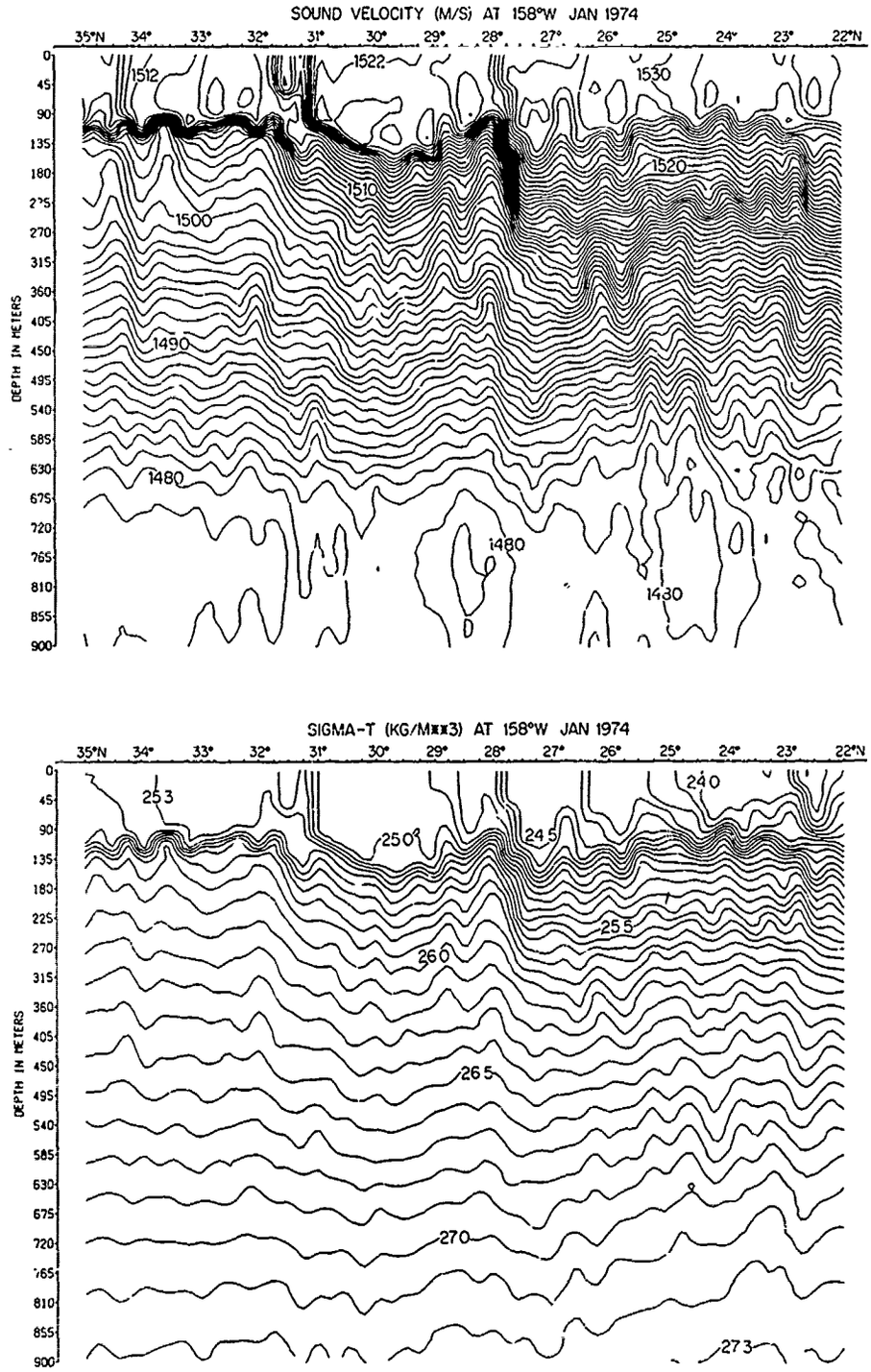

FIG. 10. Meridional sections of sound velocity (top) and density (bottom) along longitude 158°W, during the winter of 1974.

strongest, with sound velocity gradients of 8 m s^{-1} (27 km)$^{-1}$ at a depth of 90 m. Just north of this front, at depths between 90 and 135 m, a conspicuous gap occurs in the shallow sonocline. In this gap, the vertical sound velocity gradient is nearly an order of magnitude smaller than in the surrounding area. This change in vertical sound velocity structure over short distances in the vicinity of the subtropical front can be expected to have a strong effect upon underwater sound communication (Tolstoy and Clay, 1966).

Between 100 and 600 m, the sound velocity structure is complex. A frontlike feature occurs at 27°45'N, 158°W and is characterized by meridional gradients of 12 m s^{-1} (27 km)$^{-1}$. This feature is not observed at all longitudes and appears to be of local origin. There are numerous oscillations of the sonocline. Though no attempt will be made here of a spectral description of these oscillations, it is of interest to point out here that they involve a wide variety of scales and that their amplitudes and phases vary considerably with depth.

The deep sound velocity minimum shows comparatively little meridional structure. The axis of the minimum in the subtropical region north of Hawaii is located close to 750 m. Sound velocities along the axis show a slight southward increase, from 1478.5 m s^{-1} near 35°N to 1481.5 m s^{-1} near 22°N. The results are in agreement with previous investigations by Johnson and Norris (1968), which were based on coarse sampling with Nansen bottles.

d. Density and dynamic height

The meridional density distribution in the upper 900 m of the subtropical frontal zone is shown in Fig. 10 (bottom). The distribution is characterized by an isopycnal layer ~100 m deep, a sharp pycnocline between 100 and 150 m and a gradual density increase with depth below. The basic distribution is perturbed by fronts and oscillations. In the upper layer, the density fronts are weak, because of a large degree of compensation between the horizontal temperature and salinity gradients. At 34°N, this compensation is complete, so that no density front accompanies the temperature, salinity and sound velocity fronts observed there. At 31°N, a weak density front is found at the location of the well-defined subtropical thermohaline fronts. At 27°45'N, a density front is observed that extends below the upper layer into the pycnocline and is quite conspicuous there. This deep front is not found east of longitude 155°W and its origin is obscure. The Musicians Seamounts are close by and it is possible that a link exists between the front and these seamounts. The question deserves attention in future studies.

The meridional distribution of dynamic height between latitudes 28 and 35°N is shown in Fig. 11

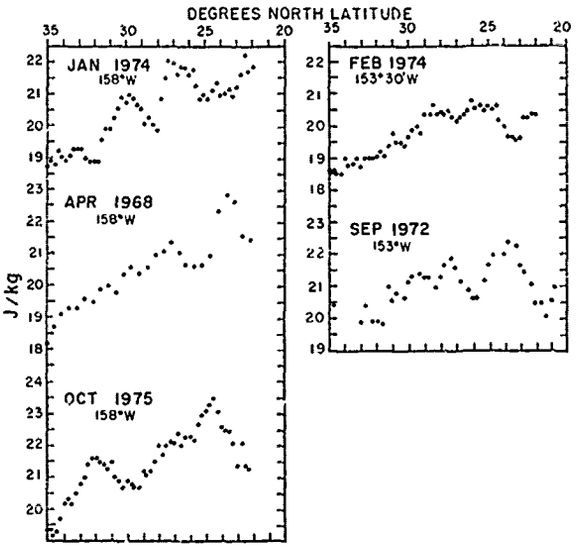

FIG. 11. Seasonal variation of the 0/1500 db dynamic heights at longitudes 158°W and 153°30'W. Based on cruises of the R. V. *Thomas G. Thompson* in the months and years shown.

for different months and longitudes. The dynamic heights are in units of Joules per kilogram, equivalent to 0.1 dyn m. An estimate of the geometric sea level height can be obtained by dividing the dynamic height values by the acceleration of gravity. From the dynamic heights, the baroclinic slopes in the subtropical frontal zone can be obtained.

The dynamic heights increase southward. The *mean slopes*, as noted earlier by Wyrtki (1975) and Roden (1977b), are quite small and show little seasonal variation. At 158°W, the mean slope is 3×10^{-6} J kg^{-1} m^{-1} and corresponds to a baroclinic current of 0.04 m s^{-1}. At 153°30'W, the mean slopes and currents are about half these values. The *perturbation slopes* are up to an order of magnitude larger than the mean slopes and vary strongly with season. The strongest perturbation slopes are 3×10^{-5} J kg^{-1} m^{-1} and correspond to a baroclinic current of 0.4 m s^{-1}. Slopes of this magnitude can be detected by satellite altimeter (Leitao *et al.*, 1978) and a potential exists for remote monitoring of their time variability. The strong time variability of the perturbation slopes was attributed to stochastic forcing by the atmosphere by Frankignoul and Müller (1979).

5. Some aspects of subtropical frontogenesis in the surface layer

The previous discussion dealt with the description of the observed thermohaline features in the subtropical frontal zone. It is of interest to investigate briefly the relationship between upper layer frontogenesis and the configurations of the Ekman and geostrophic flow fields and to determine the time needed to double the intensity of an existing front.

TABLE 2. Expressions for convergence deformation and vorticity for Ekman and geostrophic flow and representative orders of magnitude on 100 km scales for the central North Pacific. All units are in s^{-1}. The following notation is used: ϕ latitude, λ longitude, τ_λ, τ_ϕ wind stress components at the sea surface, u_g, v_g geostrophic flow components, ρ density of seawater, D mixed-layer depth, f Coriolis parameter, β its change with latitude, p pressure and α specific volume.

	Ekman flow	Geostrophic flow
Convergence	$-\left[\frac{1}{r\cos\phi}\frac{\partial}{\partial\lambda}\left(\frac{\tau_\phi}{\rho fD}\right)-\frac{1}{r}\frac{\partial}{\partial\phi}\left(\frac{\tau_\lambda}{\rho fD}\right)+\frac{\tau_\lambda}{\rho fD}\frac{\tan\phi}{r}\right]$ $\times 4\times10^{-7}$	$+\frac{\beta}{f}v_g-\rho\left(\frac{u_g}{r\cos\phi}\frac{\partial\alpha}{\partial\lambda}+\frac{v_g}{r}\frac{\partial\alpha}{\partial\phi}\right)$ 10^{-8} 10^{-11}
Normal deformation	$\frac{1}{r\cos\phi}\frac{\partial}{\partial\lambda}\left(\frac{\tau_\phi}{\rho fD}\right)+\frac{1}{r}\frac{\partial}{\partial\phi}\left(\frac{\tau_\lambda}{\rho fD}\right)+\frac{\tau_\lambda}{\rho fD}\frac{\tan\phi}{r}$ $\times 2\times10^{-7}$	$\frac{\beta}{f}v_g-\frac{2}{\rho f}\frac{1}{r}\frac{\partial}{\partial\phi}\left(\frac{1}{r\cos\phi}\frac{\partial p}{\partial\lambda}\right)+\rho\left(\frac{u_g}{r\cos\phi}\frac{\partial\alpha}{\partial\lambda}-\frac{v_g}{r}\frac{\partial\alpha}{\partial\phi}\right)$ 10^{-8} 2×10^{-7} 10^{-11}
Shear deformation	$-\left[\frac{1}{r\cos\phi}\frac{\partial}{\partial\lambda}\left(\frac{\tau_\lambda}{\rho fD}\right)-\frac{1}{r}\frac{\partial}{\partial\phi}\left(\frac{\tau_\phi}{\rho fD}\right)-\frac{\tau_\phi}{\rho fD}\frac{\tan\phi}{r}\right]$ $\times 2\times10^{-7}$	$-\frac{\beta}{f}u_g+\frac{1}{\rho f}\left(\frac{1}{r^2\cos^2\phi}\frac{\partial^2 p}{\partial\lambda^2}-\frac{1}{r^2}\frac{\partial^2 p}{\partial\phi^2}-\frac{1}{r}\frac{\partial p}{\partial\phi}\frac{\tan\phi}{r}\right)+\rho\left(\frac{v_g}{r\cos\phi}\frac{\partial\alpha}{\partial\lambda}+\frac{u_g}{r}\frac{\partial\alpha}{\partial\phi}\right)$ 10^{-8} 10^{-7} 10^{-11}
Vorticity	$-\left[\frac{1}{r\cos\phi}\frac{\partial}{\partial\lambda}\left(\frac{\tau_\lambda}{\rho fD}\right)+\frac{1}{r}\frac{\partial}{\partial\phi}\left(\frac{\tau_\phi}{\rho fD}\right)-\frac{\tau_\phi}{\rho fD}\frac{\tan\phi}{r}\right]$ $\times 2\times10^{-7}$	$\frac{\beta}{f}u_g+\frac{1}{\rho f}\left(\frac{1}{r^2\cos^2\rho}\frac{\partial^2 p}{\partial\lambda^2}+\frac{1}{r^2}\frac{\partial^2 p}{\partial\phi^2}-\frac{1}{r}\frac{\partial p}{\partial\phi}\frac{\tan\phi}{r}\right)+\rho\left(\frac{v_g}{r\cos\phi}\frac{\partial\alpha}{\partial\lambda}-\frac{u_g}{r}\frac{\partial\alpha}{\partial\phi}\right)$ 10^{-8} 10^{-7} 10^{-11}

Assume that a uniform horizontal salinity gradient of magnitude $|\nabla_H S|$ exists at the sea surface. Ignoring salt fluxes due to turbulent processes, the local time range of change of the magnitude of the surface salinity gradient can be expressed by (Roden, 1977a)

$$\frac{\partial}{\partial t}\ln|\nabla_H S| = -\frac{\partial v_n}{\partial n}, \tag{1}$$

where t is time, n the derivative normal to the front, taken positive toward increasing salinities, and v_n the velocity component normal to the front. A simple integration yields

$$|\nabla_H S|/|\nabla_H S|_0 = \exp\left[-T\left(\frac{1}{T}\int_0^T\frac{\partial v_n}{\partial n}\,dt\right)\right], \tag{2}$$

which states that the salinity front will intensify if the time average of the velocity component normal to the front decreases in direction of the front. Frontal intensification depends, therefore, on the *persistence* of the flow pattern as well as on the *intensity* of the velocity gradients. To double the intensity of the existing surface salinity front, 80 days are required for an average velocity shear of 10^{-7} s^{-1}, while only 8 days are necessary for this to occur when the average velocity shear is 10^{-6} s^{-1}. On 100 km scales, the observed horizontal velocity shears of Ekman and geostrophic flow vary mostly between 10^{-7} s^{-1} and 10^{-6} s^{-1} and thus several weeks are required to double the intensity of an existing front.

The normal derivative in (2) can be expressed in terms of convergence and deformation. If γ is the angle between the east direction and the tangent to the front

$$\begin{aligned}-\frac{\partial v_n}{\partial n} = &-\frac{1}{2}\left(\frac{1}{r\cos\phi}\frac{\partial u}{\partial\lambda}+\frac{1}{r}\frac{\partial v}{\partial\phi}-\frac{v}{r}\tan\phi\right)\\ &+\frac{1}{2}\left(\frac{1}{r\cos\phi}\frac{\partial u}{\partial\lambda}-\frac{1}{r}\frac{\partial v}{\partial\phi}-\frac{v}{r}\tan\phi\right)\cos2\gamma\\ &+\frac{1}{2}\left(\frac{1}{r\cos\phi}\frac{\partial v}{\partial\lambda}+\frac{1}{r}\frac{\partial u}{\partial\phi}+\frac{u}{r}\tan\phi\right)\sin2\gamma,\end{aligned} \tag{3}$$

where u and v are the eastward and northward velocity components, ϕ is latitude, λ longitude and r the earth's radius. The first right-hand term is the convergence, the second the normal deformation and the third the shear deformation. Expressions of these quantities for Ekman and geostrophic flow are listed in Table 2 together with magnitudes characteristic on 100 km scales in the subtropical North Pacific. It is seen that the terms containing the horizontal density gradients and those containing the latitudinal change of the Coriolis parameter are an order of magnitude smaller than the other terms. Note, in particular, that the Ekman convergence (proportional to the curl of the wind stress) is an

order of magnitude larger than the geostrophic convergence, on the scales considered here. Therefore, it follows that *upper layer frontogenesis depends essentially upon the time average of Ekman convergence and upon the time averages of Ekman and geostrophic deformation.*

a. Long-term mean fields

To determine the configuration of the wind stress field over large ocean areas and to calculate the Ekman flow, it is necessary to utilize the stress of the quasi-geostrophic wind, which can be obtained from sea level atmospheric pressure maps. The quasi-geostrophic wind is defined by

$$\mathbf{V} = -\frac{f\nabla_H p_a \times \mathbf{i}_r + \kappa\nabla_H p_a}{\rho_a(f^2 + \kappa^2)}, \qquad (4)$$

where $\mathbf{i}_r$ is a vertical unit vector, p_a atmospheric pressure, ρ_a air density, f the Coriolis parameter and $\kappa = 2.5 \times 10^{-5}$ s^{-1} is the surface friction coefficient for the wind (Defant and Defant, 1958), which allows for cross-isobar flow (12–18° in midlatitudes) toward lower pressure.

Long-term (1931–60) Ekman transports in the North Pacific are shown in Fig. 12. The outstanding feature is the confluence band in the subtropical region. In January, this band is centered near 25°N in the western Pacific and near 32°N in the region north of Hawaii. Because water of different origin is brought together in the confluence zone, temperature and salinity fronts can be expected to occur therein. This is also observed. In the western Pacific, White *et al.* (1978) found the January long-term mean position of the subtropical frontal zone to be near 25°N, while for the region north of Hawaii, the data by McGary (1956) and McGary and Stroup (1958) indicate that the January position of this front zone lies between 30 and 32°N. Though Fig. 12 is adequate to estimate the position of the subtropical frontal zone qualitatively, for a more thorough understanding of frontogenesis it is necessary to know the configuration of the velocity gradient field expressed by deformation, divergence and vorticity (Kirwan, 1975; Okubo, 1978). For Ekman flow, the gradients are proportional to those of the wind stress.

The long-term (1931–60) January mean fields of wind stress deformation, divergence and vorticity are shown in Figs. 13 and 14. The figures are based on the stress of the quasi-geostrophic wind and on a 1° latitude-longitude grid, as before. In the latitude belt between 20 and 40°N, the configuration is predominantly zonal. The normal deformation, shear deformation and divergence of the wind stress are of the same order of magnitude and vary between -2×10^{-7} and $+2 \times 10^{-7}$ N m^{-3} (1 N m^{-3} = 0.1 cgs units). The curl of the wind stress, in the other hand, is two to three times larger and varies between -4×10^{-7} and $+6 \times 10^{-7}$ N m^{-3}. In the subtropical frontal zone, the curl and the normal deformation of the wind stress are negative, while the shear deformation and the divergence are positive.

For an essentially zonal temperature and salinity distribution, observed in the central North Pacific during winter, theoretical considerations based on (2) suggest that frontogenesis occurs where the product of the initial haline gradient with the average horizontal velocity shear normal to the front has a maximum. The initial haline gradients, as indicated in Fig. 2, are strongest in the region of the subtropical front between 30 and 32°N. The horizontal velocity shear normal to the front, in view of (3) and Table 2, has a maximum in the region of large negative wind stress curl and large positive shear deformation of the wind stress, which occurs near 34°N, according to Figs. 12 and 13. Thus, a tendency exists for new fronts to form north of the subtropical front. The 34°N salinity front described earlier is an example of this.

b. Short-term mean fields

It was shown above that over long time periods an agreement exists between the observed location of the subtropical frontal zone and the Ekman confluence zone. The question arises whether such a relationship is found also on shorter time scales. The variability of the Ekman confluence zone on weekly time scales is shown in Fig. 15. The zone indicated by the dashed lines refers to the 30-year January mean discussed earlier. The zone between solid lines is for weekly means between 14 January and 10 February 1974. This time period was chosen because it coincided with the field investigations carried out on the R.V. *Thomas G. Thompson*. It is seen that in the region north of Hawaii, of interest here, the weekly position of the subtropical confluence zone varied from its mean position by about 2–4° of latitude between 21 January and 10 February. In the preceding week, however, the confluence zone was about 12° latitude south of the mean position, due to a persistent, well-developed low pressure between latitudes 35 and 40°N (National Weather Service, 1974). Does this mean that the subtropical frontal zone was displaced also 12° of latitude to the south? Obviously not, because this would imply unrealistic speeds of frontal displacement. It is more rational to assume that a new frontal zone involving different water particles was created by the southward displacement of the Ekman confluence zone. *A clear distinction must be made, therefore, between the motion of Ekman confluence zones and the motion of frontal zones on time scales of a week or shorter.* In particular, *fast moving* atmospheric disturbances with favorable wind shear zones can be expected to create *new* fronts along

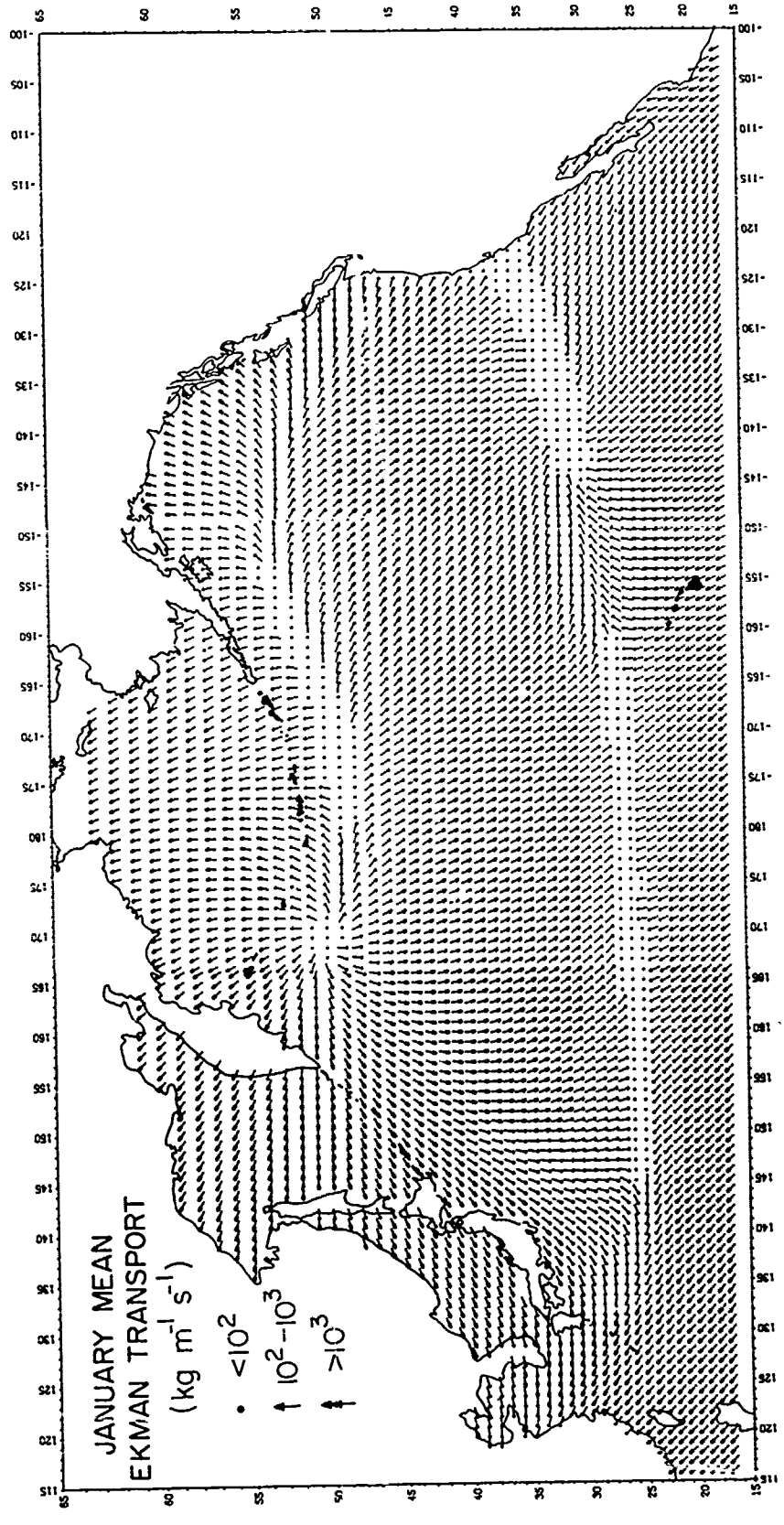

FIG. 12. Long-term mean (1931–60) Ekman transport in January. Based on the stress of the quasi-geostrophic wind evaluated on a 1° latitude-longitude grid. Note the confluence zone of Ekman transports in the subtropics.

their paths, rather than move a given front far from its original position.

6. Some aspects of subtropical frontogenesis in the lower layer

At depths, where the vertical thermohaline stratification is well developed, frontogenesis is strongly influenced by differential vertical advection, which depends on the horizontal gradients of the vertical velocity (Palmén and Newton, 1969). To estimate the significance of this process, we form the ratio of a typical horizontal advective term to a typical vertical advective term

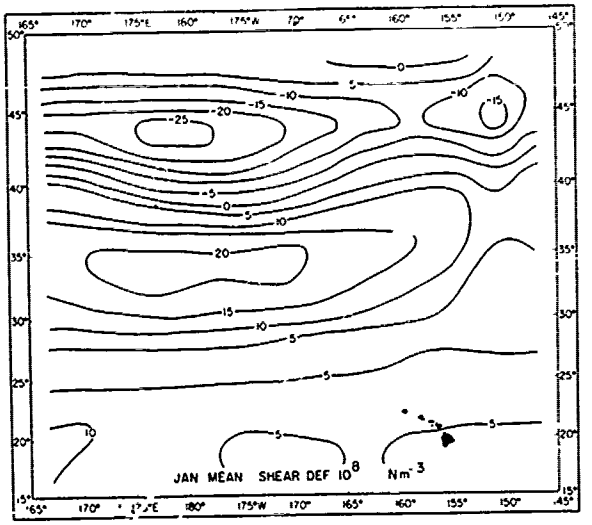

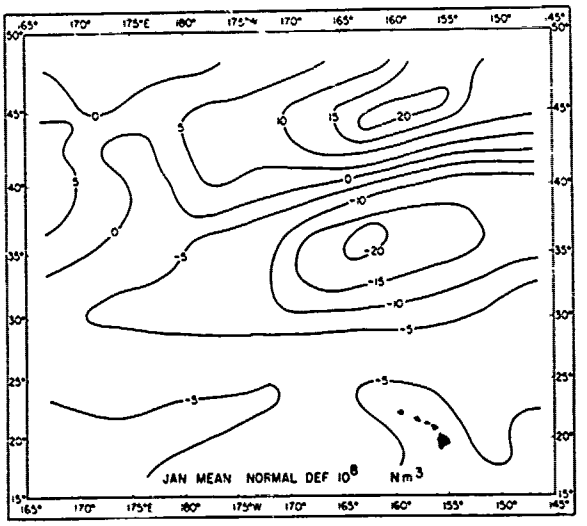

FIG. 13. Long-term mean (1931–60) fields of shear deformation (top) and normal deformation (bottom) of the wind stress. Based on the quasi-geostrophic wind evaluated on a 1° latitude-longitude grid.

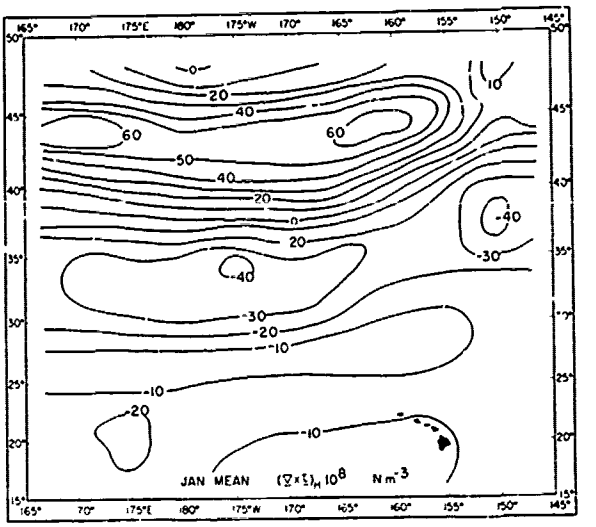

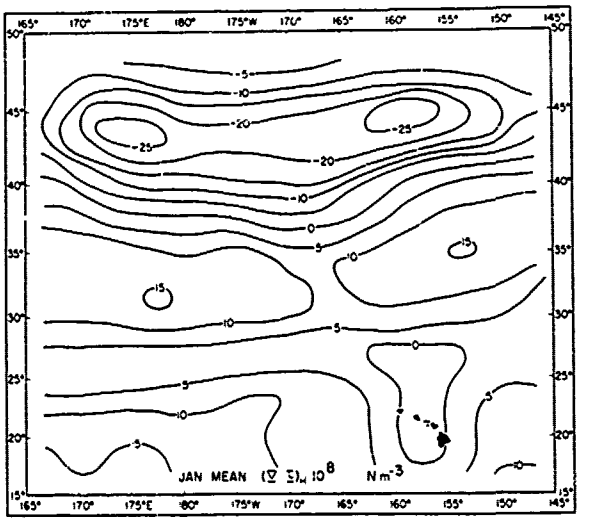

FIG. 14. Long-term mean (1931–60) fields of vorticity (top) and divergence (bottom) of the wind stress. Based on the quasi-geostrophic wind evaluated on a 1° latitude-longitude grid.

$$\gamma = \left(\frac{\partial v_n}{\partial n}\,|\nabla_H S|\right)\Big/\left(\frac{\partial w}{\partial n}\,\frac{\partial s}{\partial z}\right), \qquad (5)$$

where n is the direction normal to the front. Taking for the horizontal velocity shear 10^{-7} s^{-1}, for the vertical velocity shear 10^{-10} s^{-1}, for the magnitude of the horizontal salinity gradient 10^{-6} ‰ m^{-1} and for the vertical salinity gradient 10^{-2} ‰ m^{-1} (values applicable to the 100–150 m depth interval in the subtropical region), one finds $\gamma = 0.1$. Thus, differential vertical advection dominates.

To a first approximation, the vertical velocity can be expressed as

$$(\rho w)_{-D} = |\nabla_H \times \tau_H f^{-1}| - \beta f^{-1} \int_{-D}^{0} \rho v_g dz, \qquad (6)$$

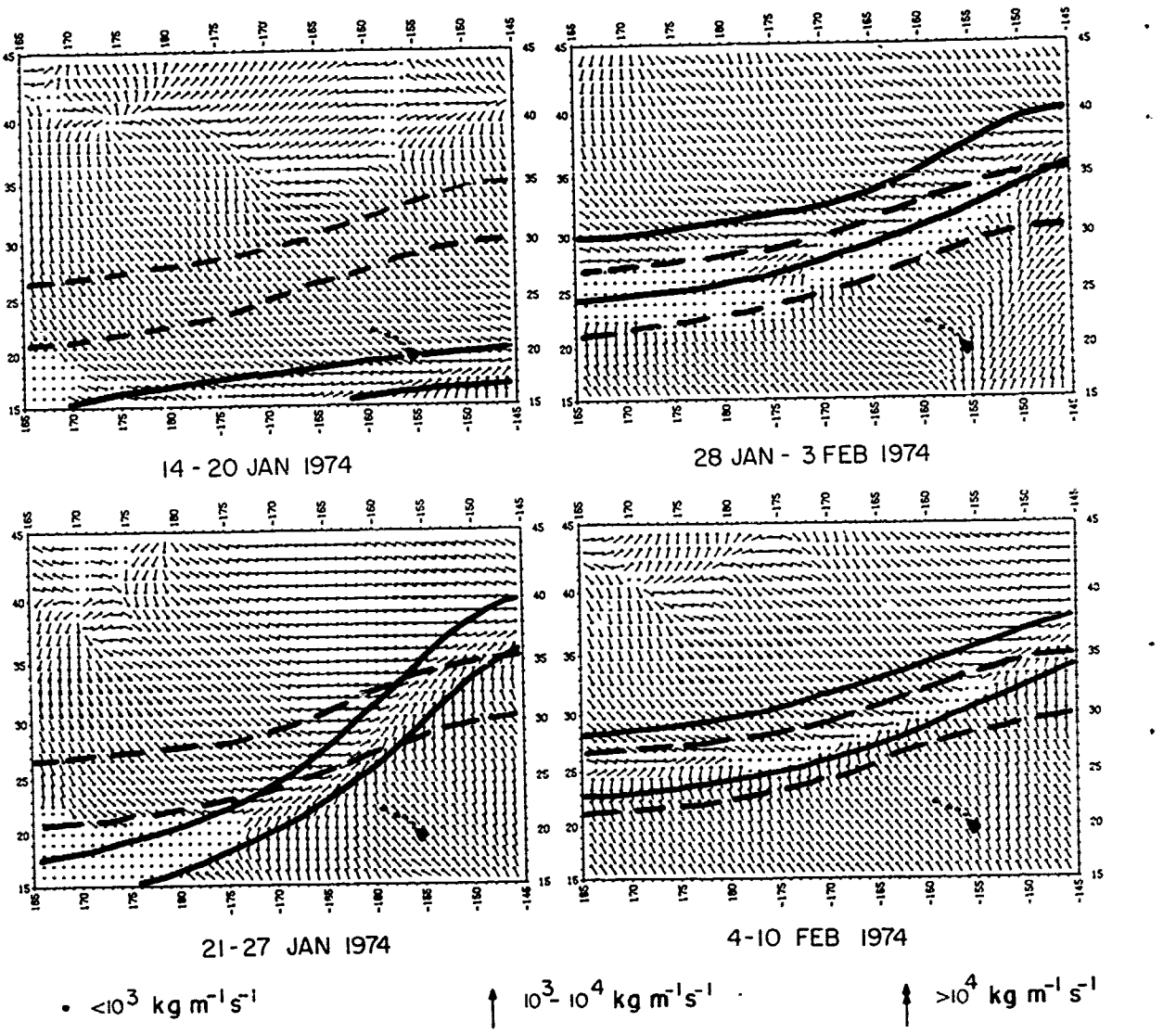

FIG. 15. Weekly mean Ekman transports during the winter of 1974. Based on the stress of the quasi-geostrophic wind evaluated on a 1° latitude-longitude grid. The zone enclosed by the dashed lines indicates the long-term mean position of the subtropical confluence zone. The zone enclosed by the solid lines shows the position of the confluence zone during the winter of 1974.

where w_{-D} is the vertical velocity at depth D, v_g the northward component of geostrophic flow and the remaining notations are as before. In the subtropical frontal zone, the curl of the wind stress is negative (Fig. 14) while the geostrophic flow has a slight southward component (Wyrtki, 1974). The former favors downwelling and the latter upwelling so that the two terms in (8) have a tendency to counteract each other. The wind stress term, however, is 5–10 times larger than the geostrophic term in regions where $v_g \leqslant 5$ cm s^{-1} and $D \leqslant 150$ m and hence the two terms normally do not cancel one another.

Frontogenesis due to differential vertical advection can be expressed by (Roden, 1977a) as

$$\frac{\partial}{\partial \tau}\left|\nabla_H S\right| = -\frac{\partial}{\partial n}\left(w\frac{\partial S}{\partial Z}\right) = -\frac{\partial w}{\partial n}\frac{\partial S}{\partial Z} - w\frac{\partial}{\partial n}\left(\frac{\partial S}{\partial Z}\right). \quad (7)$$

In the subtropical North Pacific, where the upper layer is saltier than the one below and where the halocline becomes more pronounced as one proceeds southward, both $\partial S/\partial Z$ and $\partial/\partial n(\partial S/\partial Z)$ are positive. Salinity frontogenesis can then be expected to occur where $w < 0$ and $\partial w/\partial n < 0$.

The vertical velocity distribution is shown in Fig. 16. The figure is based on the curl of the wind stress obtained from atmospheric pressure maps and aver-

aged over the period 13 January–10 February 1974. Dots indicate the cruise track of the R.V. *Thomas G. Thompson* during the same period. Areas of strong downwelling are shaded. Vertical velocities are downward south of latitude 32°N and predominantly upward north of this latitude. Two downwelling centers, at 29°30'N, 159°W and 29°N, 153°W and two upwelling centers, at 35°N, 159°W and 34°N, 152°30'W stand out. Maximum downward velocities are 10^{-3} cm s^{-1} and maximum upward velocities are 8×10^{-4} cm s^{-1}. The configuration of the vertical velocity field is favorable for salinity frontogenesis near 31°N, where the normal derivative of the vertical velocity is large and near 29°N, where the vertical velocity reaches a negative extreme. A comparison with the 150 m salinity distribution in Fig. 5 indicates the presence of increased horizontal salinity gradients and fronts near these latitudes, as expected from the vertical velocity field.

Not all prominent features in the vertical velocity field have a counterpart in the salinity distribution at 150 m, however. The large horizontal gradients of the vertical velocity associated with the upwelling center at 35°N, 159°W do not lead to significant differential vertical advection of salinity, because the vertical salinity gradients at 150 m are very small north of 32°N (Fig. 7). Consequently, frontogenesis in the salinity field cannot occur there, despite the presence of a favorable vertical velocity field.

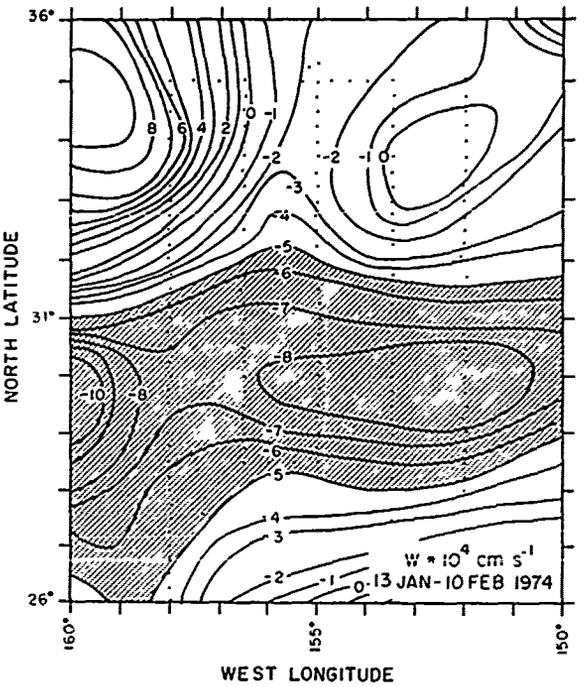

FIG. 16. Vertical velocity in the subtropical frontal zone during the winter of 1974. Based on the curl of the wind stress evaluated on a 1° latitude-longitude grid. Dots indicate station positions. Shading indicates strong downwelling.

7. Surface flux differences across the subtropical frontal zone

Subtropical frontogenesis depends on differential momentum, heat, salt and mass fluxes through the sea-air interface. It is of importance, therefore, to compare the different fluxes on either side of the subtropical frontal zone. This is shown in Table 3, which is based on information contained in the *Marine Climatological Atlas* (U.S. Navy, 1977). All the fluxes are positive upward and have been computed by the bulk parameters and equations given by Friehe and Schmitt (1976) and Roden (1977a).

Scalar wind speeds north and south of the frontal zone are of comparable order of magnitude, with differences seldom exceeding 2 m s^{-1}. Vector wind speeds across the frontal zone vary widely. The differences are most pronounced in summer, when vector wind velocities in the south are four times larger than those in the north. This is reflected also in the wind persistence factor, defined by $\gamma = |\langle \mathbf{v} \rangle| / \langle |\mathbf{v}| \rangle$. It should be noted that the *true* magnitude of the momentum flux (Pond, 1975),

$$|\boldsymbol{\tau}| = \kappa \rho_a |\langle \mathbf{v}|\mathbf{v}| \rangle| \geq \kappa \rho_a \langle |\mathbf{v}| \rangle^2 \geq \kappa \rho_a |\langle \mathbf{v} \rangle| \langle |\mathbf{v}| \rangle, \quad (8)$$

where ρ_a is density of air and κ the drag coefficient, cannot be evaluated from the scalar and vector wind velocities given in the table, because the average $\langle \mathbf{v}|\mathbf{v}| \rangle$ is not known. What is listed in the table, therefore, is a *lower limit* for the magnitude of the momentum flux, based on the middle inequality. For a wind persistence factor of unity, the difference between the true magnitude and the lower limit is proportional to the wind variance $\langle |\mathbf{v}|^2 \rangle - \langle |\mathbf{v}| \rangle^2$. Momentum flux differences across the frontal zone change sign with season. In winter, the stronger momentum fluxes occur in the north, in summer they are found in the south. This agrees with the geographical and seasonal change of the mixed layer depths across the frontal zone (Bathen, 1972).

Radiative heat flux differences across the subtropical frontal zone are large in winter and small in summer. Evaporative heat flux differences vary in the opposite sense. The resulting differences in net heat flux are such that there is a reversal in sign of the meridional heat flux gradient. In winter, this gradient points in the same direction as the meridional temperature gradient, enhancing the formation of a subtropical temperature front. In summer, the meridional heat flux gradient points in a direction opposite of the meridional temperature gradient, leading to a dissolution of the subtropical temperature front. The seasonal variation of the subtropical

TABLE 3. Sea-air energy fluxes across the sea surface north and south of the subtropical frontal zone. $\langle \mathbf{v} \rangle$ is the vector wind velocity, $\langle |\mathbf{v}| \rangle$ the scalar wind speed, γ the wind persistence factor, $|\tau|$ the magnitude of the wind stress, Q_r the radiative heat flux, Q_e the evaporative heat flux, Q_{net} the net heat flux, S the salt flux and M the mass flux. The indices 1 and 2 denote the fluxes with and without precipitation, respectively. All fluxes are positive upward.

	North of the frontal zone (35°N, 156°W)				South of the frontal zone (25°N, 150°W)			
	Jan–Mar	Apr–Jun	Jul–Sep	Oct–Dec	Jan–Mar	Apr–Jun	Jul–Sep	Oct–Dec
				Wind ($m\ s^{-1}$)				
$\langle \mathbf{v} \rangle$	2.10	1.23	1.55	2.18	3.45	5.67	6.25	4.56
$\langle \lvert\mathbf{v}\rvert \rangle$	8.83	6.50	5.41	8.60	7.55	7.06	6.83	6.91
γ	0.24	0.19	0.29	0.25	0.46	0.82	0.92	0.66
				Momentum flux ($N\ m^{-2}$)				
$\lvert\tau\rvert$	0.14	0.08	0.05	0.13	0.10	0.09	0.09	0.09
				Heat flux ($W\ m^{-2}$)				
Q_r	−32	−100	−131	−23	−91	−159	−161	−88
Q_e	72	54	72	96	111	112	129	129
Q_{net}	40	−46	−59	73	20	−47	−32	41
				Salt flux ($10^7\ kg\ m^{-2}\ s^{-1}$)				
S_1	9	6	−3	2	−7	−10	−13	−11
S_2	−11	−8	−12	−15	−18	−19	−21	−21
				Mass flux ($10^7\ kg\ m^{-2}\ s^{-1}$)				
M_1	13	28	27	36	−15	16	6	−29
M_2	−29	17	14	−48	−23	10	3	−27

temperature front is clearly seen in satellite-derived sea surface temperature maps (National Environmental Satellite Service, 1977–79).

The salt flux is shown for two cases: with consideration of precipitation and without precipitation. This was done, because available information on precipitation is quite crude and it is of interest to know how much the results are influenced by taking precipitation into account. With precipitation, the salt flux north of the subtropical frontal zone is downward only during late summer, as opposed to a year-round downward salt flux without precipitation. South of the subtropical frontal zone the salt flux is downward in both cases. The meridional salt flux gradient is fairly constant throughout the year, which contributes toward the persistence of the subtropical salinity front.

The turbulent mass flux (Kamenkovich and Monin, 1978; Dorrestein, 1979) is also given for the cases with and without precipitation. A negative sign indicates a downward flux, which can be interpreted as turbulent convection. It is seen that convection motion dominates during the colder part of the year both north and south of the front. With no precipitation, the convection lasts slightly longer than with precipitation. The meridional gradients of the turbulent mass flux are small. With no precipitation, the winter convective motion is slightly more intense north of the subtropical frontal zone than to the south of it.

8. Conclusions and discussion

The following conclusions can be drawn from an analysis of winter oceanographic and meteorological data from the region north of Hawaii:

1) The subtropical North Pacific is characterized by a broad frontal zone between latitudes 28 and 35°N in which there occur several fronts. During the winter of 1974, the most prominent of these were the 34°N front, the 31°N front and the 28°N front.

2) In the upper 100 m, the temperature and salinity fronts are largely density compensating and almost vertical. With a sampling grid of 27 km, the fronts appear ~50 km wide and have typical salinity differences of 0.4‰ across. The temperature difference across rarely exceeds 2°C and is larger in winter than in summer. Sound velocity differences across the front reach up to 12 m s^{-1} during winter.

3) Hydrostatic stabilities in the subtropical frontal zone are generally low, because of opposing vertical temperature and salinity gradients. In winter, a thin layer of increased stability (Väisälä frequency $N = 0.01\ s^{-1}$) is found between ~100 and 125 m.

4) Below the thin layer of high stability, there are prominent lateral intrusions of cool and low-salinity

subsurface water under warmer and higher salinity surface water, to the north of the subtropical front at 31°N.

5) Between 200 and 500 m, temperatures and salinities in the subtropical frontal zone decrease rather uniformly with depth. A deep salinity minimum is found near 550 m and a deep sound velocity minimum occurs near 750 m. Numerous oscillations are superimposed on the thermocline and halocline, some of which have steep frontlike features.

6) The 0/1500 db dynamic height topography bears no similarity with the configurations of the surface temperature and salinity fields, indicating that the *surface* thermohaline fronts are not determined by the baroclinic flow field.

7) The 150/1500 db dynamic height topography shows a close association with the configurations of the temperature and salinity fields at 150 m, indicating that *subsurface* thermohaline fronts below the upper mixed layer are related by the baroclinic flow field.

8) The *mean* baroclinic surface flow in the subtropical region north of Hawaii is 2–4 cm s^{-1} and to the eastward and does not depend upon season. *Perturbations* from the mean flow reach up to 50 cm s^{-1} and depend upon season, indicating possible atmospheric forcing of the perturbations.

9) On long-term time averages, the location of the subtropical frontal zone agrees with the zone of Ekman transport confluence, both occurring between latitudes 30 and 32°N in the central North Pacific. On short-term time averages, the agreement is less obvious. This is so because large departures of the confluence zone associated with fast-moving wind systems will tend to create new fronts rather than move existing fronts far from their mean position.

10) At depths below the mixed layer, frontogenesis is strongly influenced by differential vertical advection and agreement exists between the location of the thermohaline fronts and regions of large vertical velocity gradients produced by the geographical variation of the curl of the wind stress.

There are several outstanding questions to be solved in connection with the subtropical frontal zone and the atmospheric forcing of fronts, apart from the obvious problems of resolution. The *actual velocity field* in the frontal zone must be measured and compared to the calculated velocity field derived from geostrophic and Ekman flow. The *time variations in the intensity and position of fronts* must be studied in more detail, perhaps by utilization of remote sensing by satellites, in order to determine the response times to atmospheric forcing more accurately. The *mesoscale eddies* in the frontal zone need to be investigated further and the relation between these and the large-scale flow patterns must be considered. Finally, there is a need to determine the *geographical variation of the heat, salt and mass fluxes* more thoroughly in order to understand the frontogenesis processes better than can be done presently.

Acknowledgments. I am indebted to C. A. Barnes, L. H. Larsen, M. Rattray, P. Welander and A. D. Voorhis for advice. K. Bhatia carried out the programming and plotting. The scientific and operational crew of the R. V. *Thomas G. Thompson*, C. Clampitt commanding, are to be commended for outstanding performance. The research reported herein was supported by the Office of Naval Research under Contract N-00014-75C-0502 Project NR 083-012.

REFERENCES

Barnett, T. P., 1976: Large-scale variations of the temperature field in the North Pacific Ocean. *Naval Res. Rev.*, **19**, 36–51.

Bathen, K. H., 1972: On the seasonal changes in the depth of the mixed layer in the North Pacific Ocean. *J. Geophys. Res.*, **77**, 7138–7150.

Bowman, J. B., and A. Okubo, 1978: Cabbeling at thermohaline fronts. *J. Geophys. Res.*, **83**, 6173–6178.

Defant, A., and F. Defant, 1958: *Physikalische Dynamik der Atmosphäre*. Akademische Verlagsgesellschaft, 527 pp.

Dorrestein, R., 1979: On the vertical buoyancy flux below the sea surface induced by atmospheric factors. *J. Phys. Oceanogr.*, **9**, 229–231.

Eckart, C., 1960: *Hydrodynamics of Oceans and Atmospheres*. Pergamon Press, 290 pp.

Frankignoul, C., and P. Müller, 1979: Quasi-geostrophic response of an infinite beta-plane ocean to stochastic forcing by the atmosphere. *J. Phys. Oceanogr.*, **9**, 104–127.

Friehe, C. A., and K. F. Schmidt, 1976: Parameterization of air-sea interface fluxes of sensible heat and moisture by bulk aerodynamic formulas. *J. Phys. Oceanogr.*, **6**, 801–809.

Garrett, C., and E. Horne, 1978: Frontal circulation due to cabbeling and double diffusion. *J. Geophys. Res.*, **83**, 4651–4656.

Gregg, M. C., 1975: Microstructure and intrusions in the California current. *J. Phys. Oceanogr.*, **5**, 253–278.

Johnson, R. H., and R. A. Norris, 1968: Geographic variation of SOFAR speed axis depth in the Pacific Ocean. *J. Geophys. Res.*, **73**, 4695–4700.

Kamenkovich, V. M., and A. C. Monin, 1978: *Fizika Okeana I (Physics of the Ocean I)*. Vol. 1. Nauka, 454 pp.

Kirwan, A. D., 1975: Oceanic velocity gradients. *J. Phys. Oceanogr.*, **5**, 729–735.

Kuksa, V. I., 1977: Intermediate waters of the World Ocean. *Tr. Vsesoy. Nauchno-issled. Inst.* (VNIRO), **119**, 31–45.

Leetmaa, A., and A. D. Voorhis, 1978: Scales of motion in the subtropical convergence zone. *J. Geophys. Res.*, **83**, 4589–4592.

Leitao, C. D., N. E. Huang and C. C. Parra, 1978: Remote sensing of Gulf Stream using GEOS-3 radar altimeter. NASA Tech. Pap. 1209, 31 pp.

McGary, J. W., 1956: Mid-Pacific oceanography, middle latitude waters, Jan.–March 1954. *Spec. Sci. Rep. Fish.*, **180**, 173 pp.

McGary, J. W., and E. D. Stroup, 1958: Oceanic observations in the central North Pacific, September 1954–August 1955. *Spec. Sci. Rep. Fish.*, **252**, 250 pp.

Mooers, C. N. K., 1978: Frontal dynamics and frontogenesis. *Oceanic Fronts in Coastal Processes*, Springer Verlag, 16–22.

National Environmental Satellite Service, 1977–1979: Weekly maps of GOSSTCOMP sea surface temperature for the North Pacific Ocean. Series MN 180, Washington, DC.

National Weather Service, 1974: Daily maps of Northern Hemisphere sea level atmospheric pressure maps. Washington, DC.

Newton, C. W., 1978: Fronts and wave disturbances in the Gulf Stream and atmospheric jet stream. *J. Geophys. Res.*, **83**, 4697–4706.

Okubo, A., 1978: Advection-diffusion in the presence of surface convergence. *Oceanic Fronts in Coastal Processes*, Springer Verlag, 23–28.

Palmén and Newton, 1969: *Atmospheric Circulation Systems*. Academic Press, 602 pp.

Philander, S. G., 1978: Forced oceanic waves. *Rev. Geophys. Space Phys.*, **16**, 15–43.

Pond, S., 1975: The exchanges of momentum, heat and moisture at the ocean-atmosphere interface. *Numerical Models of Ocean Circulation*. Nat. Acad. Sci., 26–38.

Rattray, M., and J. G. Dworski, 1978: The effect of bathymetry on the steady baroclinic ocean circulation. *Dyn. Atmos. Ocean.*, **2**, 321–339.

Reid, J. L., 1965: *Intermediate Waters of the Pacific Ocean*. Johns Hopkins Press, 85 pp.

Reid, J. L., and R. S. Arthur, 1975: Interpretation of maps of geopotential anomaly for the deep Pacific Ocean. *J. Mar. Res.*, **33**(Suppl), 37–52.

Roden, G. I., 1975: On North Pacific temperature, salinity, sound velocity, and density fronts and their relation to the wind and energy flux fields. *J. Phys. Oceanogr.*, **5**, 557–571.

——, 1977a: On subarctic fronts of the central Pacific: structure and response to atmospheric forcing. *J. Phys. Oceanogr.*, **7**, 761–778.

——, 1977b: On long-wave disturbances of dynamic height in the North Pacific. *J. Phys. Oceanogr.*, **7**, 41–49.

——, 1979: On the depth variability of meridional gradients of temperature salinity and sound velocity in the western North Pacific. *J. Phys. Oceanogr.*, **9**, 756–767.

——, and J. D. Irish, 1975: Electronic digitization and sensor response effects on salinity computations from CTD field measurements. *J. Phys. Oceanogr.*, **5**, 195–199.

——, and D. F. Paskausky, 1978: Estimation of rates of frontogenesis and frontolysis in the North Pacific Ocean using satellite and surface meteorological data from January 1977. *J. Geophys. Res.*, **83**, 4545–4550.

Seckel, G. R., 1968: A time sequence oceanographic investigation in the North Pacific tradewind zone. *Trans. Amer. Geophys. Union*, **49**, 377–387.

Sverdrup, H. U., M. W. Johnson and R. H. Fleming, 1942: *The Oceans*. Prentice Hall, 1087 pp.

Tolstoy, I., and C. S. Clay, 1966: *Ocean Acoustics*. McGraw-Hill, 293 pp.

Turner, J. S., 1973: *Buoyancy Effects in Fluids*. Cambridge University Press, 367 pp.

Uda, M., 1938: Researches on "siome" or current rip in the seas and oceans. *Geophys. Mag.*, **11**, 307–372.

U.S. Navy, 1977: *Marine Climatological Atlas of the World*, Vol. 2, *North Pacific Ocean*. Govt. Printing Office, 388 pp.

Väisälä, V., 1925: Uber die Wirkung der Windschwankungen auf die Pilotbeobachtungen. *Soc. Sci. Fenn. Comment. Phys. Math.*, **II-19**, 37.

Voorhis, A. D., E. H. Schroeder and A. Leetmaa, 1976: The influence of deep mesoscale eddies on sea surface temperature in the North Atlantic subtropical convergence. *J. Phys. Oceanogr.*, **6**, 953–961.

White, W. B., K. Hasunuma and H. Solomon, 1978: Large-scale seasonal and secular variability of the subtropical front in the western North Pacific from 1954 to 1974. *J. Geophys. Res.*, **83**, 4531–4544.

Wyrtki, K., 1974: The dynamic topography of the Pacific Ocean and its fluctuations. Rep. HIG-74-5, Hawaii Institute of Geophysics [contains bimonthly maps of dynamic height and standard deviations].

——, 1975: Fluctuations of dynamic topography in the Pacific Ocean. *J. Phys. Oceanogr.*, **5**, 450–459.

Upper Ocean Workshop

Timberline Lodge, Oregon – 3-5 March 1980

Summary Report

APL-UW TN 3-80
April 10, 1980

Prepared by:
Michael C. Gregg
Applied Physics Laboratory - University of Washington - Seattle, Washington 98105

CONTENTS

SUMMARY

Approximately 30 academic physical oceanographers interested in observational programs in the upper ocean met for informal discussions from 3-5 March 1980 at Timberline Lodge, Oregon. The emphasis was on ideas for future research, including that work concerned with the direct response of the upper ocean to atmospheric forcing. Since most of the investigators who took part in MILE and JASIN are now planning further observations in the upper ocean, the meeting began with short presentations in which the participants outlined their new projects. Following this there were discussions of some major questions concerning the upper ocean; these were pursued in smaller groups as well as by the full workshop. Finally, the proposed observational programs were considered again since many of the participants recognized opportunities for cooperation. This summary report has been prepared as a reminder for the participants and to provide a synopsis for others interested in upper ocean work.

The most significant conclusion to emerge from the meeting was that observational capabilities in the upper ocean are improving rapidly. New instruments made possible the MILE and JASIN programs, and now a second generation is being developed, including some for the purpose of upper ocean work during storms. Important discoveries have resulted almost every time new instruments have been used, and more can be expected. Since most of the investigators using these tools are studying particular processes, e.g., internal waves, intrusions, or small-scale mixing, their observational approach is to do joint programs to obtain those complementary measurements that are most directly necessary to understand the processes of interest. Until these immediate linkages are understood, the benefit to be gained from additional even larger programs is secondary. As an example, microstructure work has reached the point where the dissipative quantities χ and ε must be related to the local shear. Until this is done the relationship of the mixing events to mesoscale eddies or direct wind forcing is secondary; restricting the observations to only those large-scale experiments that can define the eddy field will not yield progress consistent with the effort involved.

The programs presented by the participants extend until 1984 in some cases. Much of the work is exploratory, reflecting the fact that our knowledge is severely restricted by the lack of any observations that define whether particular processes are important in even one situation. The diversity of the programs indicates that the question of which processes are important is a statistical problem and must be addressed at many times and places. Several of the efforts are of the same scope as MILE.* Compared with the effort in the upper ocean five years ago, this represents a large increase in the total effort and in the cooperation between individual research programs.

In short, rapid progress is being made in our understanding of the upper ocean and, although continued and even enhanced communication and cooperation will be beneficial, a significantly different way of working together, or a major new community-wide experiment is not warranted at this time.

In the following, the summaries of the presentations and discussions are grouped into scientific questions, instrumentation, and observational programs.

GENERAL SCIENTIFIC QUESTIONS

1. It was generally agreed that we still have much to learn about the mechanisms by which momentum, heat and chemical constituents are transferred at the sea surface and within the mixed layer.

   Very near the surface, which itself is poorly defined, we need to improve our understanding of how surface waves effect momentum exchange and how much of the Ekman transport may be carried by them. The presence of bubbles and spray may significantly affect transport of scalar properties but we do not yet know how to observe this.

*The Mixed Layer Experiment (MILE), which took place in August-September 1977, involved 14 principal scientists from 6 institutions, and some $1.5 million in funding, including analysis. It was conceived in 1975, and the major scientific papers began to appear in 1979.

Within the mixed layer we are still ignorant of the dominant sources of energy for mixing and of the structure of the turbulence. In generating turbulence, what is the relative importance of wave breaking and production by shear near the surface, in the interior of the layer, and at the base of the mixed layer? If waves are dominant, one would hope to observe microstructure and turbulence modulation related to breaking events. If surface shear is dominant, a dependence of turbulence on wind stress but little wave breaking modulation is expected. If shear at the mixed layer base is critical, then turbulence would be modulated by the shear at the bottom of the mixed layer that is more closely related to the relative phases of inertial motions above and below the mixed layer base than to wind stress. If turbulence production within the layer is important, a dependence of microstructure on internal shear and the Monin-Obuhkov length is expected. Observations that give evidence of several of these sources have been reported; however, there is insufficient evidence to determine under what situations different sources are dominant.

The need for vertical profiles of temperature and velocity microstructure as indicators of the location of turbulent energy sources in the column is great. Few measurements of this type have been made within 10 m of the surface during even moderate winds because present instruments behave poorly under such conditions, particularly during launch. The need for two- and three-dimensional cuts through the mixed layer on various scales was also emphasized. These are essential to define any large scale structures (Langmuir cells, convection plumes, shear instability billows, etc.) important in the mixing process, and to define the lateral intrusive processes that are observed when horizontal inhomogeneities relax. Similarly the "roughness" of the base of the mixed layer is believed to be important in generation of internal waves, and the structure of the near surface "micro-bubble cloud" discloses features of the turbulence near the surface. As an example of this strategy, Thorpe has monitored the bubble cloud in Loch Ness using

an acoustic sounder and found that (a) the bubble cloud depth varied almost linearly with wind speed, showing dependence of the turbulence on wave-breaking or near-surface shear, (b) bubble cloud depth did not respond to Langmuir cell slicks, suggesting that the cells are restricted to only a few meters depth or are very weak, and (c) distinct forms of roughness in the cloud's roughness corresponded to periods of convection, wave breaking and large shear.

2. Several points of particular concern for models of mixed layers were discussed. The goal was to pose observational questions that would test major assumptions of different models. In large measure the subjects of concern to modelers parallel the interest of the observationalists

A. Is the deepening of mixed layers controlled by a critical Richardson number across the interface at the bottom? (This is a key assumption in Mellor's model.) Or, is the deepening related more closely to the wind stress, as supposed in models of the Kraus-Turner sort?

B. How should the flux from the seasonal thermocline into a stationary mixed layer be parameterized? By gradient diffusion?

C. How should the energy-containing turbulent components be parameterized? Some models use an integral length scale to describe the energy-containing motions, and this in turn forms the basis for parameterizing ε, the rate of dissipation of turbulent kinetic energy. Large-scale models assume that the integral scale depends upon latitude. Some of the observationalists felt that the dependence of models on an unknown integral scale was more a modeling convenience than something that could be related to measurements.

D. How does kinetic energy leave the mixed layer? Can the rate of decay of inertial energy in the mixed layer be reconciled with the downward flux of near-inertial energy in the

thermocline? Or is it possible that the energy leaks out as high frequency internal waves generated by mixed layer turbulence?

E. Are there significant [illegible] and three-dimensional phenomena in the mixed layer? If [illegible]t are they and how may their effects be parameterized?

F. Do frontal dynamics (e.g., convergence zones and jets) strongly alter mixed layer dynamics?

3. What is the importance of flows below the surface mixed layer? Two aspects of such flows were considered. The first concerned the role of Ekman divergence (convergence) on mixed layer dynamics. This has been incorporated into models, but never observed. If it is important, what are the time and length scales? Closely coupled to this is the general role of bulk Ekman dynamics. Over what space and time scales is it relevant? The second aspect of deeper flows was the role of intrusions, which have been observed directly at the base of the mixed layer as well as throughout the upper ocean. Are they major factors in the response of the ocean to atmospheric forcing, or are they more occasional happenings?

4. Motions of tidal and near-inertial frequency dominate the spectra of moored time series. What are the mechanisms for generating these motions and what are their spatial scales? The near-inertial motions are believed to have scales on the order of 100 km or more in the mixed layer, which are established by atmospheric forcing. (This is not well established, however.) The scales observed below the mixed layer are more on the order of 10 km. Why the difference? Do the shorter scales "leak out" more effectively? How do the leakage rates depend upon the depth of the mixed layer and on its three-dimensional structure? Briscoe pointed out that strong harmonics and mixing of the tidal and inertial signals are found in records from the upper ocean but not in those from several

kilometers deep. Are the harmonics smeared by nonlinear interactions?

5. Although not restricted to the upper ocean and atmospheric forcing, there was considerable interest in improving our understanding of the nature of small-scale vertical mixing in the seasonal and main thermocline. Measurements of temperature microstructure indicate that the gradient heat flux is quite low in the main thermocline but can be large in the seasonal thermocline beneath strong storms. These measurements are a very limited sample in space and time. Much more information needs to be obtained about the seasonal and geographical variability. It is also important to determine how χ and ε are related to the variability in the shear field. What effect do the dissipative events have on the internal wave spectrum? Are critical layers as important in the ocean as in the atmosphere? Or is most of the energy lost from the internal wave field in bottom and side wall boundary layers?

6. The transition from the mixing layer to the upper thermocline is a region of strong shear and intense gravity wave activity which continues into the thermocline. Many questions remain unanswered about the interaction of internal waves in shear flows. Is the internal wave directional spectrum affected by propagation of waves in a shear? How does this process affect wave-wave scattering, mixing and Reynold's stresses? How does the critical layer phenomenon actually operate in the presence of large amplitude waves with a continuous spectrum? A large part of the short-scale vertical shear is associated with quasi-inertial oscillations. How do high frequency internal waves interact with these time-dependent shears? Is there evidence for mixing events and transfer of momentum associated with critical layers?

INSTRUMENTAL DEVELOPMENTS

The capability of making observations of structures and motions in the upper ocean has increased greatly in recent years and was the basis for the MILE and JASIN programs. (The vector-measuring current meters developed by Weller and Davis may be available commercially by late 1980.) The next steps are the development of long-term upper ocean moorings (Halpern and Briscoe are both working on these), and the further development and refinement of towed and profiling instruments that can work efficiently in heavy sea states.

During the past year Sanford and Drever completed development of an expendable velocity profiler (XTVP) that produces data of quality comparable to their large EMVP. Osborn and Lueck are working on an expendable ε profiler using the shear foil probes that were successful on CAMEL. Miyake has been testing XCTD probes that are being produced commercially. Caldwell and Dillon at OSU and Oakey at Bedford have developed lightweight tethered profilers for microstructure in the upper ocean. A refinement of the OSU probe can be dropped and retrieved from a ship underway at 6-7 knots. Gregg and Lahore are developing an automatic profiler for temperature and velocity microstructure and density finestructure that can be deployed under strong storm conditions. In an effort to measure ε directly to the surface, Osborn's new internally-recording instrument will record data during its ascent.

Two other profiling systems are being developed which are probably not suitable for strong wind forcing but will work in the upper ocean under moderate conditions. Cox is completing a drifting yo-yo electromagnetic velocity profiler, which he calls the Cartesian Diver. It will have its first trial next autumn. It has a maximum depth of 1 km and will usually be operated between the surface and several hundred meters. The vertical water velocity will be determined by recording the rotation induced by paddles on the case as the vehicle rises (similar to the approach of Voorhis). Sanford and Gregg are developing a multiscale profiler (MSP) that combines the electromagnetic velocity data with an acoustic current meter and temperature, salinity and velocity microstructure information. The instrument will operate in the upper 1 to 1.5 km and can be used in moderately heavy sea states.

The ability to do horizontal measurements is also increasing. Paulson's towed thermistor chain was used to depths of 90 m during the FRONTS cruise. He plans to add conductivity cells and possibly other sensors. Gregg is studying the dynamic response of temperature and conductivity probes in an effort to improve the horizontal mapping of temperature and salinity with the APL-UW depth-cyling towed body. He also intends to add an O_2 sensor.

Osborn and Gargett are developing turbulence instrumentation for use on the USS Dolphin. The measurements include velocity, salinity, temperature and acceleration. They anticipate that observations can be made close to the surface and that the ship can be a component of future mixed layer programs.

Pinkel's development of remote probing of the near-surface velocity field from FLIP is being extended so that he can search for patterns in mixed layers. Using one sonar beam, the velocity can be sensed to a precision of ~1 $cm \cdot s^{-1}$ after 30 seconds averaging.

McWilliams and Niiler are designing six surface drifters for deployment during STREX in October 1980. A 120 m-long cable with 10 thermistors and 3 pressure sensors will be suspended below the floats, which will house atmospheric pressure and oceanic near-surface temperature. The data will be transmitted via satellite, providing 3 hour means and variances.

OBSERVATIONAL PROGRAMS

The observationalists discussed their plans for future work, which in some cases was foreseen to about 1984. Many of the plans involved cooperative endeavors of varying size; in some cases other participants indicated a desire to join the work. The following summaries describe the joint programs and do not include the solo investigations that were discussed. These projects are either funded, proposed, or "at the tip of the pen." Two additional themes emerged--studies of near-inertial motions and of deep convective mixed layers--in which many participants expressed strong interest for future cooperation. The table at the end indicates the estimated times of the programs.

1. STREX. Atmospheric scientists are planning measurements at Station P in the autumn of 1980 to examine air-sea transfers under storm conditions. Several oceanographers would like to participate in what are basically independent measurements-of-opportunity. The McWilliams and Niiler drifters have already been mentioned. Sanford has requested funds to deploy his XTVP to determine whether there is an increase in near-inertial storms. A highly energetic structure (a peak amplitude of 0.5 $m \cdot s^{-1}$ at 200 m depth) found north of Hawaii suggests the range of intensity of these features is not known. Also, deSzoeke would like to deploy four moored thermistor chains to examine convectively-dominated mixed layers during STREX.

2. FLIP-based observations of the near-surface velocity field will be made by Pinkel and Weller in May 1980 off Southern California. The acoustic Doppler system will be used to examine near-surface internal wave propagation and the directional spectrum of the near-surface internal wave field. Current and CTD profiles will be used to form the gradient Richardson number. The effect of FLIP's drift will be monitored using LORAN-C navigation. At the end of their observations, Sanford will take several patterns of XTVP profiles for an intercomparison and to examine the structures with scales greater than the range of the acoustic beams.

3. In mid-1982 or 1983 Pinkel, Weller, and Price plan to concentrate on structures within mixed layers, including some biological measurements. Attempts will be made to study the horizontal structure of the velocity field within mixed layers, including Langmuir and convective cells. It was suggested that Thrope's use of bubbles as tracers might be fruitful. It also might be advisable to direct the beams at a sufficient angle to the vertical to obtain a Doppler component from the stronger vertical motions in any cells.

Other investigators who expressed interest were Gregg, Osborn, and Sanford, who could base their yo-yo or expendable profilers on FLIP and use the acoustic signals for background. Osborn

and Gargett were interested in possibly operating the USS Dolphin nearby. Pinkel encouraged other measurements that could examine horizontal structures around FLIP.

4. Chris Mooers stressed the need to test the various numerical models (including those that will be used for operational forecasts) of the upper ocean thermal structure against common data sets. (Atmospheric scientists have found such prediction experiments beneficial; so probably will oceanic scientists.) He envisioned a program that would include repeated AXBT patterns, as well as current and wind measurements, to obtain multiple realizations of the evolution of forced events. This prediction experiment (PREDEX) could incorporate process studies of Ekman pumping/suction and near-inertial motion radiation; i.e., a comprehensive study of the ocean's adjustment/response to atmospheric forcing by storms and larger scale, larger term forcing. This experiment could commence in one-to-three years.

5. Briscoe emphasized that the next stage in long-term studies of the upper ocean is the deployment of near-surface moorings for several seasons to obtain adequate statistics based on multiple forcing events. He has proposed that such a mooring be established at 32°N, 57°W for a period of two years, beginning in late 1981. The site was chosen to provide occasional mesoscale forcing as well as direct wind events. A need exists for some more detailed measurements near the moorings on an occasional basis; this is also an opportunity for those wishing to use the moored data as background for their observations.

6. Niiler underscored the deeper response of the ocean to divergences and convergences in the shallow atmospherically-forced flow. He is preparing a proposal to study the low-frequency circulation of the Northeast Pacific. This would involve the installation in the summer of 1981 of two densely instrumented subsurface moorings along 150°W at 29°N and 42°N. Based on

the results of the first one-year deployment, larger arrays would be installed for up to two years. Specific moorings to study the upper ocean would be added for shorter periods.

7. Gregg and Sanford expressed their intention to explore signals in microstructure and near-inertial motions under strong storms. Gregg's motivation is the observation of Cox numbers changing from 6 to 1000 and back to below 10 as a storm passed over the MILE site. Sanford stressed the structure found in January 1980, which contained about 100 times the kinetic energy of the typical near-inertial feature; he believes that the feature was generated by the strong storms that had recently passed through the site. They will try to use ships of opportunity to explore the conditions under strong forcing events.

   The above programs have their principal effort directed toward the direct response of the ocean to atmospheric forcing events. Several others are concerned with the upper ocean but have at most an indirect connection to atmospheric forcing.

8. Terry Joyce described the Warm-Core-Ring Experiment which has been proposed as a multidisciplinary program involving biologists and chemists as well as physical oceanographers. The objective is to examine contained systems having strong lateral gradients. The interaction of rings with the shelf water is also of interest. In the center of the rings, mixing processes are believed to be primarily vertical. Within the rings mixed layers are 20 to 30 m deep in summer, deepening to 350 m in winter, while in the slope water outside the rings the mixed layer depth is only 150 m. Lateral variability in these layers will be examined with CTD to-yo's. Several participants at the workshop suggested that this promises to be an opportunity to examine a unique mixed layer regime and should be viewed in the larger context of convectively-driven mixed layers; measurements should be made that can be repeated in the deep mixed layers south of the Gulf Stream.

On the edges of the rings, the many thermohaline intrusions found in the upper 300 m suggest that lateral mixing is dominant, which gives rise to the question of why the rings live so long. A series of to-yo's is planned to obtain statistics of intrusions through the boundaries.

Osborn plans to obtain ε profiles in the rings. Joyce expressed a need for temperature microstructure measurements and more detailed horizontal observations than can be obtained with to-yo's.

Leaman plans to deploy a Cyclesonde, and Gregg and Sanford said they expected the MSP to be ready for the 1983 program.

9. The Subtropical North Atlantic Gyre Experiment was described by Schott as being focused on the main thermocline near 26°N in the Western North Atlantic. The goal is to observe low-frequency variability, e.g. the changing amplitude of the Antilles Current. Moored current meters will be placed in the zone from 100 m to 1000 m, and the vertical velocity will be inferred assuming the Beta Spiral.

10. Several investigators expressed interest in further measurements in the Equatorial Undercurrent. Hayes and Halpern are now doing so as part of EPOCS. The PEQUOD program is trying to develop an upper-ocean program; as part of this, Pinkel is considering taking FLIP to the equator and letting it drift for nearly a month to examine the generation of internal waves in the strong shear zone. This would be done in either 1983 or 1984. Gregg is planning to use the microstructure yo-yo, and Osborn expressed interest in using his expendables.

11. Gregg discussed a plan to examine the transport of scalar quantities from the seasonal thermocline into the mixed layer under the trade winds. In these locations the observed microstructure levels have been far lower than would be expected from the gradient fluxes required to sustain the standing crop

observed by biologists. The yo-yo will be used to obtain an extensive set of microstructure measurements following a tagged water parcel. Davis expressed interest in releasing a cluster of floats instrumented with temperature, and possibly conductivity, sensors.

12. Following the meeting Chip Cox provided the following summary of his proposals for future observations.

A. *Experiments on measuring the spatial structure of currents (frequency < coriolis frequency)*

(1) The goals are to describe the fine scale of currents in the surface mixed layer and in the thermocline. Frontal systems at the surface and intrusions at depth are examples of structures that have smallish scales of the currents. Fronts can also exist below the surface--for example, the formation of intrusions from unique surface conditions. Some of the questions to be asked are:

(a) What are the cross-sectional scales of these flows? Do the flows form a filamentous structure? What are the meander forms? What time scales are involved?

(b) How are small-scale flows maintained? Is there interaction with internal waves that tends to accentuate or diminish small-scale structure? What are the shears (vertical, horizontal) in the flow and how do they interact with internal waves and currents?

(2) Techniques needed to attack these questions are <u>continuous</u> in nature because discrete observations with fixed current meters cannot (unless very closely spaced) avoid aliasing spatial scales. Examples of continuous shear recorders are the EMVP of Sanford, the Cartesian Diver (both vertical profilers) and the Doppler devices of Pinkel and Regier (mixed horizontal, vertical profilers). An experiment with

these devices should be accompanied by CTP observations in a close spaced network and probably with moored current meters for reference information.

B. *Stormy weather and its influence on internal motion*

(1) So far in the study of near surface properties of the ocean it has not been possible to evaluate the relative influence of storm events vs long-term less intense conditions for establishing the mean climatology of the ocean as a whole. In particular some questions which badly need answers are:

(a) How is the internal wave climate maintained? Is it supplied by energy in bursts which then supports the calm weather internal wave energy by spreading widely through the ocean? What is the energy flux into internal waves in stormy conditions? Does this locally enhance wave energy with associated dissipative events? How much wave energy can escape from the stormy region? How deeply does it penetrate into the sea?

(b) By what amount are dissipative events enhanced by enhanced internal wave and other shear flows? What is the role of inertial oscillation in these processes? How deeply does the dissipation extend? How much turbulent transport of properties is brought about by these processes? Can storm-generated events provide the "missing" eddy fluxes which have been inferred from chemical measurements of average mixing?

(2) Techniques that can be applied to these questions must be capable of operation under stormy conditions. Our experience has so far been unsuccessful (mostly) for these extremes, but efforts are under way in two directions. (a) Expendable probes launched from shipboard may be practical. (Question: how do we avoid having a connecting link to ship blown back in our faces by wind?) (b) Probes and moorings that can be launched and recovered between storms may be successful (moored C.M.'s certainly are). The Cartesian Diver is intended to work in this way.

C. The mutual influences of quasi-steady shear flows, internal waves, and turbulence need to be examined. If shear flows can produce some types of anisotropy in internal wave spectra, this should lead to rapid momentum fluxes. Strong shears may lead to critical layers from certain internal waves. If formed, these are important influences on the shear flow itself, on the internal waves and on mixing. Some questions are (a) what is the degree and type of anisotropy of internal waves in shear flows? Is there a measurable Reynold's stress? What is the interaction of high frequency internal waves with shear of strong, short vertical wavelength inertial oscillation? (b) Do critical layers develop in these or in steady shears? What is the nature of nonlinear interactions in shear flows? Does this interaction tend to reduce the importance of critical layers? What is the nature of dissipative processes in critical layers? How does the critical layers phenomenon affect the spectrum of internal waves in the neighborhood of shear flows? (c) Does shear instability develop in the absence of critical layers because of instability of intense internal waves?

These and related questions require new observations combined with the best theoretical work to guide experiments and to help explain the results. The development over the past several years of shear probes such as the EMVP and Cartesian Diver and Doppler sonar will provide some of the required tools.

D. Some other processes that interest me and are not described above are the following:

(a) What is the nature of the sharp and regular stair step profile in the vertical which only occasionally appears, but has been described several times? Sometimes, but not always, it seems to be the signature of a double diffusive process.

(b) How does the internal wave energy in the deep water manage to maintain itself almost at a constant level? What about diffusion of internal wave energy vs radiative transport? What is the degree to which the I.W. spectrum on equilibrium or quasi-equilibrium form?

Discussion was begun of two observational programs that were of interest to many people attending the workshop--Near-Inertial Motions and Deep Convective Mixed Layers. Some of the scientific questions concerning near-inertial motions have already been discussed. Further consideration is expected. Sanford suggested a special session at the Fall AGU, which Mooers agreed to organize.

Most of the attention that has been given to mixed layer experiments has been concerned with wind-forced events. Many think that convectively-dominated regimes merit investigation, especially since these are the source of most of the intermediate water. Some of the particular questions raised were: Is it possible to measure latent heat flux from a buoy? Is the dissipation really different in a convectively-dominated regime? What is a first-order description of the horizontal structure in such a regime?

Joyce and Briscoe pointed out that Worthington is planning an investigation of the Gulf Stream and the transport of the 18° water for 1982 and 1983. Observations of the deep convective mixed layers south of the Stream would complement that work. Mooers suggested the Texas shelf as an alternate site, due to the frequent, strong "northers" there and the subsequent outbreaks of cold air. Since the probability of finding a convectively-driven deepening event is low during any 3-week cruise, Briscoe offered to consider moving his proposed mooring to this site if there was sufficient interest. Further discussions are expected. There was also interest in whether any of the proposed drilling sites for the Glomar Explorer would provide a good location for extended profiling measurements.

Table I. Observation Programs for Which Dates (Firm or Tentative) Have Been Set

	1980	1981	1982	1983	1984
STREX	X				
FLIP - Seasonal Thermocline	X				
FLIP - Mixed Layer			X		
FLIP - Equatorial Undercurrent					X
Briscoe - Atlantic Moorings			—	—	
Niiler - Pacific Moorings		—	—	—	—
Warm-Core-Rings			—	—	
Subtropical N. Atlantic Gyre		—			

WORKSHOP PARTICIPANTS

U.C., San Diego

Russ Davis
Charles Cox
Rob Pinkel
Steve Thorpe - Visitor
Thomas Osborn - Visitor

Oregon State University

Peter Niiler
Clayton Paulson
Thomas Dillon
Roland deSzoeke
Murray Levine

Woods Hole Oceanographic Inst.

Melbourne Briscoe
Terrence Joyce
James Price
Robert Weller
Douglas Caldwell - Visitor
Lynne Talley - Student
Eric d'Asaro - Student

Naval Postgraduate School

Chris Mooers
Roland Garwood

NASA

Larry McGoldrick

University of Washington

Thomas Sanford
Michael Gregg

PMEL - Seattle

David Halpern
Stan Hayes

NCAR

James McWilliams

University of Miami

Fritz Schott
Kevin Leaman

Nova University

Pijush Kundu

Pat Bay Ocean. Lab.

Ann Gargett
Michael Miyake

ONR

Lou Goodman

APPENDIX

In preparation for the meeting, most of the participants prepared one page summaries of their personal research goals. Two participants elected to include their summaries here.

SOME HIGHLIGHTS OF PERSONAL INTEREST: from the modeling viewpoint

Roland William Garwood, Jr.
Department of Oceanography, Naval Postgraduate School

I. Spring Transition in the Oceanic Planetary Boundary Layer (OPBL)

Fig. 1 shows a model climatology (17-year mean) for the variance in mixed layer depth at a site in the North Pacific. The largest variance is in the late winter, and there is a very rapid reduction in the month of April. The peak value in March is associated with year-to-year variability in the time of spring transition. This result further (Elsberry and Garwood, 1978: Bull. Am. Meteorol. Soc., 59) emphasizes the importance of the March and April air-sea interaction in temperate latitudes. Future field and modeling programs should recognize the significance of this time period during which the ocean is most sensitive to variations in atmospheric forcing. In addition to the annual and longer-scale climatic implications, the spring transition has significance for the survival of fish larvae (Lasker, 1978: Rapp. P.-v. Reun. Cons. int. Explor. Mer, 173).

Fig.1 Variance in mixed layer depth

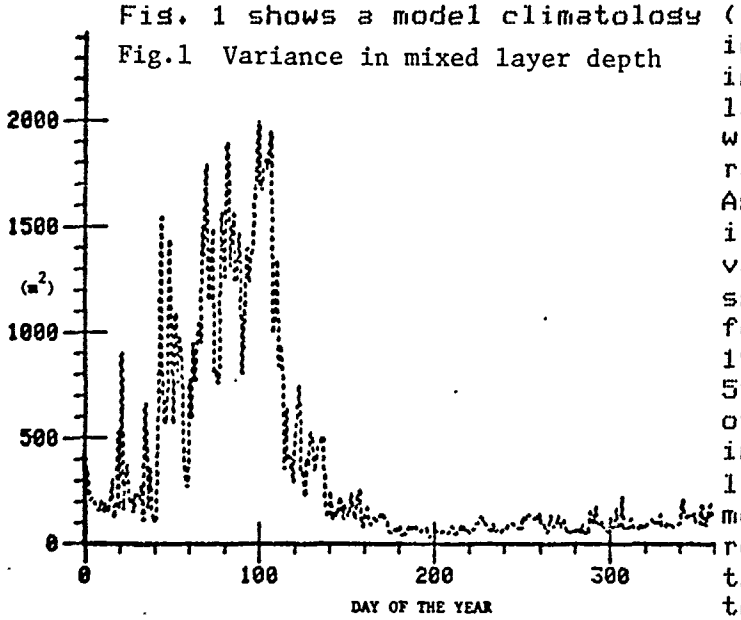

II. Surface Density Fronts

Interaction between frontal circulation and OPBL processes are being studied with the aid of a new coupled OPBL-General Circulation Model (Adamec, et al, 1980: in prep.). Initial results suggest that wind direction relative to the local frontal azimuth and stratification due to surface heating are important in determining cross-frontal mixing and upwelling and downwelling circulations at the interface between water masses. Fig. 2 shows T(x,z) sections under combinations of heating and wind direction conditions after 12 hours.

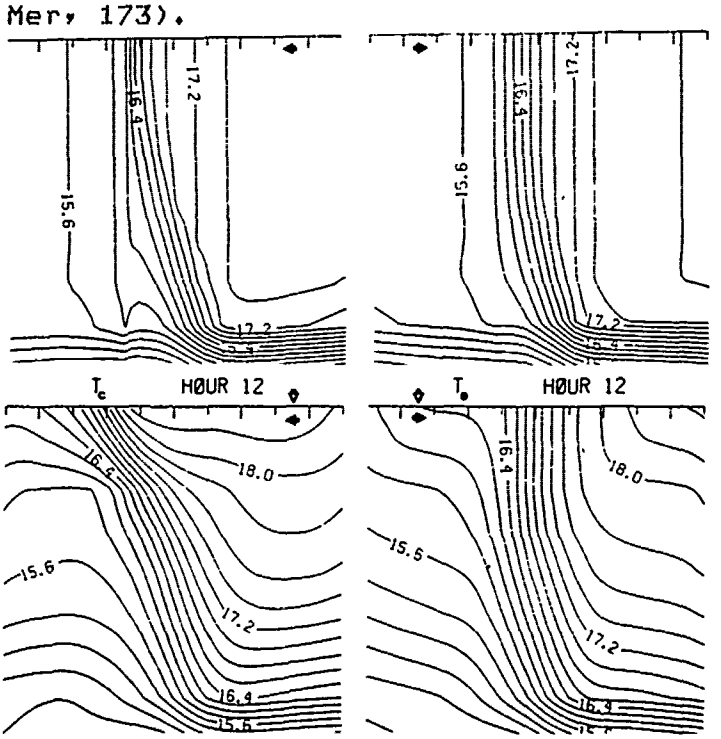

Fig. 2 Model results with identical initial conditions. Open arrows show direction of net surface heat flux, and closed arrows give direction of Ekman transport. Horizontal tick marks are at 5 KM spacing, and the vertical scale is 50 M overall.

Brief Statement of Upper Ocean Research Plans

Christopher N. K. Mooers
Department of Oceanography
Naval Postgraduate School

The general topic of interest is the prediction of upper ocean thermal structure and all that implies. The ability to make a short range (few days), limited area (10^4 km^2) forecast of the field of mixed layer depth and temperature, to some as yet undefined accuracy, in a general oceanic region would be significant. The basic questions are: "How do you do it? and "How do you know when you have done it?" Component questions of interest include:

a. How "good" do the atmospheric forcing data have to be? Some sensitivity tests would be needed.
b. How well can they be determined from satellite or other remote sensing? Is an atmospheric model needed to make a good estimate?
c. Can we use satellite or other remote sensing data, together with climatology and geostrophic and Ekman dynamics, to make an initial analysis?
d. Given the initial analysis and some estimates of boundary conditions, and forecasts of atmospheric forcing, do we have an upper ocean thermal structure forecast capability or are we limited by our ability to parameterize transfer processes, initialize, or verify?

Sometimes, it is interesting to contemplate a series of prediction experiments. You probably would like tests under storm conditions. Quickly, there would arise the question of anyone's ability to resolve spatially the atmospheric forcing induced by a storm without a storm model.

A more specific problem of strong personal, professional interest is the theory of the generation of near-inertial motions by atmospheric forcing, their propagation (especially in oceanic frontal zones), their role in mixing via the shear instabilities they may induce, and parameterization of any such turbulent mixing. Results from several studies, apparently including FRONTS, lend some vitality to this avenue of investigation.

Another topic of very strong interest to me is the interaction of the eddy stream of the California Current, irregular coastal bathymetry, and the sequence of synoptic disturbances (weather cycles) of the Northeast Pacific with the West Coast upwelling regime, which presumably leads to offshore entrainment in the upper layer of upwelled waters so provocatively and seemingly apparent in satellite IR imagery.

One can also wonder about the California Current System. For example, what-in-the-world are its three traditional seasons: upwelling, oceanic, and Davidson Current? How do the waters and flow of the California Current, Undercurrent, and Countercurrent "tie-in" with the general circulation of the North Pacific, especially considering the hints now available regarding intra-annual and interannual variability in all components of the System? Are mesoscale coastal wind systems of importance to evolving the state of the oceanic upper layer? In the coastal ocean? Elsewhere?

1 March 1980

Reprinted from JOURNAL OF PHYSICAL OCEANOGRAPHY, Vol. 10, No. 1, January 1980
American Meteorological Society
Printed in U. S. A.

Signatures of Mixing from the Bermuda Slope, the Sargasso Sea and the Gulf Stream[1]

M. C. GREGG AND T. B. SANFORD

Applied Physics Laboratory and Department of Oceanography, University of Washington, Seattle 98105

(Manuscript received 15 February 1979, in final form 20 August 1979)

ABSTRACT

Nearly simultaneous profiles of temperature microstructure and velocity shear were made adjacent to the island of Bermuda. Profiles with elevated microstructure levels were found in close association with regions of pronounced steplike finestructure, which contained nearly adiabatic regions from 2 to 10 m thick. The temperature spectra and the presence of numerous centimeter-scale temperature inversions gave evidence that active turbulent mixing was occurring in some of these regions. These were the locations in which large-scale surveys, reported by Hogg *et al.* (1978), found that eddies impinging on the island were forcing alongshore flow.

Although the mixing was intense by comparison with profiles in the thermocline, the limited geographical extent of the affected areas and the moderate levels indicate that mixing adjacent to islands is of minor importance on a global basis.

A very limited number of profiles taken in the Sargasso Sea found microstructure levels in the thermocline that were similar to previous data from the Pacific. In both sets of observations the microstructure levels are consistent with K_z levels significantly below 10^{-4} m^2 s^{-1}. Although the surface winds were very light, a 135 m deep mixed layer was turbulent. The spectral forms showed general, but not exact, agreement with the "universal" spectral forms.

The microstructure activity in the Gulf Stream was dominated by double-diffusive signatures on the upper and lower boundaries of the numerous thermohaline intrusions that were present. Thus the high shear values, 10^{-2} s^{-1}, did not inhibit the formation of double-diffusive structures. In intervals not containing inversions, the microstructure levels were little different from those in the Sargasso Sea. These levels are much lower than those found in the Equatorial Undercurrent and are not consistent with the values assumed for vertical turbulent diffusivities in models of the Stream.

1. Introduction

Inferences about the presence and intensity of small-scale turbulent mixing must be made to construct analytical and numerical models of oceanographic features. The parameterization of turbulent fluxes plays a particularly prominent role in models of mixed layers, the main thermocline, and jetlike flows such as the Equatorial Undercurrent and the Gulf Stream. In the absence of a theoretical framework for understanding mixing, particularly in stratified fluids, estimates of turbulent fluxes are obtained as the residuals required to balance fluxes from other processes, which are presumably better known.

The objective of microstructure measurements is to improve the understanding of mixing by direct observation, with an ultimate goal of measuring the fluxes. Since observational techniques are presently inadequate for direct flux measurements, more limited results must be accepted. Currently, most of the information is based on consistency tests, in which the observed microstructure levels are compared with those that would accompany the turbulent fluxes assumed by large-scale models, and pattern recognition in which small-scale mixing processes are identified by comparison with laboratory experiments.

Since fluctuations occur over a wide range of scales, it is necessary to distinguish those scales at which molecular processes are important from larger features. Because gradient structures with thicknesses <0.5 m are required to produce significant viscous or diffusive transport, that range of feature has been termed microstructure. Larger structures can also be produced when mixing occurs but, without accompanying microstructure observations, it is often difficult to distinguish this irreversible finestructure from reversible finestructure, which is formed by internal wave deformation.

In this paper we use simultaneous microstructure and finestructure observations to investigate mixing at several locations in the northwestern Atlantic Ocean. The observations were made from the R/V *Knorr* during the Fine and Microstructure Experiment (FAME), which was performed in the autumn of 1975. The primary objective was to study mixing

[1] Department of Oceanography, University of Washington Contribution No. 1049; Woods Hole Oceanographic Institution Contribution No. 4319.

0022-3670/80/010105-23$09.75

processes in the vicinity of Bermuda with moorings, CTD casts, and a variety of free-fall instruments. Observations more limited in scope were also made in the Gulf Stream and in the Sargasso Sea; while at the latter site we found a deep turbulent mixed layer, which provided an excellent opportunity to examine the characteristic signatures in the *absence* of stratification.

Using these sets of observations in consistency tests of the turbulent fluxes used in some models provides strong evidence about the correctness of the models. In addition, comparison of the levels and characteristics of the microstructure at the FAME sites, as well as with those made in the central Pacific (Gregg, 1976a, 1977b) the California Current (Gregg, 1975) and the Equatorial Undercurrent (Gregg, 1976b; Crawford and Osborn, 1979), affords considerable insight into the small-scale mixing in the northwestern Atlantic.

In view of the presently incomplete understanding of mixing, it is not possible to state the results in a brief, simple manner without first going into the details of the observations. Since these details are not of interest to many readers who, nevertheless, are concerned with the basic conclusions, we present in the next section a discussion of measurement and analysis methods that will provide sufficient background for the summary and discussion of the conclusions in the final section.

2. Background

a. Bermuda

The suggestion that the most intense small-scale mixing occurs adjacent to solid boundaries of the ocean is an old one. However, more recently specific mechanisms have been proposed for this mixing: the breaking of internal waves on slopes (Wunsch, 1969), buoyancy boundary layers (Wunsch, 1970), and turbulent boundary layers over the sea floor driven by large-scale flows due to tides or eddies (Armi, 1978). All of these mechanisms are likely near Bermuda, which is an isolated mountain with steep sides.

The observational evidence of oceanic mixing has generally consisted of steplike finestructure that was presumed to have been formed by small-scale turbulent mixing that went to completion. A particularly interesting example of the latter was the discovery of 30 to 50 m thick steps in the thermocline close to Bermuda (Wunsch, 1970, 1972). In response to these findings, theoretical arguments by Hogg (1972) showed that a steady flow incident on the island could produce large-scale, up to 500 m thick, shear instabilities on the left side (looking downstream) and in the island wake.

The results of the large-scale survey work during FAME have been reported by Hogg *et al.* (1978, henceforth referred to as HKS). Current meter records, Geomagnetic Electrokinetograph (GEK) traverses and CTD surveys showed that several mesoscale rings or eddies were impinging upon the island. The situation was thus quite different from that treated by Hogg (1972); in particular, there was no broad flow incident on the island and the velocities were generally low. Although no steplike structures were found in the CTD profiles, an increase of a factor of 10 in the temperature finestructure levels was observed as the island was approached from any direction. This increase in the finestructure was shown by plotting the variance of the temperature gradient contained between wavelengths of 25 to 5 m and between 1.0 and 0.2 m for all of the CTD casts. (Although some thermohaline intrusions were found in the CTD surveys, they were not responsible for the increase in variance levels near the island, which occurred in monotonic profiles.) In addition to the general increase, three regions of maximum variance levels were found where the low-frequency eddies forced alongshore currents. The patterns of the variance levels were very similar for both wavelengths.

Elevated finestructure levels, or even step structures, are not evidence per se that mixing, an irreversible process, is taking place. To the contrary, Garrett and Munk (1975) have assumed that all of the finestructure to scales of 2 cpm in monotonic profiles is formed reversibly by internal wave strain. In addition, the laboratory work of Baker (1971) and Calman (1977) has shown that reversible step structures can be created under high-Richardson-number conditions in a rotating salt-stratified tank; their steps were dynamical features connected with a larger flux of momentum than of salt and disappeared much more rapidly when the forcing was removed than could be accounted for by diffusion. Since Wunsch reported a Richardson number of 23 from current meters moored near the island, a question arises whether the steplike structures he observed or the elevated finestructure levels reported by HKS were formed reversibly or irreversibly.

In this paper, data obtained by simultaneous profiles of the Microstructure Recorder (MSR) and the Electromagnetic Velocity Profiler (EMVP) are used to assess the level of irreversible mixing activity near Bermuda and to investigate its relationship to the finestructure.

First, bulk averages of microstructure activity are examined and compared with the patterns in the finestructure levels found by HKS and with those in other locations. The Cox number, defined as

$$C \equiv \frac{\langle (\nabla T')^2 \rangle}{\langle \partial T/\partial Z \rangle^2}$$

is the primary statistic. The definition above uses the three components

$$(\nabla T')^2 = \left(\frac{\partial T'}{\partial X}\right)^2 + \left(\frac{\partial T'}{\partial Y}\right)^2 + \left(\frac{\partial T'}{\partial Z}\right)^2,$$

where $\nabla T' \equiv \nabla T - \langle \nabla T \rangle$ in the numerator. Although a thermistor mounted on the tip of one of the rotating wing blades on the MSR is used to measure the horizontal components of $\nabla T'$ it does not have adequate spatial resolution to obtain their variances. However, since to scales of 10 cm there is little indication of isotropy in the thermocline, we use $C \approx \langle (\partial T'/\partial Z)^2 \rangle / \langle \partial T/\partial Z \rangle^2$. The same practice was followed with the MSR data taken in the Pacific.

Second, in the regions with the largest Cox numbers some unique features in the finestructure were found. Probability distributions of the gradients, i.e., $\Delta T/\delta$, where ΔT is the temperature difference over an interval $\delta = 0.8$ m, are used to characterize this finestructure and to compare it with records from less active locations near Bermuda and with the Pacific data. These distributions were chosen as measures of the degree to which the profiles could be characterized as "well mixed." Spectral slopes in the microstructure range are used to distinguish those well-mixed regions that appeared to have turbulent stirring from those in which the turbulence had decayed.

b. The Sargasso Sea

Before the last decade the central regions of the subtropical gyres were believed to have relatively simple dynamics in the main thermocline and below. The nearly exponential temperature profile was modeled as a steady-state balance between a presumed uniform, slow, upward advection of deep water and an enhanced downward transport of heat due to small-scale turbulence (Munk, 1966). Independent estimates of the upwelling velocity (~1 cm day^{-1}) yielded an intensity of the turbulent heat flux equivalent to an eddy coefficient $K_z = 10^{-4}$ m^2 s^{-1} (1 cm^2 s^{-1})

The assumptions made in this model of a "diffusive" thermocline are equivalent to those in the "gradient flux" approach in atmospheric boundary layer work, where K_z is inferred from $\langle (\nabla T')^2 \rangle$. As was pointed out by Osborn and Cox (1972), if these assumptions are fulfilled, then

$$K_z = k \frac{\langle (\nabla T')^2 \rangle}{\langle \partial T/\partial Z \rangle^2}, \qquad (1)$$

where k is the thermal diffusivity. Thus $K_z = 10^{-4}$ m^2 s^{-1} corresponds to a Cox number of 710.

Microstructure observations from the subtropical gyres in both the North and South Pacific found average Cox numbers far lower than 710; three separate cruises to 28°N, 155°W had average Cox numbers of 2, 10 and 59. As stated above, $\langle (\partial T'/\partial Z)^2 \rangle$ was used rather than $\langle (\nabla T')^2 \rangle$. However, even if full isotropy had been assumed, the levels were so low that they implied weak turbulent fluxes. The microstructure measurements do not give reliable estimates of the vertical heat fluxes, but they do make a strong consistency test of supposed K_z values; turbulent fluxes cannot occur in a stratified profile without producing microstructure signatures with magnitudes equivalent to Eq. (1).

In transiting the Sargasso Sea to make the observations near Bermuda, we decided to allocate a small amount of time to first look at microstructure levels in the subtropical gyre of the North Atlantic. The main result is the comparison of the Cox numbers obtained with those from the Pacific.

As an unexpected benefit from the mid-gyre data, analysis of the MSR temperature microstructure records revealed a strongly turbulent mixed layer. A request was made to Ann Gargett that she analyze the nearly simultaneous velocity microstructure profile taken with T. Osborn's profiler "Camel" for intercomparison of the spectra. These data are compared with the Kolmogorov and Batchelor spectral forms and interpreted in light of larger scale measurements of the vertical and horizontal velocities in the mixed layer.

c. The Gulf Stream

It has been generally assumed that intense currents such as the Gulf Stream and the Equatorial Undercurrent are turbulent jets, and relatively high values of vertical mixing have been used in the parameterization of these features in analytical and numerical models. For example, Orlanski and Cox (1972) (quoted by Niiler, 975) used $K_z \approx 10^{-3}$ m^2 s^{-1} in a model of western boundary currents. In view of the strong stratification associated with these currents such high levels of small-scale turbulence must have signatures in the temperature microstructure of equivalent intensity.

Observations in the Equatorial Undercurrents of the Pacific (Gregg, 1976b) and the Atlantic (Crawford and Osborn, 1979; Osborn and Bilodeau, 1979) have found regions of intense mixing in the high shear regions above and below the velocity maximum. The Cox numbers averaged over the 30 m thick patches were (3–4) × 10^3 (with no allowance for isotropy.) The MSR density profiles from the Pacific showed intense overturning activity over scales of ~1 m in these patches, while intense velocity microstructure was reported in the measurements with Camel from the Atlantic. Both the patterns of the activity and the magnitudes of the Cox numbers were in good agreement with the model proposed by Robinson (1966).

Using the large-scale shear profiles obtained with EMVP to identify the Gulf Stream, we compare the Cox numbers with those in both the mid-gyre

regions and the Equatorial Undercurrent. In addition, the signatures in the profiles are examined to identify the processes producing the microstructure.

d. Instrumentation and methods

The instrumentation and analysis methods are similar to those used previously and described by Gregg (1977b) and Sanford *et al.* (1978), except that the performance of the MSR was substantially upgraded.

A 16-bit digital data system in the MSR provided a factor of 10 improvement in the dynamic range of the temperature gradient data so that the high-frequency noise level in the high-pass microstructure channels was only a factor of 2 above the Johnson noise of the thermistors. These high-pass data were recorded at 50 Hz. The low-pass temperature data were digitized at a 5 Hz rate with a least count of ~0.3 m°C. An additional temperature channel, also digitized at a 5 Hz rate, used a Wien bridge oscillator with a thermistor in one of the reference legs. The stability of this device (Pederson, 1969) permitted the determination of the mean temperature gradients over scales of 1 m to an accuracy of $\pm 1.2 \times 10^{-4}$ °C m^{-1}. This proved to be essential for the description of the nearly homogenous regions found in the thermocline.

Since the analysis of these data was completed, dynamic response calibrations have been completed on thermistors similar to those used on the high-pass channels during FAME. The double-pole form of the transfer function was verified but the time constants were found to be less than those used previously. For the nose sensor, which had a speed of 0.08 m s^{-1}, the new calibrations give $\tau = 20.9$ ms (compared to 35 ms used before), while $\tau = 10.0$ ms was obtained for the wing-tip probe, which had a speed of 0.60 m s^{-1}. Previously $\tau = 22.0$ ms had been used for the wing probe. The new time constants will obviously result in lower Cox numbers. However, the changes are not large as can be seen by examining Fig. 7b in Gregg (1977b), which compared the effect of a much larger range of time constants on the variances. Therefore, the Cox numbers have not been recomputed and the values are therefore directly comparable with the previous data. However, in two cases in this paper arguments about the nature of the turbulence producing the microstructure are based on spectral slopes. The new time constants were used in preparing these figures.

The MSR fell at ~1 m s^{-1} until a preset depth where the wings were deployed and the descent slowed to a mean rate of 0.08 m s^{-1}. The recording duration of 51 min spanned ~250 m.

An improved pressure gage used during FAME permitted a study of fluctuations in the fall rate, which were found to be directly related to the vertical velocity of the internal wave field (Desaubies and Gregg, 1978). Use is made of this technique in estimating vertical velocities in the active mixed layer found in the Sargasso Sea.

Most of the MSR launches were coincident with EMVP drops. In some cases, the EMVP, with a descent/ascent rate of 1 m s^{-1}, was launched after MSR so that it overtook the MSR at an early part of its recording cycle. At other times, both vehicles were released within several minutes of each other so that MSR sampled water up to an hour after the velocity profiler had passed through.

Since the pressure gages of the two instruments were not calibrated with the same standard, temperature proved to be the best reference for relating the two data records. We estimate that it was possible to match the profiles to ±10 m by using the large-scale features of the temperature structure, e.g., the base of the mixed layer or the curvature of the main thermocline. Closer alignment was not generally convincing due to displacement differences arising from internal waves and possible lateral drift. Since the MSR was not acoustically tracked, precise estimates of drift are not available. However, the separation of the various instruments on their return to the surface was usually no more than a few hundred meters, and sometimes less than 10 m.

Since no 30–50 m thick layers were found near Bermuda, the identification of finestructure features common to the records from different instruments had to be attempted over scales of 2–10 m in most cases. Except for some prominent temperature inversions in the Gulf Stream, the matching of common structures was not successful, due to differences in the spatial resolution of the instruments and to the apparently short horizontal scales of the finestructure. Consequently, the comparison of shear and temperature microstructure was limited to bulk, as opposed to more event-oriented, statistics. This restriction is regrettable, but necessary, until simultaneous velocity and microstructure measurements can be made from a single instrument. The comparison was based on estimates of the Richardson number computed using the temperature, salinity and velocity data from EMVP. To obtain values in the range of Ri = 1 to 10 with no more than 50% statistical uncertainty [refer to Gregg (1979) for details] a ΔZ of 50 m was chosen. The summary plots of the data from the Gulf Stream and the Sargasso Sea include these Richardson numbers with the corresponding Cox numbers.

3 Bermuda

a. Average levels

The locations of the 15 MSR records taken in the environs of Bermuda are shown (Fig. 1) superimposed on the large-scale flow field reported by HSK

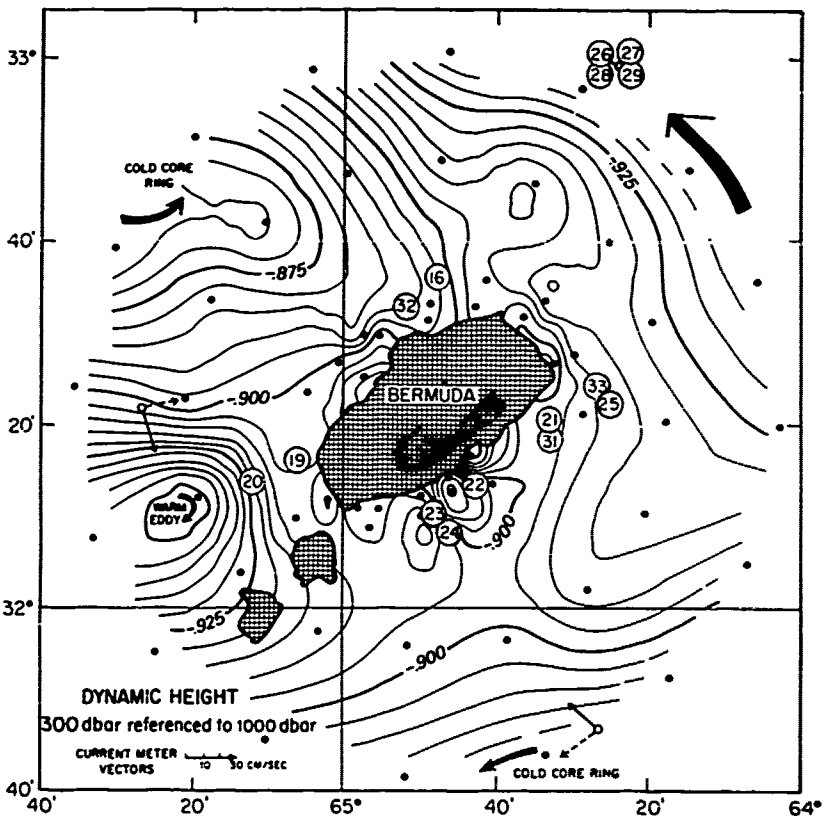

FIG. 1. Locations of the MSR drops adjacent to Bermuda are shown by the numbers superimposed on the large-scale flow field obtained by HKS. The contours are the dynamic height anomaly at 300 db referenced to 1000 db. The three open circles represent the mooring locations; four MSR drops were made near the mooring to the northeast of the island. HKS identified three eddies or rings in the flow field.

(their Fig. 2). The velocity structure was interpreted as the effect of three mesoscale eddies, or rings, which were observed passing by the island. The locations of the microstructure drops were chosen after a preliminary analysis at sea of the large-scale survey and ranged from within a few kilometers of the shore to one of the offshore moorings (shown in the upper right of Fig. 1).

Since the vertical extent of the MSR profiles was twice as long as those taken in the Pacific, the average Cox numbers were computed over the upper and lower halves of the records in order to be comparable to the previous results. The mean of the 30 values is 117, which is high in relation to averages of 2, 10 and 59 found during the three separate two-week-long cruises in the mid-gyre (Gregg, 1977b). However, since there appears to be little evidence for isotropy at the small scales, the average near Bermuda is low in relation to the value of C = 710 equivalent to $K_z = 10^{-4}$ m^2 s^{-1}.

Few temperature inversions were present in the Bermuda MSR data, and those were in the offshore profiles, MSR 26–29. Except for one inversion in MSR 33, the other records had monotonic temperature decreases on the finescale, and hence the higher microstructure levels are not due to the activity usually associated with intrusions. The lowest microstructure levels (C = 10 to 20) are similar to values from the Pacific, but the highest (C = 745) is greater than any found in the previous results, except in the Equatorial Undercurrent or on intrusions.

b. Horizontal distribution of the activity

The upper panel in Fig. 2 shows the contour map of the finestructure variances produced by HKS (their Fig. 8a). Comparison with Fig. 1 shows that the three regions of elevated finestructure occur where the mesoscale flow impinges on the island, forcing alongshore flow. The numbered circles on the map indicate the locations of MSR drops. In the lower panel of Fig. 2 the Cox numbers of these drops are plotted over the appropriate pressure intervals. It is seen that the records with the highest microstructure levels (MSR 19, 32 and 33) occurred in the places where HKS found the most intense finestructure activity, while the profiles south of the island (MSR 22–24) had lower than average values.

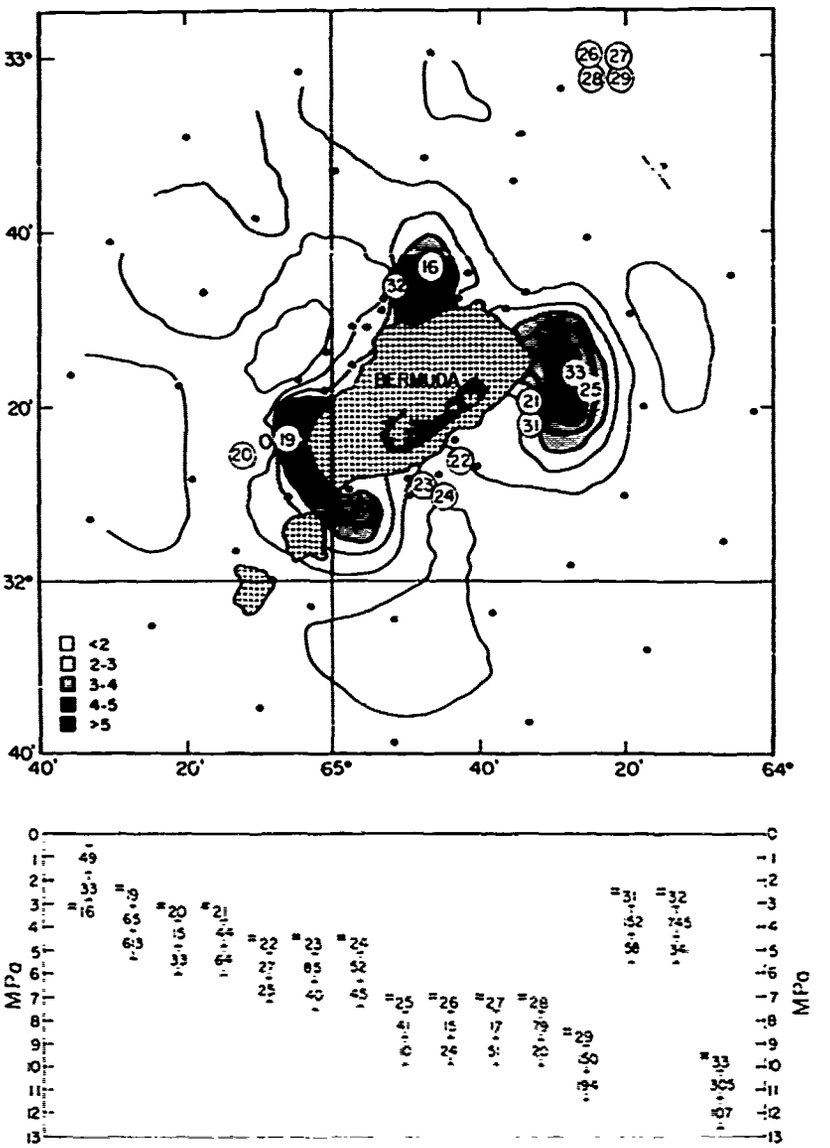

FIG. 2. Locations of the MSR drops in relation to the average finestructure intensity over the range 200–400 db obtained from CTD records by HKS. The measure for finestructure intensity is the contribution to the temperature gradient variance between scales of 0.2 to 1.0 m. The pressure intervals (given in units of MPa, where 1 MPa = 100 db) and average Cox numbers for the upper and lower half of each MSR drop are shown in the lower panel. The most active microstructure records, MSR 19 and 32, were in regions of the most intense finestructure.

as did those near the mooring (MSR 26–29) except for one that had several inversions. The relationship between the HKS finestructure levels and the Cox numbers is not fully consistent, however; note that MSR 16 also occurred in an intense finestructure region but had relatively low Cox numbers. Since the finestructure maps were taken at a different time from the microstructure observations, we believe that this is due to the basic intermittence of the processes producing the microstructure.

The significance of Fig. 2 is that the high Cox numbers occurred only in the regions with elevated finestructure levels and not in other locations. Even though the microstructure sampling was quite limited and at different times and locations from the CTD profiles reported by HKS, the incidence of the high Cox numbers in the regions with elevated finestructure implies that strong mixing may have produced the finestructure. To be certain, a more detailed examination of the profiles is required.

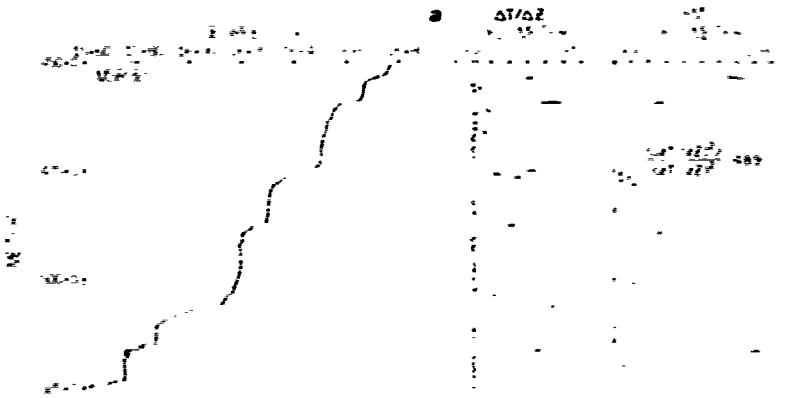

FIG. 3a. Expanded plot of the part of MSR 32 containing the steplike structures and the highest microstructure levels. From the middle trace, it is apparent that over most of this section it is possible to make an unambiguous separation between the low-gradient and high-gradient regions, and thus to uniquely define the step structures.

c. Relationship between the microstructure and the finestructure

In addition to the relatively large values of some of the Cox numbers in the regions with high finestructure levels, additional evidence for irreversible mixing comes from signatures in the profiles. Distinct steplike regions are apparent in MSR 32 and 19, two active records from the regions with elevated finestructure. These features do not occur in any of the other data. The contrast between these steplike regions and the other records can be observed in the expanded-scale plots of Fig. 3. MSR 20 was a low-activity record slightly offshore from one of the strong finestructure regions. In the case of the lower part of MSR 32 it is possible to make a reasonably objective separation of the profile into high- and low-gradient sections, e.g., by choosing the mean gradient as an indicator level: in this case the distinction between high and low gradients does not change rapidly as the indicator level is varied about the mean gradient. By contrast, for MSR 20 the separation between high and low gradients changes much more rapidly as the indicator level is varied. Thus there is not a clear distinction between high- and low-gradient regimes for a record such as MSR 20, which is typical of the thermocline.

In Fig. 4 the mean gradients and Cox numbers are shown for the stair-step regions in MSR 32 and 19. The intervals have been chosen to correspond to regions with nearly uniform values of $\Delta T/\Delta Z$, where ΔZ is 0.8 m. The most prominent characteristic of these figures is the very low value of the gradient in some of the well-mixed regions: some of the gradients are only 1% of the mean gradient and correspond to the adiabatic lapse rate. By contrast, the high-gradient interfaces between these layers are only two to three times the average gradient. The

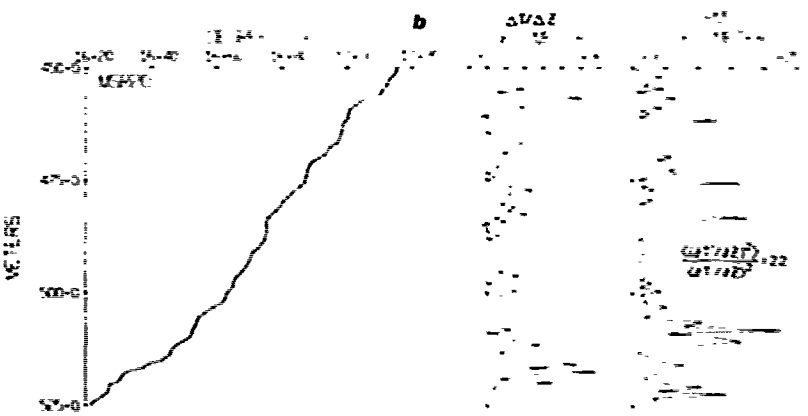

FIG. 3b. A section from a low-Cox-number record MSR 20 for comparison with Fig. 3a. Although there is one well-mixed region in the center of the record, the profile is "irregularly steppy" with no unique means of distinguishing between high- and low-gradient regions.

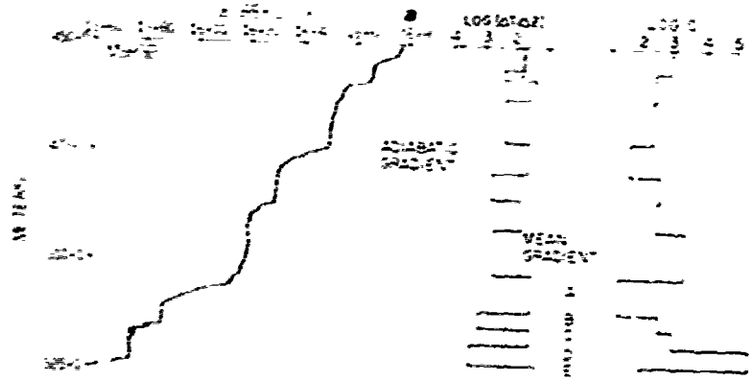

FIG. 4a. The active section of MSR 32 has been sectioned into depth intervals over which the finescale temperature is nearly uniform. Two 4 m thick regions near the bottom of the record are nearly adiabatic. The upper one, B, has a Cox number shown on the far right that is typical for the entire section, while the lower one, D, has an extremely high Cox number. The high-gradient region in the middle of these well-mixed zones appears to be overturning.

difference between the stair-step records and the data from typical thermocline profiles is shown most clearly by comparing histograms of the 0.8 m $\Delta T/\Delta Z$ values (Fig. 5a).

The most probable gradient value for the MSR 32 data was the lowest bin, which contained 28% of all values, while for MSR 20 the lowest bin contained less than 10% of the values and was not the most likely. Although the total number of samples for these histograms is too low to allow much confidence in the probability distributions, the plot for MSR 20 has a basic structure similar to that of the main thermocline. An example prepared from an ensemble of many drops in the Pacific (Fig. 6) shows a very skewed distribution with the most probable value between the mean gradient and zero. Very weakly stratified sections are much less probable than those with half of the mean gradient, unlike the situation in MSR 32 where the probable value occurs in the bin with the lowest positive gradient.

Also shown in Fig. 5 are plots of the cumulative distribution of the gradient values and of the net temperature difference ΔT. As an example, 70% of the 0.8 m averages for MSR 32 are less than the mean gradient (which is unity on the abscissa) and collectively account for less than 20% of the temperature difference across the section. For the Pacific data, 60% of the values are less than the mean and account for 30% of the net temperature change. The larger separation between these curves for MSR 32 is due to the contribution of a few very high gradient values.

The Cox numbers in Fig. 4 range from less than 10 to more than 10^5. The largest values occur in the low

FIG. 4b. Finestructure in the active microstructure region of MSR 19 also showing striking stair-steps.

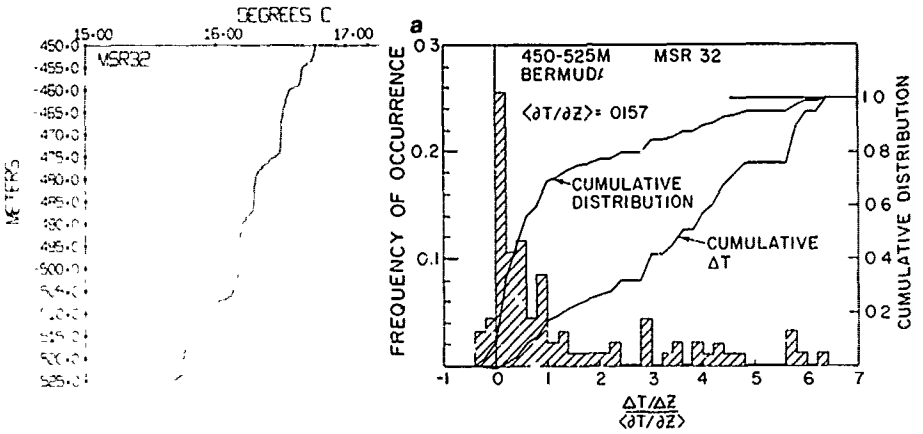

FIG. 5a. Histogram of 0.8 m averages of $\Delta T/\Delta Z$ for MSR 32. This stair-step record is characterized by a much larger number of weakly stratified sections than is typical of the main thermocline. The number of high gradient regions is also increased, leading to a pronounced separation of the cumulative distribution and ΔT curves.

gradient sections, which is not surprising since such low values occur in the denominator of the Cox number. In the well-mixed sections large Cox numbers can be due to either active turbulence throughout the layer or to gradient structures formed by entrainment at the boundaries, in which case only very weak turbulence need be present in the layer itself. Further evidence of active turbulence is provided by the spectra slopes in the different regions.

d. Spectral slopes

In stratified profiles turbulence will produce density inversions with scales as small as a few centimeters. As discussed by Gregg (1977b) some of the observed patches of temperature microstructure are associated with distinct 0.5–1 m thick density instabilities, while others appear to be stable over these scales, but have numerous temperature inversions over scales of 0.1 m and less. Due to difficulties in measuring salinity at scales of a few centimeters, it has not been possible to determine what fraction of these small temperature inversions are also density inversions. However, several lines of indirect evidence suggest that many of the patches are associated with active turbulence in which the velocity microstructure has not completely decayed.

In a laboratory study of the wake of a turbulent grid that was dragged through a salt stratified tank, Lange (1974) found that the spectral slopes of the vertical salt gradients were +0.5 to +1.0 while the wake was growing; the accompanying optical ob-

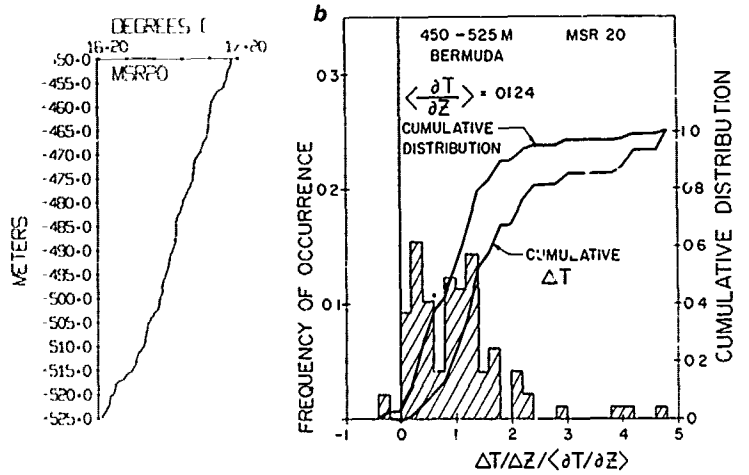

FIG. 5b. Histogram of 0.8 m averages of $\Delta T/\Delta Z$ for MSR 20. This record is similar to those in the main thermocline, e.g., Fig. 6. Note the much lower frequency of occurrence of the lowest positive bin compared to that in Fig. 5a.

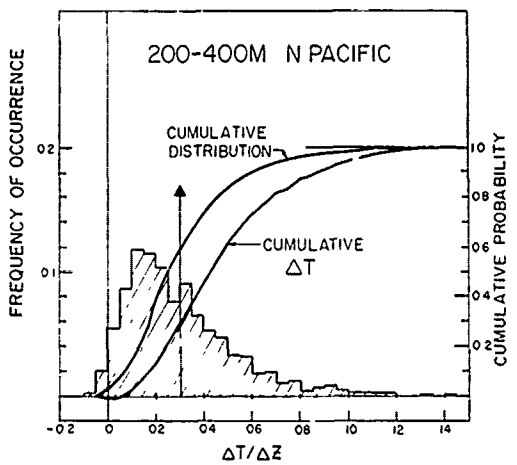

FIG. 6. Histogram of 1.0 m averages of $\Delta T/\Delta Z$ for an ensemble of many records from the main thermocline of the Pacific. The distribution is highly skewed with a most probable value at half of the mean gradient, which is shown by the arrow, and a decaying tail toward higher gradients. Unlike MSR 32, very weakly stratified regions are less likely than ones with half the mean gradient.

servations also re ied intense turbulence in the wake. As the wake ollapsed, the spectral levels at high wavenumbers decreased more rapidly than those at lower wavenumber, causing the slopes to decrease. By three buoyancy periods the profile was restratified, but strongly layered, and by 16 periods the spectral slopes were −1, and the turbulence was completely decayed into a field of internal waves.

The temperature gradient spectra from the Pacific thermocline show slopes from +1 to −1 in the microstructure range; the positive slopes are associated with the patches having many centimeter-scale inversions. This is consistent with Batchelor's (1959) viscous-convective subrange for passive scalars; the occurrence of this range is not dependent on high-Reynolds-number turbulence, but is possible with the weak turbulence that appears to exist in the thermocline. Due to the uncertainty of the thermistor response, discussed in more detail in Gregg (1977b), the scale at which these rising spectra are cut off by diffusion had not been clearly defined.

Gradient spectra from subsections of MSR 32 are shown in Fig. 7. In these plots comparison of data from the wing probe, which had an angle-of-attack of 6° to the horizontal, provides a measure of the isotropy of the small-scale temperature fluctuations. A marked difference is apparent between the spectra of the two well-mixed regions B and D; the maximum of the former occurs at 5 cpm, while that of the latter is quite broad and nearly a decade higher on the wavenumber axis. The structures in region B are well resolved in both wing and nose records and appear to be nearly isotropic. Since the spectrum from section B is falling in the normal microstructure range while that of the deeper section D is rising with an approximately +1 slope, we conclude that active mixing was occurring in the latter, but not in the former.

Great differences are apparent in the microstructure records from the strongly stratified regions as

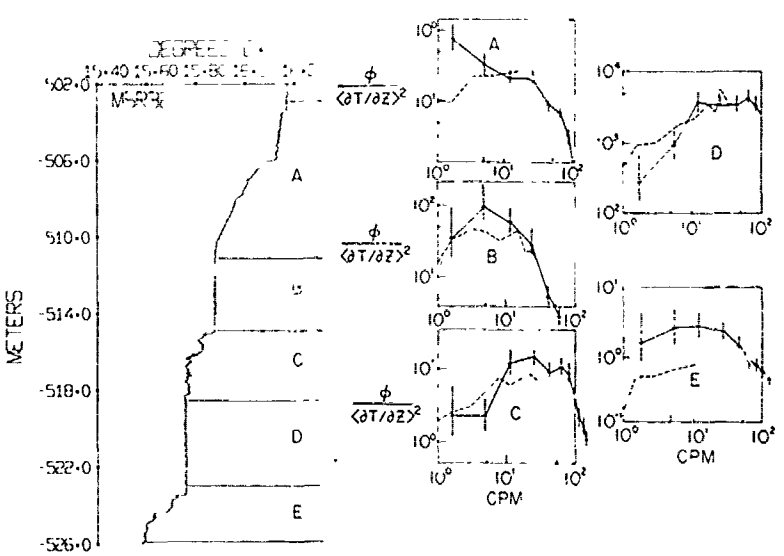

FIG. 7. Average temperature gradient spectra for different sections in the steplike region of MSR 32. Spectra of vertical profiles are shown by solid lines while those from the corresponding wing records are given by dashed lines. Regions A, B and E have falling spectra in the microstructure range, while C and D do not. The difference between the two well-mixed regions (B and D) is particularly notable and implies turbulent stirring in D but not in B.

well as the homogeneous layers. The upper stratified zone A has low normalized spectral levels and a falling spectrum with a Cox number of 20. There is thus no evidence for active mixing. By comparison the high-gradient region C has a Cox number of 1000, numerous small-scale temperature inversions, and a prominent spectral maximum in the microstructure wavenumber range. This 4 m thick interface appears to be actively mixing. The possibility that some of the fluid from this apparent overturning zone may have been carried upward could account for the high Cox numbers but nonturbulent spectra in B.

e. Discussion

From moored observations of temperature and current made on the Bermuda slope, Ericksen (1978) found instances of low Richardson numbers and of internal wave breaking. The occurrence of these events, which Ericksen took to be Kelvin-Helmholtz instabilities over O(1) meter vertical scales, was equally likely at all frequencies in the internal wave band. This picture of mixing events randomly distributed in space and time is consistent with microstructure observations in the main thermocline of the open ocean and in the lower activity regions around Bermuda. However, when the entire perimeter of the island was surveyed by HKS, localized regions of elevated finestructure levels were found in regions of high boundary-eddy flow interaction.

Several mechanisms, for example, lee wave production over bottom topography, with subsequent breaking, and bottom-generated turbulence, were considered by HKS to be possible sources of the enhanced temperature finestructure. However, the lack of a corresponding signal in the shear profiles led them to conclude that most of the finestructure was a remnant of mixing that occurred prior to the observations.

The microstructure observations discussed above offer direct evidence that active vertical mixing was occurring in the regions of high finestructure levels. However, the mixing was quite localized, and occurred over the relatively small part of those sections where steplike profiles were encountered. Possible explanations for this are as follows:

(i) The step structures were formed irreversibly by overturning activity. This activity could have been occurring intermittently throughout the steplike region and was active at the time of the observation at only a few sites. Or it could have been sustained over more restricted depth intervals for a limited time and then ceased. In the latter case only the bottom sections of Figs. 4a and 9 were still mixing when the observation was made.

(ii) The step structures were formed reversibly by high-mode internal wave activity near the island. Shear instabilities occurring in only a small part of the internal wave field produced the observed microstructure.

In view of the nearly adiabatic gradients and sharp boundaries of many of the sections of Fig. 4, alternative (ii) seems quite unlikely. For example, we consider a nearly homogenous region formed reversibly from an initially linear profile. If Δ is the equilibrium separation of the isotherms bounding the region, and δ their instantaneous separation, then the instantaneous gradient will be $dT/dZ = (\Delta/\delta) \times \langle dT/dZ \rangle$, where $\langle dT/dZ \rangle$ is the initial linear gradient. For some of the sections in MSR 32, the required strain, $(\delta - \Delta)/\Delta$, is as high as 30–80. Such high values seem quite unlikely.

From the high Cox numbers and spectral slopes we conclude that active mixing was occurring in the high-finestructure regions near the island and that the elevated finestructure levels were not just remnants of previous mixing, nor were they due solely to internal wave strain. However, sustained mixing prior to the microstructure observations must have occurred to produce the nearly adiabatic regions.

4. Microstructure in the Sargasso Sea

A site (35°N, 66°30′W) in the Sargasso Sea was occupied on the way to Bermuda from Woods Hole and again for one day on the return leg. During the second set of observations the surface water was found to be moving to the southeast at a speed of ~0.5 m s^{-1} with respect to the deeper water. As seen in Fig. 8, this produced a shear of ~0.007 s^{-1} from shallower than 100 m to 225 m, a value comparable to that of the Gulf Stream. Due to the limited observations in space and time, the process producing the shear could not be determined, but the fact that it showed little variation during the observations suggests that it may have been due to a mesoscale eddy.

a. The mixed layer

Conditions within the mixed layer, presented in Fig. 9, were markedly different when the data from the second set of measurements (9 November) are compared with the first (10 October).

On the large scale the transition at the base of the MSR 37 mixed layer (second set of observations) is thin and sharp, while that of MSR 10 is much thicker and more diffuse. In a series of mixed-layer observations in the Pacific, Gregg (1976a) found that a similar contrast in transition regions occurred between times of active mixing and quiesence. In that case these times were well correlated with

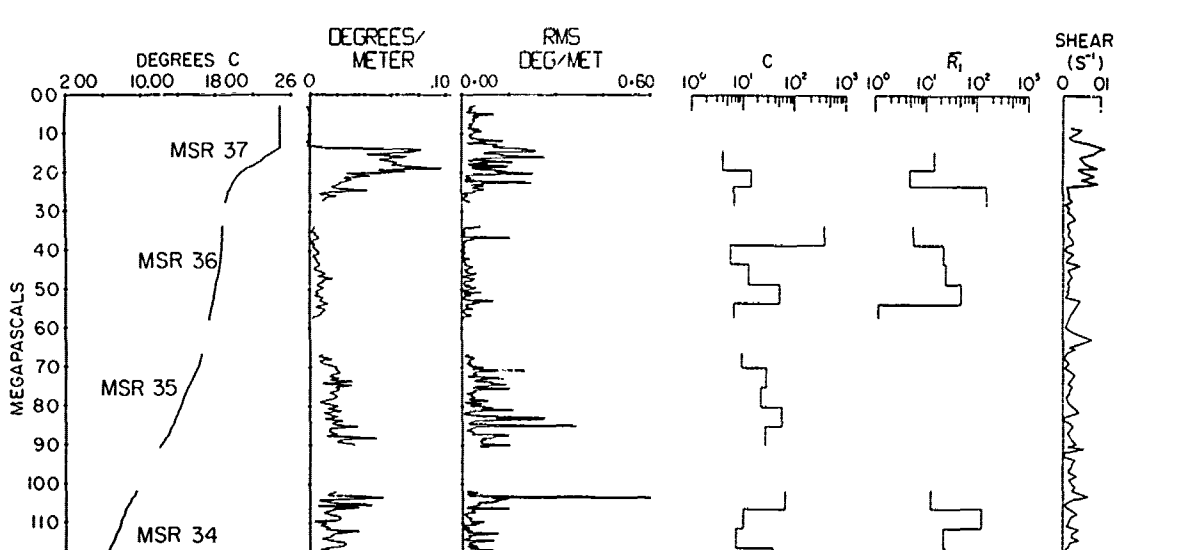

FIG. 8. Summary plots of the MSR drops in the Sargasso Sea are given in the first four columns. The last column shows shear obtained from a typical EMVP drop at that site while the fifth column shows Ri obtained from EMVP drops that were simultaneous with MSR. A strong shear zone, with a mean shear of 0.007 s^{-1}, spanned most of the seasonal thermocline and extended into the lower part of the mixed layer. The shear was not sufficient to cause significant mixing in the seasonal thermocline, but based on the relatively high rms gradients in the mixed layers it may have caused the observed mixing across the base of the layer. Most of the mixing activity in the 18°C water (MSR 36) and below the main thermocline occurred in a few events, while that in the main thermocline (MSR 35) occurred over a larger fraction of the record. There was no consistent correlation between the Cox and Richardson numbers averaged over 50 m.

meteorological conditions, while the situation for the present data is much less clear, as will be discussed subsequently. The large-scale shear is also quite different; there is a high shear across the thin step-like transition of MSR 37 but not of MSR 10.

Evidence that the MSR 37 surface layer was being strongly stirred comes from the large fluctuations in vertical velocity, $\Delta W = 0.066$ m s^{-1}. Since these measurements were made from a slowly descending body, their structure is smeared between spatial and temporal sampling. However, the similarity between the magnitude of these fluctuations and those of horizontal velocity ($\Delta U \approx 0.05$ m s^{-1}) is consistent with the existence of cellular convection within the layer. The fluctuations of vertical velocity in MSR 10 were much lower by comparison.

The levels of temperature microstructure are much higher throughout the MSR 37 layer with a strong increase in the bottom 15 m. No corresponding increase is apparent in the MSR 10 data. Spectra of the temperature records show similar differences; that of MSR 37 shows good agreement with the "universal form", while that for MSR 10 does not. In addition, comparison of the MSR 37 wing and nose spectra (Fig. 10) shows isotropy for $k > 0.2$ cpm, while this is only true for $k > 2$ cpm in MSR 10. Thus, all of the microstructure measurements confirm the larger scale evidence for strong stirring in MSR 37 but not in MSR 10.

The observations from the Pacific had spectra similar to those expected for fully developed turbulence during a mild storm when the Monin-Obukhov length L_B exceeded the depth of the mixed layer, indicating that forced or free convection should be present throughout the layer. The data recorded in the *Knorr* log are not suitable for estimating L_B, although it is clear from the wind records that mechanical turbulence could not have extended very far into the mixed layer during the second set of observations. Convection, however, was possible; the air temperatures during the November profiles were in the range 21–22°C, while the bucket temperatures were ~23°C and the underlying surface layer 24.8°C. Thus, the Rayleigh number greatly exceeded the critical value, indicating that convection should have been occurring.

Additional support for the occurrence of convection comes from a comparison of CTD profiles made during both periods of observation. In the intervening 19 days, the mixed layer deepened ~21 m, cooled from 25.6 to 24.8°C and increased in salinity from 36.333 to 36.356‰. If the deepening had been driven solely by mechanical mixing, the layer should have cooled 0.1°C and increased in salinity by

12 ppm. Thus the change in salinity agrees well with that expected for the observed deepening but the cooling was much greater than that due to mechanical driving.

Within 20 min after MSR 37 was launched, a profile was begun with Camel. Comparison of the Camel spectrum (kindly supplied by Ann Gargett) with the MSR temperature spectrum (Fig. 11) shows that both exhibit general agreement with the forms expected for a strongly turbulent flow. To our knowledge, this is the first demonstration of these forms from simultaneous, or nearly so, observations from separate bodies. Integration of these spectra yields a rate of turbulent energy dissipation ϵ of $(1.4–1.5) \times 10^{-7}$ W kg^{-1} (Gargett *et al.*, 1979) and a rate of diffusive smoothing of the temperature gradients χ of 5.42×10^{-9} °C^2 s^{-1}. In both cases, full isotropy was assumed based on Fig. 10.

Using these values for ϵ and χ a more detailed comparison with the "universal" forms for the temperature spectrum can be made. The solid line under the temperature spectrum in Fig. 11 with the $-5/3$ slope was plotted from the form for the convective subrange (corresponding to the inertial subrange in velocity) given by

$$\phi_T(k) = \beta_1 \chi \epsilon^{-1/3} k^{-5/3}, \qquad (2)$$

with the value $\beta_1 = 0.31$ determined by Grant *et al.* (1968). [Note that the levels must be corrected for spectral units of °C^2 cpm^{-1} rather than the

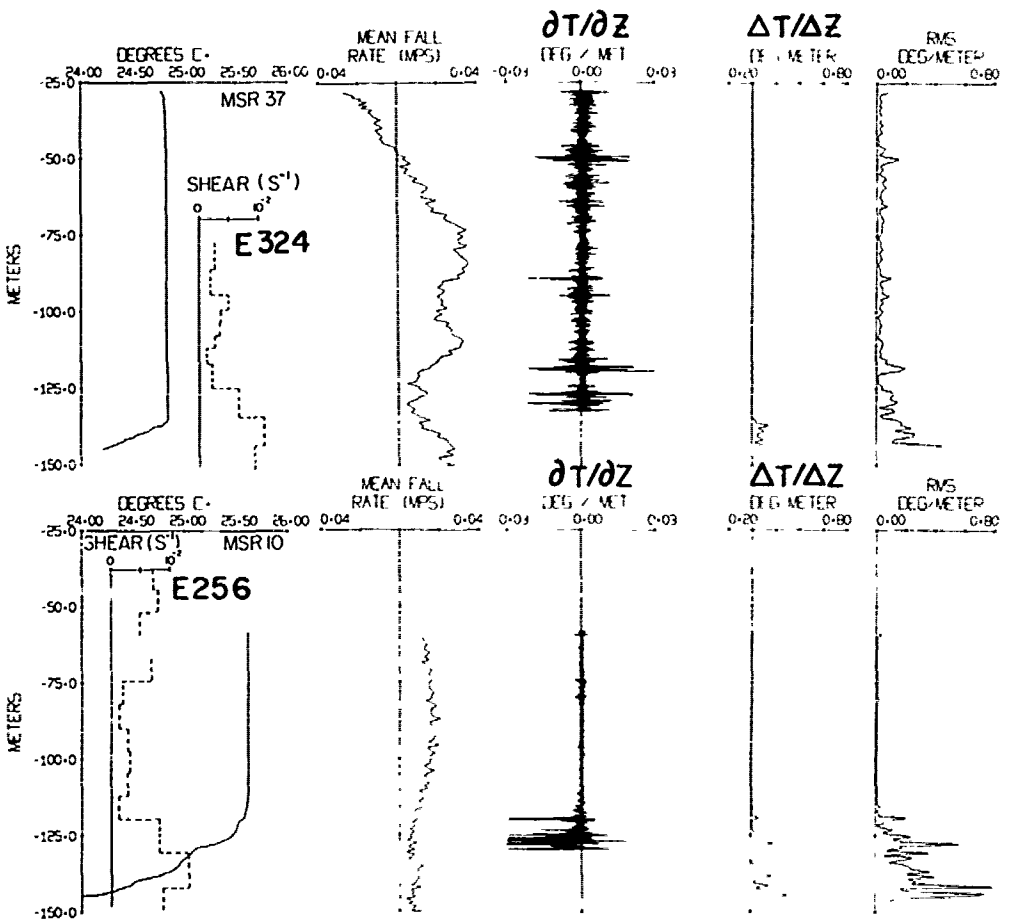

FIG. 9. Details of the mixed layers during the first (MSR 10) and the second (MSR 37) occupations of the site in the Sargasso Sea. The abrupt termination of the mixed layer in MSR 37 is consistent with active turbulence within the layer while the more diffuse transition in MSR 10 implies the absence of vigorous turbulence. In both cases the shear levels increased near the base of the mixed layer; however, those in MSR 37 had a maximum across the transition while those in MSR 10 reached a maximum in the stratified region below the mixed layer. MSR 37 also had large changes in the vertical water velocities, ± 0.04 m s^{-1}, inferred from changes in the MSR fall rate. Those for MSR 10 were about ± 0.005 m s^{-1}. The other traces are, from the left, the microstructure temperature gradients over scales < 0.01 m, the mean T Grad averaged over 0.8 m, and the rms T Grad over the same interval. Note that the rms T Grad for MSR 37 begins increasing above the base of the mixed layer, implying mixing across the transition region.

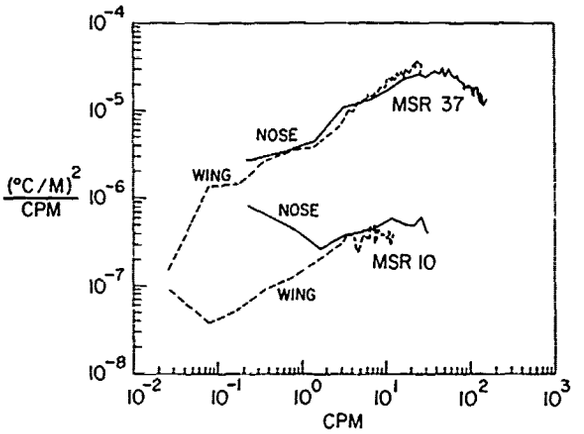

FIG. 10. Average temperature gradient spectra from wing and nose probes in the mixed layers of MSR 10 and 37. The MSR 37 data are consistent with isotropy from 0.3 to 30 cpm, while structures in the MSR 10 data are not isotropic for $k < 2$ cpm. Confiidence limits for the spectral estimates are similar to those shown in Fig. 11.

$°C^2$ rad^{-1} cm^{-1} used by Grant *et al.* (1968).] The agreement is excellent.

The solid curve at higher wavenumbers is the best overall fit of the Batchelor model spectrum to the observations using the same methods as Grant *et al.* (1968). This model spectrum is given by

$$\phi_T(k) = q^{3/2} 2\sqrt{\pi} k_T^{1/2} \nu^{3/4} \epsilon^{-3/4} \chi \times \left[\frac{\Phi(x)}{x} - \int_x^\infty \Phi(x)dx \right], \quad (3)$$

with

$$x = \frac{(2q)^{1/2}k}{k_B}, \quad k_B = \epsilon^{1/4}\nu^{-1/4}k_T^{-1/2},$$

$$\Phi(x) = (2\pi)^{-1/2} \exp(-\tfrac{1}{2}x^2).$$

(k_T is the thermal diffusivity and ν the kinematic viscosity.)

The scaling constant q was evaluated as 3.9 ± 1.5 by Grant *et al.* Using the value of the parameter x obtained by our "best fit" curve gives $q = 57$, a value in serious disagreement with the above value. On the other hand, if $q = 3.9$ is used with the measured values of ϵ and χ to evaluate (3), only a small part of the measured spectrum is fitted.

We interpret the above disagreement of the scaling constants of the Batchelor spectrum to be further evidence that (3) is only an approximate form that is exactly fulfilled in the "roll-off" wavenumber range only under limited conditions if at all. The verification of the Batchelor spectrum (Gibson and Schwarz, 1962; Grant *et al.* 1968) was based only on fits over the k^{-1} range; higher wavenumbers were limited either by noise or spatial attenuation of the probes. This would be equivalent to considering only $k < 10$ cpm in Fig. 11.

Elliott and Oakey (1976) also found that the roll-off portion of temperature spectra from the data in the thermocline did not follow (3) but had a less rapid decrease with increasing k. By obtaining a similar result in a fluid that was homogenous in the mean and had other evidence for turbulent stirring, it appears that the differences between the observations and (2) are not solely an effect of stratification. It follows that attempts to infer ϵ from the high wavenumber shape of temperature spectra are open to serious question.

b. Below the mixed layer

As can be seen in Fig. 10, the Cox numbers averaged over 50 m thick sections vary from 4 to 400 because of the highly intermittent character of the microstructure. As discussed in more detail in Gregg (1977b), the presence of one strong patch often determines the Cox number for the section. For example, note in Fig. 8 the two strong events in the upper sections of MSR 34 and 36 and the resulting large Cox numbers. The records are far too few to warrant any conclusions about average

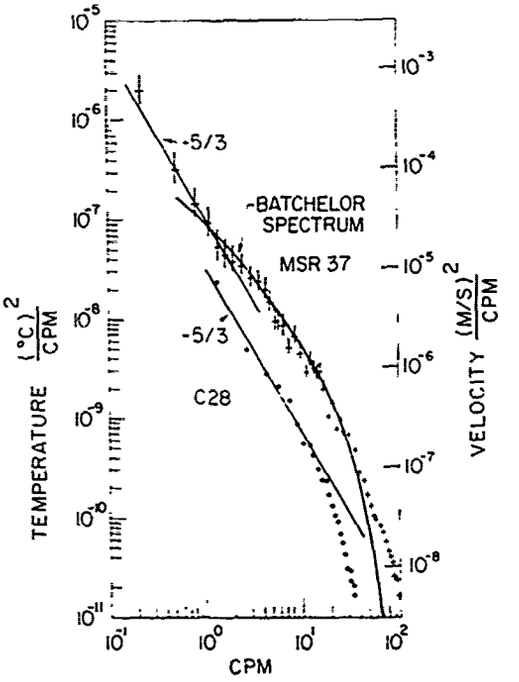

FIG. 11. Comparison of MSR temperature spectrum in the MSR 37 mixed layer with a velocity spectrum from a nearly simultaneous Camel profile. Both are generally consistent with the forms expected for fully developed, homogeneous turbulence. (It should be noted that the velocity spectrum is of the component transverse to the motion of the profiler.) The solid $-5/3$ line for the temperature spectrum was plotted from the observed values of ϵ and χ with the scaling constant determined by Grant *et al.* (1968). The curve for the Batchelor spectrum is a visual best fit. It is apparent that no shifting of the curve can give agreement with the data throughout the full wavenumber range.

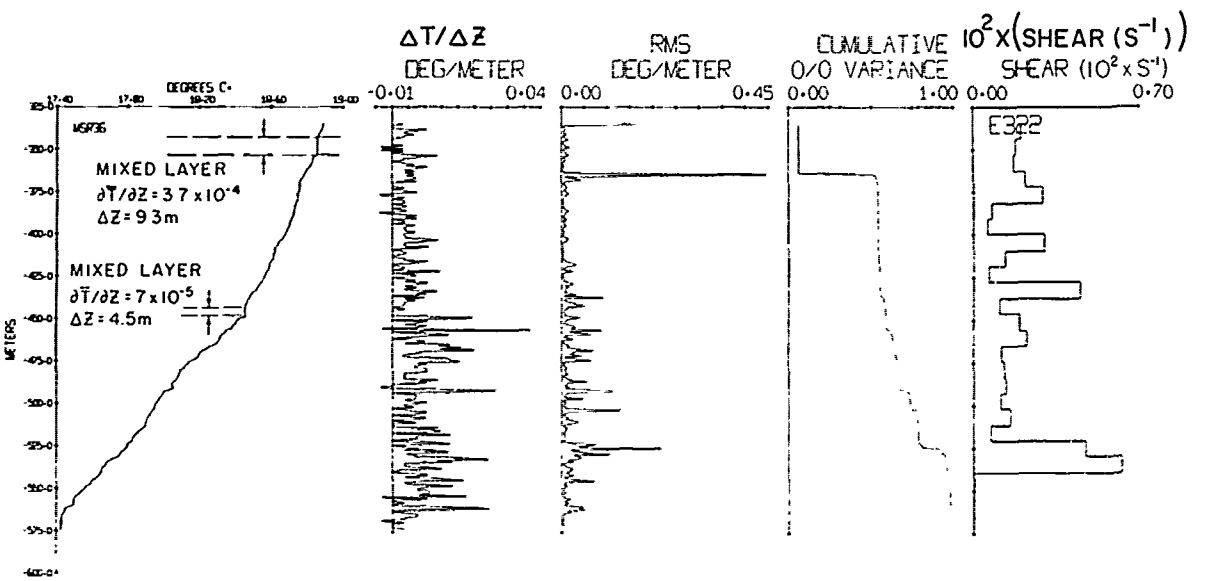

FIG. 12. Summary plot of MSR 36 compared with 10 m shear values from a simultaneous EMVP drop. The two most active mixing regions are in high shear zones. Note the two well-mixed regions.

levels, but the range of values is consistent with that found during the most active of three cruises to the central North Pacific.

Although some of the larger Cox numbers appear to occur with the lower Ri estimates, there is no significant correlation between the two. As an example, note the very low Ri value at the bottom of MSR 36 and the equally low Cox number. Although statistically significant estimates of Ri could not be made to scales < 50 m (Gregg, 1979), shear values could be obtained to 10 m. Fig. 12 shows the shear values for the record in the 18°C water. It is seen that the two large contributions to the temperature gradient variance occur near 365 and 530 m, and are in regions with higher than average shear.

The two subsurface well-mixed regions in MSR 36 are very close to being adiabatic. Although similar regions had been occasionally noted in the Pacific data, the stability of the temperature circuit used at that time was not sufficient to accurately determine their mean gradients. In view of the relatively low mixing efficiency in stratified fluids (Thorpe, 1973), the existence of these subsurface layers implies that *sustained* mixing events have occurred. Isolated Kelvin-Helmholtz instabilities studied in the laboratory by Thorpe (1973) and Koop (1976) do not produce such complete mixing.

5. Temperature microstructure in the Gulf Stream

Three MSR drops were made at shallow depths in the vicinity of 38°N, 69°W. MSR 38 was obtained toward the northern edge of the Gulf Stream, while two others, MSR 39 and 40, both simultaneous with EMVP records, were made through the Stream's core.

A summary plot of MSR 38 is given in Fig. 13, while the other two records are combined in Fig. 14. EMVP 326 was simultaneous with MSR 39 but on the scale shown in the summary figure the velocity structure had no significant changes between the two drops. Annotations on Fig. 14 denote particular signatures in the finestructure and microstructure.

a. Thermohaline intrusions and double diffusion

The most striking feature of the observations in the Stream was the ubiquitous presence of salt-stabilized temperature inversions. A comparison of several CTD profiles made in a nearly north-south line shows that these represent intrusions formed by interleaving across the Stream. (Inversions with increases as large as 5°C were found in the CTD casts.) Toward the northern edge, there was a thick zone in the upper 100 m with multiple, sharp inversions having scales as small as 2 m (note the upper part of Fig. 13). To the south where the intrusions occurred at greater depths (Fig. 14) in the core of the Stream, the inversions were more isolated, thicker, and had more diffuse boundaries.

Several of the inversions show the same patterns of microstructure activity as found in less energetic locations such as the California Current. The inversion in Fig. 15 shows all of the features discussed in detail by Gregg (1975). There is a 2 m thick nearly isothermal section above the inversion with three distinct temperature steps below. An equally large contribution to the rms temperature

gradient occurs on the lower boundary of the intrusion. From a comparison of the temperature and salinity records through similar features, Gregg and Cox (1972) identified the steps on the upper boundaries of the intrusions as the diffusive case described by Turner (1968). Although the increased activity on the lower boundary is in a region where salt fingering is possible, there are no steps or other features to uniquely identify the process as double diffusive. However, Gregg (1968) and Linden (1971) showed that although mechanical turbulence easily destroys the regularity of the fingers, the enhanced diffusive fluxes continue until very high levels of turbulence are present. Thus, it is likely that the structures on the lower boundary of the inversion are produced by a combination of shear-generated turbulence and salt fingering.

At greater depths, another profile (Fig. 16) did reveal a prominent sequence of nearly adiabatic layers beneath a temperature inversion. This is the first clear sequence of such a series of distinct layers obtained from the many MSR drops through similar inversions, and is additional evidence for the presence of salt fingering on the undersides of inversions. We have no explanation for the presence of the steps under this intrusion but not beneath the others.

A comparison of the MSR profiles with those of Williams' Self-Imaging-Micro-Profiler (SCIMP) illustrated the previously mentioned difficulty of comparing data from different profilers. With the aid of acoustic tracking, the ship was positioned directly over SCIMP when MSR was launched. Since MSR was not tracked, the subsequent lateral separation is not known; however, with a mean shear of 0.018 s^{-1}, the separation when both instruments passed through the inversion in Fig. 15 should have been less than 100 m. A comparison of the Gross Temperature Record from MSR and the Brown CTD on SCIMP in Fig. 17 shows that both instruments passed through essentially the same inversions, although they were distorted by the internal wave field, and there is a difference in the absolute temperature calibrations of the instruments. The intrusion at 100 m is half as thick in the SCIMP profile as in the MSR data. Although this may be due to lateral variations, it could also be due to deformation by the intense internal wave field (Desaubies and Gregg, 1978). The difficulty in comparing finescale features below the inversions is readily apparent.

The steps on the upper boundary of the inversion in the MSR record are clearly not present in the SCIMP data. Although this absence could be due to lateral variability in the intrusion, no steps were observed by SCIMP on any of the other intrusions. A comparison of temperature gradient spectra from matching sections of MSR and SCIMP records showed attenuation of the SCIMP data at scales $\lesssim 1$ m (P. Hendricks, personal communication). Since both instruments had similar descent rates, the comparison of their spectra is a good indication of their relative dynamic response as a function of frequency. The SCIMP data were obtained with a microstruc-

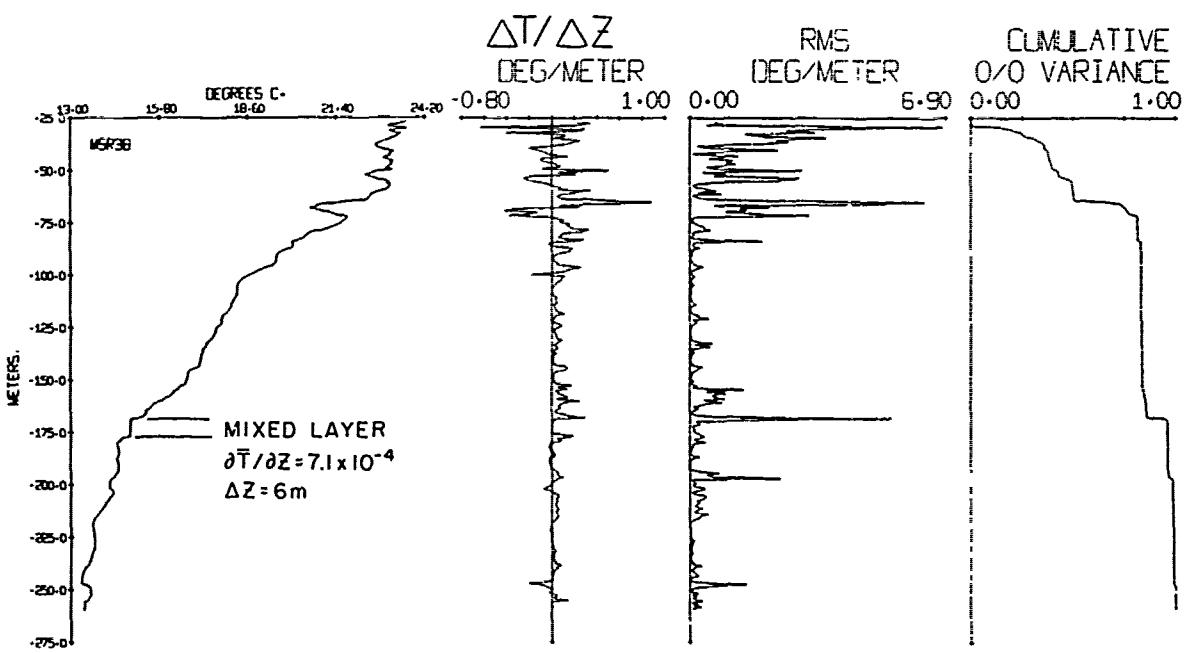

FIG. 13. A shallow MSR record taken toward the northern edge of the Gulf Stream shows that most of the microstructure activity is associated with temperature inversions. The accompanying CTD observations show that the inversions are of advective origin.

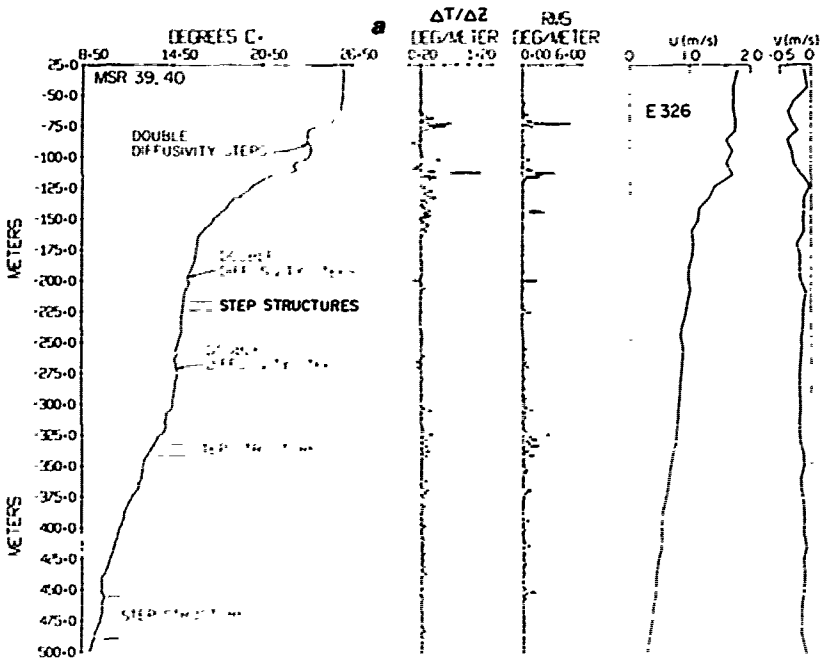

FIG. 14a. Summary plots of two MSR records taken in the middle of the Gulf Stream with the velocity profile from an EMVP record. The double diffusivity steps are on the upper boundaries of salt-stabilized temperature inversions. Some of the step structures in monotonic regions may be due to salt fingering.

ture version of the N. Brown CTD. Although the CTD uses a glass-rod thermistor, which is like that on MSR, as a dynamic correction to the platinum wire probe, it appears that the complete system response is much slower.

Movies made with the optical system on SCIMP,

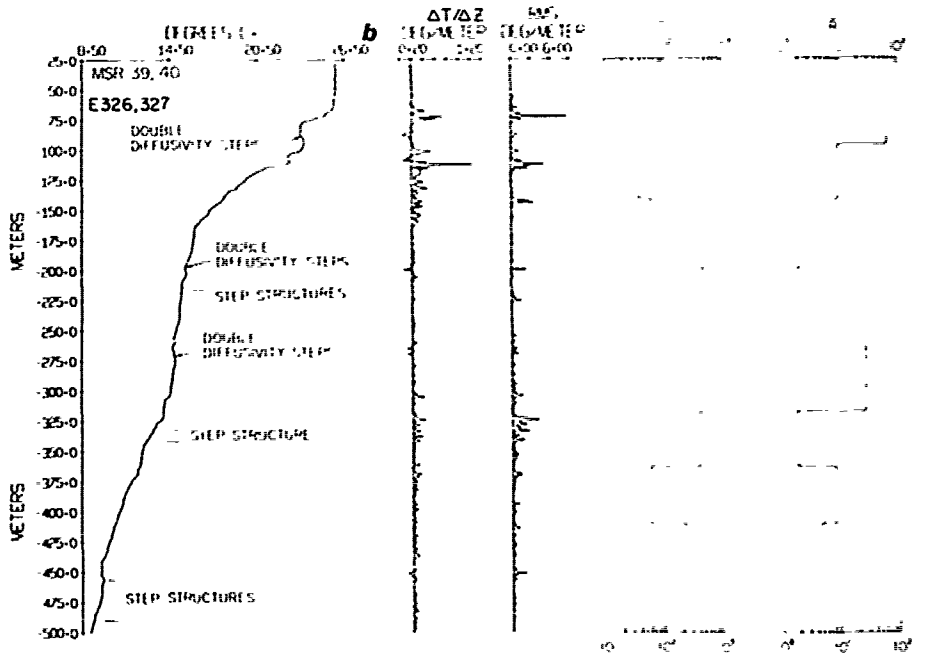

FIG. 14b. Cox and Richardson numbers computed over 50 m scales from simultaneous drops in the Gulf Stream. It is seen that many of the higher Cox numbers are associated with the diffusive steps on the temperature inversions. There is no consistent relationship between the Cox and Richardson numbers.

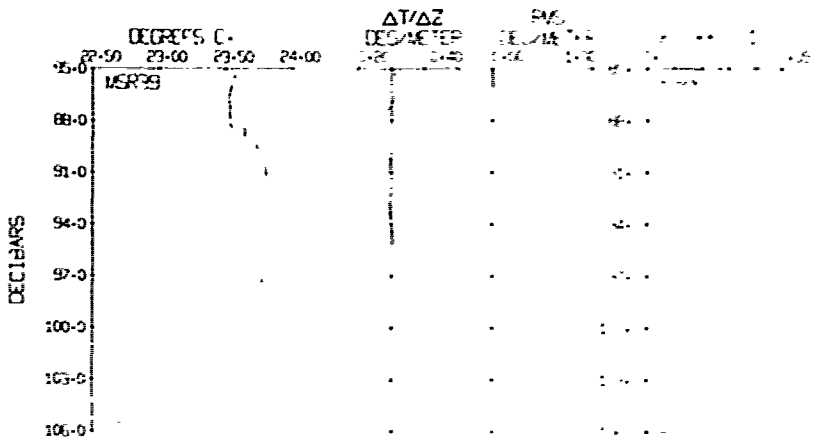

FIG. 15. Detail of the upper temperature inversion from Fig. 14 showing the same pattern of microstructure activity as found on inversions in regions with low mean shear such as the California current. As seen on the plot on the far right, the mean shear across the feature was 0.01 s^{-1}.

however, did show horizontally banded structures on the temperature inversion with thicknesses similar to those of the steps in the MSR temperature record (A. J. Williams, III, personal communication). Much fainter, irregular structures were observed on the underside of the inversion where the rms temperature gradient showed a large increase. These structures have previously been interpreted as the product of a combination of shear-generated turbulence and salt fingering.

Finally, the highest levels of $\langle(\partial T'/\partial Z)^2\rangle^{1/2}$ in Fig. 14 occurred on the underside of a temperature inversion situated at the base of the mixed layer. There the temperature profile decreases smoothly through this region (Fig. 18) indicating the absence of any overturning with scales ≥ 0.1 m. The SCIMP shadowgraph films showed a banded structure indicative of tilted salt fingers. From the EMVP data the mean shear in this region was 10^{-2} s^{-1}. The slow vertical motion of salt fingers would produce a

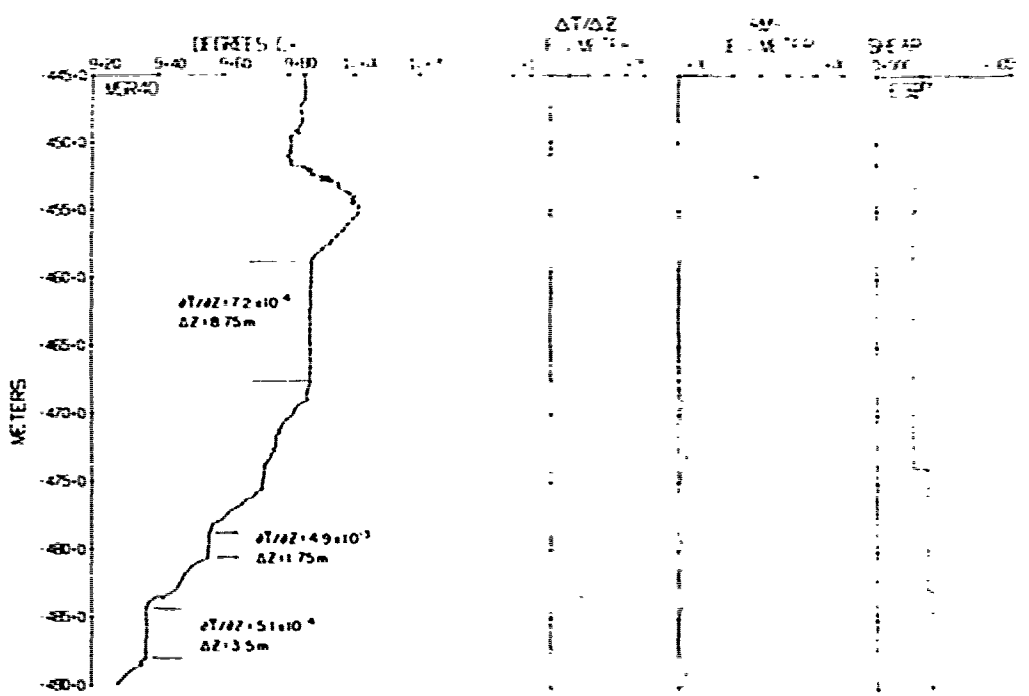

FIG. 16. Sequence of well-mixed regions below a temperature inversion in the Gulf Stream. Their location beneath the inversion suggests that these may be formed by salt-fingering.

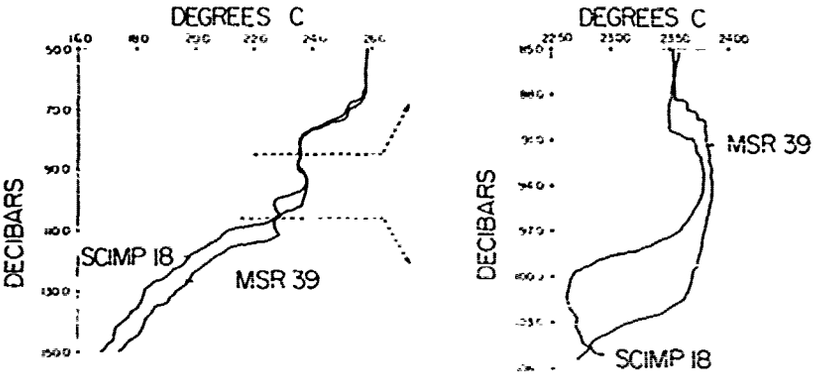

FIG. 17. Nearly simultaneous profiles obtained by SCIMP and MSR in the Gulf Stream. The Brown Microprofiler CTD on SCIMP did not show the sharp steps on the upper boundary of this intrusion, nor any of the other intrusions where they appeared in the MSR data. A comparison of temperature spectra indicates that this is due to smoothing by the CTD. Shadowgraph movies on SCIMP did show distinctive structures on the boundaries of the intrusion.

significant tilt in such a shear and hence appear as a strong signal in a vertical profile allowing a descent/ascent rate of 1 mm s^{-1} and a 0.2 m thick fingering region gives a mean inclination of 60° to the vertical. Thus, a strong rms gradient signal should appear in a vertical profile through a fingering region.

b. Monotonic sections and turbulence

Some dissipative structures are found in regions where the temperature decreases monotonically in the finescale range, with no apparent influence of intrusions. The most prominent of these (Fig. 19) contains a sequence of stair-steps, the bottom two of which are very well mixed. This record was not simultaneous with a SCIMP profile and there is no firm basis for distinguishing between turbulence and salt fingering. From Fig. 14b it is noted that the mean Richardson number is about 2 across the region, so mechanical mixing due to shear instabilities over scales less than 50 m is a possibility.

From Fig. 14b it is also seen that the 50 m average Cox numbers range from 36 to 600. All of the higher values include one or more of the intrusive features discussed above. The two 50 m thick regions that have monotonic temperature profiles without step structures have C = 60, values that are typical of mid-gyre thermoclines.

Due to the small number of profiles and the intermittent nature of turbulent mixing it is possible that such activity frequently occurs in the Gulf Stream but was missed by these observations. However, just the existence of 50 m thick regions with Cox numbers of 40–60 in the high-shear zone of the current is in striking contrast to Cox numbers 100 times greater found during observations in the Equatorial Undercurrents of the Pacific and the Atlantic.

Evidence that the low microstructure levels are not completely misleading comes from comparison with a previous set of microstructure observations in the Gulf Stream made along a north–south track at 63°W by Oakey and Elliott (1977) in the fall of 1972 and the spring of 1974. Their casts, spaced ~20′ apart in latitude, were averaged over 100 m thick sections to examine the change in the bulk statistics of microstructure and finestructure across the Stream. Relatively constant levels (normalized by

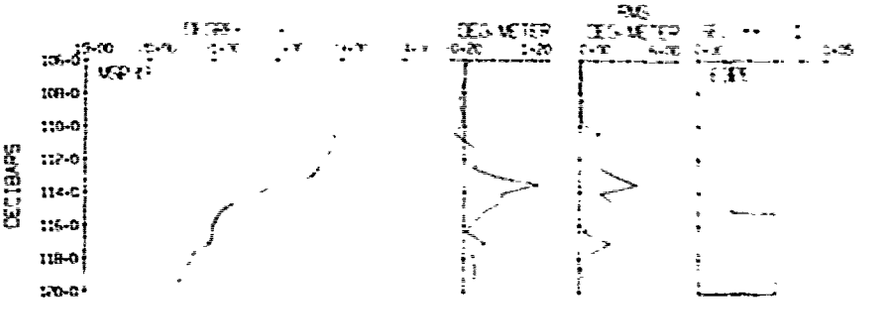

FIG. 18. Section from the Gulf Stream with the strongest microstructure. The SCIMP observations show banded structures on the same feature that suggest salt fingers.

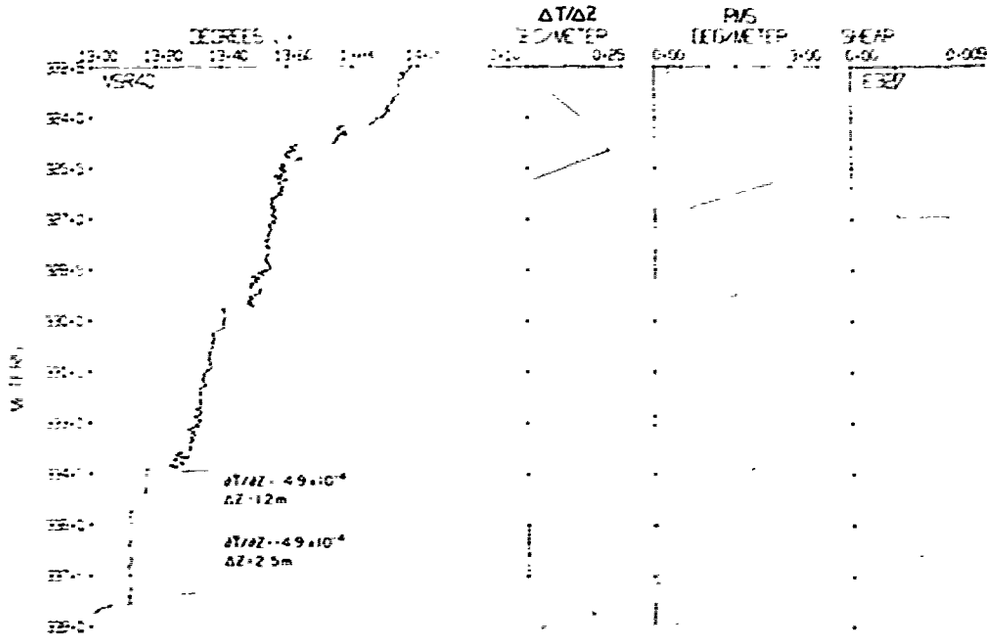

FIG. 19. Two sections that appear to be actively mixing lie above two thinner, nearly adiabatic regions. The evidence is not sufficient to distinguish mechanical mixing from salt fingering.

the mean gradients) were established over a wide range of depths and positions within water masses on the *T-S* diagram. The Cox numbers in the Stream, which they located from the isotherm slope, ranged from 20 to 520. Higher values were found in the slope water to the north. From the relatively constant ratio between the microstructure and fine-structure levels, they suggested that the dissipation of internal waves at finestructure features was a possible mechanism for generating the microstructure.

Although they did not examine the signatures in the profiles, from our observations we believe it likely that much of the activity they observed in both the Stream and the slope water was associated with double-diffusive activity on intrusions.

In view of the comparison that can now be made between the Gulf Stream and many other locations, we conclude that the parameterization of vertical turbulent transport in the Stream with eddy coefficient values similar to those used in models of the Equatorial Undercurrent, e.g., 10^{-2} m^2 s^{-1}, is not appropriate. If the double-diffusive contribution is removed and the remaining microstructure attributed to shear instabilities, then the regions with Cox numbers of 40 would give $K_z^T < 5 \times 10^{-1}$ m^2 s^{-1}, and possibly lower than 1×10^{-2} m^2 s^{-1} if some of the microstructure in monotonic regions is also due to salt fingering.

6. Summary and discussion

The interpretation of these observations has some implications for the large-scale dynamics of the ocean, as well as for the characterization of small-scale mixing. These two aspects are considered separately in the following summary and discussion.

a. Large-scale implications

1) Active turbulent mixing was occurring during FAME in localized regions immediately adjacent to the island of Bermuda. The microstructure measurements, at least in this instance, verified that the elevated finestructure levels found by HKS were in fact indications of active mixing and not just the products of previous mixing or intense internal wave strain. The mechanism producing this mixing could not be determined but HKS made a plausible demonstration that it was related to the flow field of three mesoscale eddies, or rings, impinging on the island.

Although the levels of mixing activity adjacent to Bermuda varied from 3 to 100 times those found in the thermocline, the areas involved were quite limited. If the levels and extent of strong mixing found in these observations are typical of island-induced effects, then, in view of the limited volume of water near islands compared to that in the thermocline, one must conclude that island-induced mixing is of minor importance on a global basis.

2) A very limited data set from the upper kilometer of the Sargasso Sea did not reveal any surprises when compared to more extensive observations in the subtropical gyre of the Pacific: the microstructure levels were significantly below those consistent with $K_z = 10^{-4}$ m^2 s^{-1}.

The Atlantic microstructure levels were equivalent to those found during the more active of the three cruises to the Pacific site. Although both locations were in subtropical gyres, the more western location of the Sargasso Sea site is in a region of higher energy in the eddy field than would be expected at the Pacific site. Much more extensive observations at both sites are required to determine whether a significant difference exists in the long-term-average Cox numbers.

3) After the identifiable signatures due to double diffusive activity on thermocline intrusions were removed, the remaining microstructure levels in the high-shear core of the Gulf Stream are much less than those consistent with the levels of small-scale turbulence assumed, i.e., $K_z = 10^{-2}$ m^2 s^{-1}, in models of the Stream. Our observations suggest levels of $K_z^T < 5 \times 10^{-5}$ m^2 s^{-1}, and possibly lower than 1×10^{-5} m^2 s^{-1} due to small-scale turbulence. Since vertical heat fluxes have been found to result from thermohaline intrusions (Turner, 1978; Gregg and McKenzie, 1979) it appears that this mechanism and not small-scale turbulence is the major agent for vertical, as well as lateral, heat and salt fluxes in the Gulf Stream.

The low levels of turbulent activity in the Gulf Stream, which were comparable to those in the Sargasso Sea, are particularly notable when compared to the 30 m thick patches in the Equatorial Undercurrent. Although the region of major activity in the Pacific Undercurrent was diffusively stable, the Cox numbers were up to 100 times larger than those in the sections of the Stream that did not contain intrusions. This situation agrees with the dynamical constraints on the two jets (P. Niiler, personal communication); a large turbulent vertical viscosity is necessary on the equator since the horizontal pressure gradient cannot be balanced by a lateral Corioles force. The Gulf Stream does not have this constraint.

4) A 135 m deep, turbulent mixed layer was found in the Sargasso Sea during a period with very low winds. Although auxiliary measurements, e.g., large-scale vertical and horizontal velocity and small-scale isotropy, were made the origin of the turbulence could not be determined; both free convection and the high mean shear within and across the base of the layer were possible driving forces.

b. Characterization of small-scale mixing processes

1) The intense microstructure near Bermuda was embedded in distinct steplike profiles. In these sections, unlike the situation in less energetic regions where the profile has very irregular gradient structures, it was possible to make a clear distinction between nearly adiabatic mixed regions and the interfaces between them. As one evidence of the steplike profiles, histograms of the gradients over scales of 1 m were markedly different from those in profiles from less active regions near Bermuda or the open ocean. Since the strain required to form these structures from a smooth profile by internal wave deformation is unreasonably high, the nearly homogenous regions must have been produced by mixing. Some of the interfaces between the well-mixed layers showed intense centimeter-scale inversions that suggest overturning activity. In these sections, and in some of the well-mixed layers, spectra of the temperature gradients showed extensive wavenumber bands with slopes of nearly $+1$ in the microstructure range, which are typical of active mixing.

These data show a more direct relationship between finestructure and microstructure than has been observed in previous data. When the microstructure levels from monotonic profiles were compared with those with thermohaline intrusions, Gregg (1975) found that using the finestructure variance (defined as the integral of the gradient spectrum from 0.01 to 1 cpm) provided a much better normalization of the data than did the Cox number. However, when only monotonic profiles from the same site were compared, the microstructure levels over 125 m thick sections varied by a factor of 100 (Gregg, 1977b) while in the same sections there was no statistically significant variation in the finestructure level (Gregg, 1977a). The difference between the open ocean observations in the Pacific and the Bermuda results is that the mixing near the island was sufficiently sustained and produced regions in which the profile became fully mixed. Sequences of such well-mixed regions have not been found in the mid-gyre thermocline, implying that the mixing in these regions is not as sustained.

2) Isolated mixed layers up to 10 m thick having mean gradients as low as 10^{-4} °C m^{-1} were found in the main thermocline of the Sargasso Sea as well as near Bermuda and in the Gulf Stream. Similar structures may have been present in the Pacific data but were not detected due to a less sensitive, and less stable, temperature circuit. In view of the low efficiency of mixing in stratified fluids, the existence of these layers implies that sustained turbulent mixing events have occurred, or the existence of an isolated layer formed by salt fingering.

3) Following verification of the Kolmogorov spectrum using measurements by a towed body in a turbulent tidal channel by Grant *et al.* (1962) there was optimism that the "universal" form would be commonly found in the upper ocean. When the measurements were extended to the ocean, Stewart and Grant (1962) found difficulties due to vibrations of the towed body when operated under surface waves and to the much lower ϵ levels. Based on the tidal channel results, they proposed a procedure

to obtain an upper limit to ϵ by "obtaining any measure of the spectral level at any wavenumber" if it could be assumed that the "universal" spectral form was actually present in the data. The Grant *et al.* (1968) evaluation of the scaling constants β_1 and q was based on fitting the universal forms to the data to obtain ϵ and χ. However, in these cases there were extensive low wavenumber regions that did match the universal forms.

The difficulty with this approach is that there has not as yet been established any understanding of what conditions are sufficient for the universal form, particularly in the roll-off portion of the high wavenumber spectrum, neither is there a criterion for deciding when a portion of a spectrum exhibits a fit that is good enough. In view of the evidence accumulated over the last decade that shows discrepancies with the various universal forms (Nasmyth, 1970; Gregg *et al.*, 1973; Elliott and Oakey, 1976; Gregg, 1977b), further application of the Stewart and Grant (1962) approach to obtaining ϵ and χ by fitting to a limited portion of a spectrum seems to be unwarranted and unnecessary since these parameters can be obtained by direct integration of the spectra.

The mixed-layer spectra reported here showed a much closer fit to the universal spectral forms than those from the thermocline or from some of the other mixed-layer observations. Although the scaling of the temperature spectrum in the $-5/3$ range showed excellent agreement with the value given by Grant *et al.* (1968) that in the viscous-convective range did not, even though the supporting measurements gave evidence for isotropy and large-scale stirring of the mixed layer. More extensive measurements, e.g., time series, of all of the parameters measured will be required to determine whether this is a general or a particular result.

4) The existence of active double diffusive signatures on the intrusions in the core of the Gulf Stream shows that high shear levels do not necessarily inhibit the formation of these structures. The possibility of such inhibition had been viewed as a limitation on the applicability of double diffusive laboratory experiments to the ocean.

The interpretation of the microstructure data was greatly aided by the simultaneous use of several instruments and the HKS surveys adjacent to Bermuda. Further progress will require more detailed horizontal information than was done in FAME and integration of the different measurement techniques into a single instrument; the short horizontal scales of the finestructure and the vertical displacements by the internal wave field make comparison of the results from individual instruments very difficult, particularly in the main thermocline.

Acknowledgments. In doing this work, we have benefited from the efforts and cooperation of many people. The extraordinary efforts of Mr. Art Pederson in the re-design and operation of MSR were crucial. Messrs. Le Olson and Eric Aagaard made valuable contributions in the mechanical design of the vehicle and probes, and Ms. Gaye Anthony has performed the data analysis with skill and dedication. Mr. Bob Drever was responsible for the operation of EMVP with essential support from Messrs. Ed. Denton and Art Bartlett. Mr. John Dunlap has performed the EMVP data analysis.

In this analysis, we have benefited from discussions and data exchanges with Drs. Nelson Hogg, Ann Gargett and Sandy Williams.

The work was supported by the Office of Naval Research, Code 481, under Contract N00014-75-C00502 to APL/UW and N00014-79-C-0071 NR 083-004 to WHOI.

REFERENCES

Armi, L., 1978: Some evidence for boundary mixing in the deep ocean. *J. Geophys. Res.* **83**, 1971–1979.

Baker, D. J., Jr., 1971: Density gradients in a rotating stratified fluid: Experimental evidence for a new instability. *Science* **172**, 1029–1031.

Batchelor, G. K., 1959: Small-scale variation of convected quantities like temperature in turbulent fluid. Part I. General discussion and the case of small conductivity. *J. Fluid Mech.*, **5**, 113–133.

Caiman, J., 1977: Experiments on high Richardson number instability of a rotating stratified shear flow. *Dyn. Atmos. Oceans*, **1**, 277–297.

Crawford, W. R., and T. R. Osborn, 1979: Microstructure measurements in the Atlantic Equatorial Undercurrent. *Deep-Sea Res.* (in press).

Desaubies, Y. J. F., and M. C. Gregg, 1978: Observations of internal wave vertical velocities by a free fall vehicle. *Deep-Sea Res.*, **25**, 933–946.

Elliott, J. A., and N. S. Oakey, 1976: Spectrum of small-scale oceanic temperature gradients. *J. Fish. Res. Bd. Can.*, **33**, 2296–2306.

Erickson, C. C., 1978: Measurements and models of fine structure, internal gravity waves, and wave breaking in the deep ocean. *J. Geophys. Res.*, **83**, 2989–3009.

Gargett, A. E., T. B. Sanford, and T. R. Osborn, 1979: Surface mixing layers in the Sargasso Sea. *J. Phys. Oceanogr.*, **9**, 1090–1111.

Garrett, C., and W. Munk, 1975: Space-time scales of internal waves: A progress report. *J. Geophys. Res.*, **80**, 291–297.

Gibson, C. G., and W. H. Schwarz, 1962: The universal equilibrium spectra of turbulent velocity and scalar fields. *J. Fluid Mech.*, **16**, 365–384.

Grant, H. L., R. W. Stewart, and A. Moilliet, 1962: Turbulence spectra from a tidal channel. *J. Fluid Mech.*, **12**, 241–268.

——, B. A. Hughes, W. M. Vogel, and A. Moilliet, 1968: The spectrum of temperature fluctuations in turbulent flow. *J. Fluid Mech.*, **34**, 423–442.

Gregg, M. C., 1968: Mechanical stirring and salt fingers. WHOI Summer Institute Geophys. Fluid Dynamics Reports, Vol. II.

——, 1975: Microstructure and intrusions in the California Current. *J. Phys. Oceanogr.*, **5**, 253–278.

——, 1976a: Fine and microstructure observations during the passage of a mild storm. *J. Phys. Oceanogr.*, **6**, 528–555.

——, 1976b: Temperature and salinity microstructure in the Pacific equatorial undercurrent. *J. Geophys. Res.*, **81**, 1180–1196.

——, 1977a: A comparison of finestructure spectra from the main thermocline. *J. Phys. Oceanogr.*, **7**, 33–40.
——, 1977b: Variations in the intensity of small-scale mixing in the main thermocline. *J. Phys. Oceanogr.*, **7**, 436–454.
——, 1979: The effects of bias errors and system noise on parameters computed from *C, T, P,* and *V* profiles. *J. Phys. Oceanogr.*, **9**, 199–217.
——, and C. S. Cox, 1972: The vertical microstructure of temperature and salinity. *Deep-Sea Res.*, **19**, 355–376.
——, C. S. Cox, and P. W. Hacker, 1973: Vertical microstructure measurements in the central North Pacific. *J. Phys. Oceanogr.*, **3**, 458–469.
——, and J. H. McKenzie, 1979: Cross isopycnal intrusions. *Nature*, **280**, 310–311.
Hogg, N. G., 1972: Steady flow past an island with applications to Bermuda. *Geophys. Fluid Dyn.*, **4**, 55–81.
——, E. J. Katz, and T. B. Sanford, 1978: Eddies, islands and mixing. *J. Geophys. Res.*, **83**, 2921–2938.
Koop, C. Gary, 1976: Instability and turbulence in a stratified shear layer. Ph.D. dissertation, Dept. Aerospace Engineering, University of Southern California, USCAE 134, 245 pp.
Lange, E., 1974: Decay of turbulence in stratified salt water. Ph.D. dissertation, University of California, San Diego, 157 pp.
Linden, P. F., 1971: Salt fingers in the presence of grid-generated turbulence. *J. Fluid Mech.*, **49**, 611–624.
Munk, W. H., 1966: Abyssal recipes. *Deep-Sea Res.*, **13**, 707–730.
Nasmyth, P. W., 1970: Oceanic turbulence. Ph.D. dissertation, University of British Columbia, 69 pp.
Niiler, P. N., 1975: Deepening of the wind-mixed layer. *J. Mar. Res.*, **33**, 405–422.
Oakey, N. S., and J. A. Elliott, 1977: Vertical temperature gradient structure across the Gulf Stream. *J. Geophys. Res.*, **82**, 1369–1380.
Orlanski, J., and M. D. Cox, 1972: Baroclinic instability in ocean currents. (Unpublished manuscript).
Osborn, T. R., and C. S. Cox, 1972: Oceanic finestructure. *Geophys. Fluid Dyn.*, **3**, 321–345.
——, and L. Bilodeau, 1980: Temperature microstructure in the equatorial Atlantic. *J. Phys. Oceanogr.*, **10**, 66–82.
Pederson, A. M., 1969: An accurate, low-cost temperature sensor. *Trans. Marine Technology Society Temperature Measurements Symp.*, 135–154.
Robinson, A. R., 1966: An investigation into the wind as the cause of the equatorial undercurrent. *J. Mar. Res.*, **24**, 179–203.
Sanford, T. B., R. G. Drever, and J. H. Dunlap, 1978: A velocity profiler based on the principles of geomagnetic induction. *Deep-Sea Res.*, **25**, 183–210.
Stewart, R. W., and H. L. Grant, 1962: Determination of the rate of dissipation of turbulent energy near the sea surface in the presence of waves. *J. Geophys. Res.*, **67**, 3177–3180.
Thorpe, S. A., 1973: Experiments on instability and turbulence in a stratified shear flow. *J. Fluid Mech.*, **73**, 731–751.
Turner, J. S., 1968: The behavior of a stable salinity gradient heated from below. *J. Fluid Mech.*, **33**(Part I), 183–200.
Wunsch, C., 1969: Progressive internal waves on slopes. *J. Fluid Mech.*, **35**, 131–144.
——, 1970: On oceanic boundary mixing. *Deep Sea Res.*, **17**, 293–301.
——, 1972: Temperature microstructure on the Bermuda slope with application to the mean flow. *Tellus*, **24**, 350–367.

JOURNAL OF GEOPHYSICAL RESEARCH, VOL. 85, NO. C5, PAGES 2704–2710, MAY 20, 1980

On the Variability of Surface Temperature Fronts in the Western Pacific, as Detected by Satellite

GUNNAR I. RODEN

Department of Oceanography, University of Washington, Seattle, Washington 98195

The variability of sea surface temperature fronts in the western North Pacific is investigated by using satellite and shipboard data On a 100 km by 100 km grid and on a time step of 1 week the satellite recognizes the subarctic front, the subtropical fronts, and one to two fronts associated with the Kuroshio intrusion. The subarctic front is centered near 42°N and can be seen throughout the year. Frontal gradients vary from 5°C/100 km in winter to 2°C/100 km in summer, and deviations from the mean latitude are small. The subtropical front is seen only from late fall to early summer in the latitude range between 28°N and 33°N. Maximum frontal gradients are of the order of 3°C/100 km and occur in late spring. Kuroshio fronts occur sporadically in the latitude range between 35°N and 37°N. Because of the meandering nature of this current and of the rather coarse resolution used, these fronts are not consistently seen. The findings by satellite are in broad agreement with those derived from shipboard observations employing a similar sampling scheme. To study the relationship between satellite-derived temperature fronts and atmospheric flow patterns, the subtropical front was related to the configuration of the wind stress field. It was found that the oceanic front occurred near a persistent atmospheric front in a region where the vorticity and deformation of the wind stress change sign.

INTRODUCTION

The western North Pacific is noted for three principal fronts. In the north there is the subarctic front, which meanders between latitudes 40°N and 43°N and extends from Japan toward the central Pacific. It is clearly defined on satellite infrared images [*Legeckis*, 1978], on surface temperature maps (contoured maps of sea surface temperature west of longitude 180° [*Japan Meterological Agency*, 1956–1979]), and on hydrographic sections [*Uda*, 1938; *Roden*, 1972]. Between 34°N and 38°N the Kuroshio front is encountered, which extends in a meandering fashion east-northeastward from Cape Inubozaki in central Japan to the Emperor seamount chain at longitude 170°E. This front is seen clearly in high-resolution satellite infrared images [*Legeckis*, 1978], aircraft surveys [*Cheney*, 1977], and shipboard observations [*Kawai*, 1972; *Roden*, 1975] during the colder part of the year. During summer, when intense solar radiation diminishes the horizontal temperature contrast at the sea surface, the Kuroshio front cannot always be detected by remote sensing or by analyzing surface observations collected by ships, though this front remains well defined below 50 m. In the south the subtropical front is found. At the sea surface this front exists only during winter and spring, when it is encountered between latitudes 28°N and 33°N. Observations by satellite [*National Environmental Satellite Service*, 1977–1978] indicate that it occurs intermittently and that its position varies widely within the above mentioned latitude limits.

The Kuroshio front results from the large-scale intrusion of warm and saline water into higher latitudes. The front is deep, highly baroclinic, and in quasi-geostrophic balance. The strongest temperature contrasts occur at the northern boundary of this intrusion. The southern boundary of this intrusion is normally not visible in the surface temperature field because of the small temperature contrasts. The subarctic and subtropical fronts are related to Ekman-type convergence and deformation [*Roden*, 1975]. They are typically shallow, well defined in temperature and salinity, but only weakly baroclinic. The weak baroclinicity results from the near balance of the horizontal temperature and salinity gradients such that the resulting horizontal density gradients are small. At the sea surface the subarctic front is a temperature and salinity front throughout the year, while the subtropical temperature front vanishes during summer because of intense solar radiation.

It is of interest to investigate the variability of these fronts as seen by satellite, to compare the results to those obtained in presatellite days, and to relate the fronts to the atmospheric flow field.

DATA

The basic data used in this investigation are (1) weekly sea surface temperature maps based on infrared measurements on earth-orbiting satellites, known as Gosstcomp (Global Operational Sea Surface Temperature Computation) and issued by the *National Environmental Satellite Service* [1977–1978]; (2) 10-day sea surface temperatures based on shipboard observations [*Japan Meteorological Agency*, 1975, 1976*a*, *b*] (the 1975 atlas contains monthly normal sea surface temperatures for 1956–1970, digitized on a 1° latitude-longitude grid; the 1976*a* atlas contains 10-day normal sea surface temperatures for January–June 1956–1970 and standard deviations of monthly normal sea surface temperatures, both digitized on a 1° latitude-longitude grid; the 1976*b* atlas contains 10-day normal sea surface temperatures for July–December 1956–1970 and maximum and minimum values of monthly mean sea surface temperatures, all digitized on a 1° latitude-longitude grid), and (3) northern hemisphere sea level atmospheric pressure maps issued daily by the *National Weather Service* [1977–1978]. The maps were digitized at 1° latitude-longitude intersections for use in further computations.

A description of the methods used to reduce infrared measurements from satellite to sea surface temperatures is given by *Brower et al.* [1976]. Basically, retrieval temperatures are corrected for effects of atmospheric attenuation by utilizing time coincident measurements of a vertical temperature profile radiometer. The input into the Gosstcomp sea surface temperature maps is based on averaging these data in both space and time. The spatial averaging is done in 100 km by

Paper number 9C1729.
0148-0227/80/009C-1729$01.00

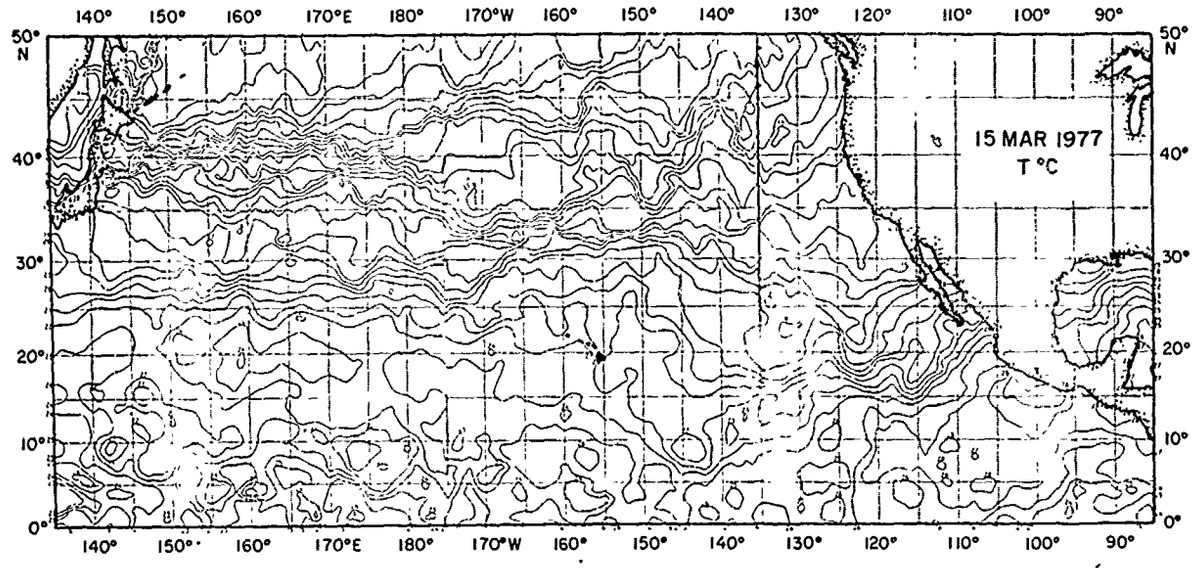

Fig. 1. Satellite map of sea surface temperature for March 15, 1977, based on Gosstcomp maps [*National Environmental Satellite Service*, 1977–1978].

100 km squares, and the time averaging is done over a period of 1 week. Thus only large-scale and persistent fronts occur on these maps. Small-scale and transient meandering fronts are eliminated by the averaging procedure.

Errors arise principally from the uncertainties connected with correcting for atmospheric attenuation [*Barnett et al.*, 1979]. The accuracy of the horizontal temperature gradient is difficult to estimate from the available information. When the horizontal temperature gradient occurs in an area of uniform atmospheric attenuation, the uncertainty is of the order of 0.5°–1°C/100 km [*Chahine et al.*, 1977]. When the horizontal temperature gradient lies in a region of variable atmospheric attenuation, the uncertainty is likely to be larger.

Results From Satellite Observations

Satellite views of sea surface temperature in the North Pacific are shown in Figures 1 and 2 for both winter and summer. Temperatures are resolved on a 100 km by 100 km grid. In the western Pacific, two fronts stand out clearly: the subarctic front between 41°N and 44°N and the subtropical front between 25°N and 30°N (winter) and 28°N and 33°N (summer). Both fronts are about 150–200 km wide and are well defined between longitudes 140°E and 180°E. Meridional gradients dominate. At the subarctic front these are of the order of 3°C/100 km, and at the subtropical front they are up to 2°C/100 km. The Kuroshio front is seen only vaguely in the Gosstcomp maps: on March 15, 1977, it is visible between 35°N and 38°N and 155°E and 175°E, while on June 14, 1977, it is seen mostly off central Japan. The sporadic visibility of the Kuroshio front in the Gosstcomp maps is believed to be due to spatial and temporal averaging procedures, which tend to suppress transient meandering features on subgrid scales.

The week-to-week variability of the meridional temperature gradient along longitude 165°E is shown in Figure 3.

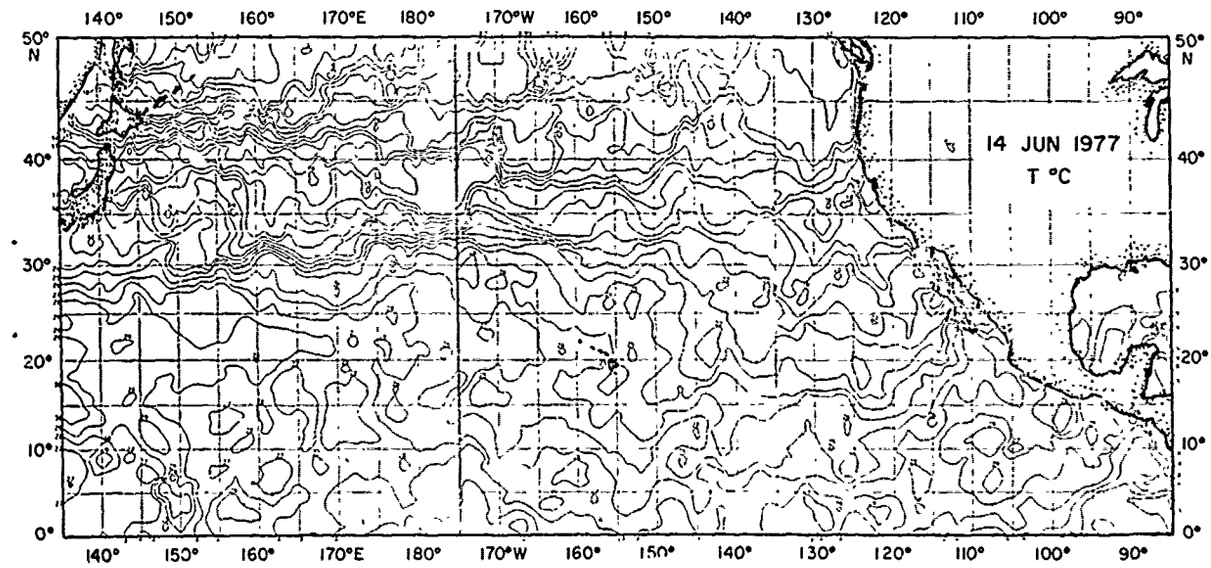

Fig. 2. Satellite map of sea surface temperature for June 14, 1977, based on Gosstcomp maps [*National Environmental Satellite Service*, 1977–1978].

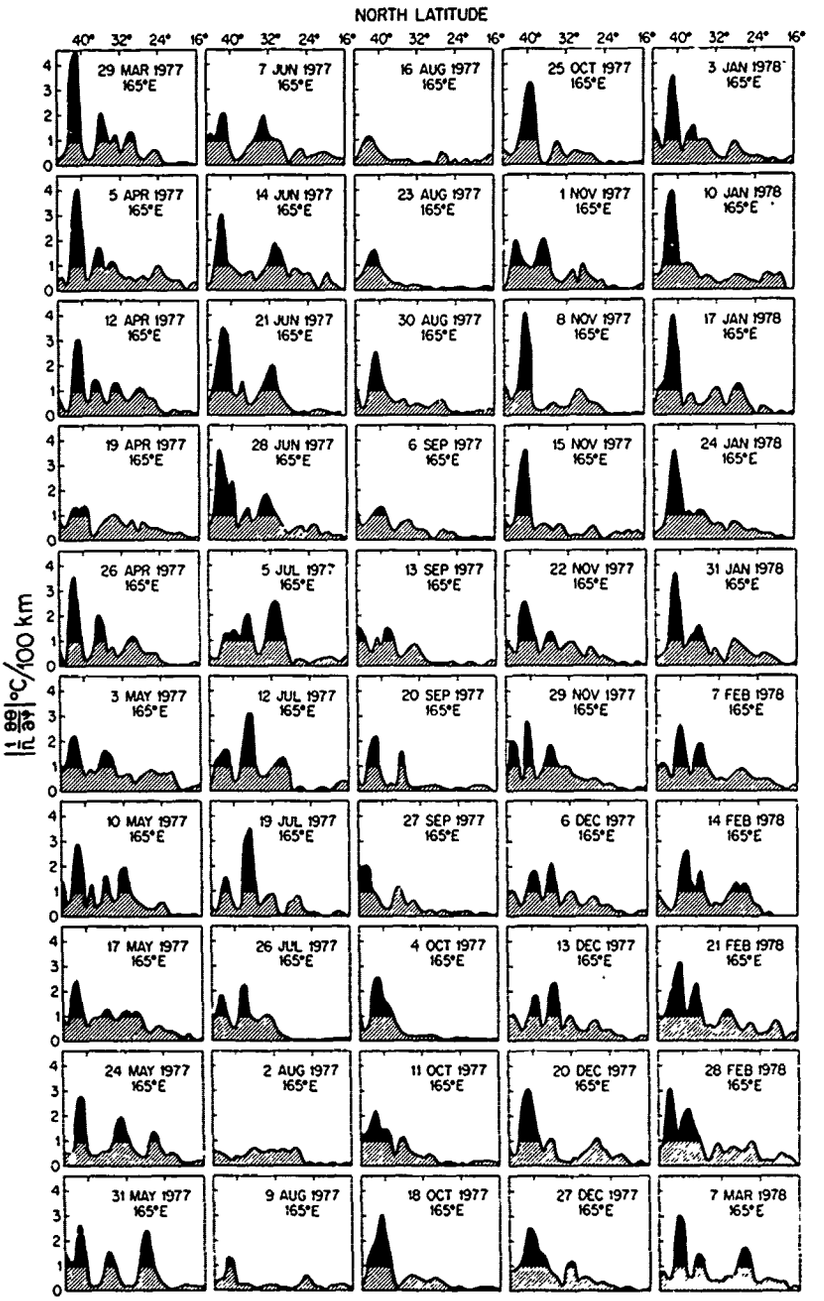

Fig. 3. Week-to-week variability of the magnitude of the meridional temperature gradient based on Gosstcomp maps [*National Environmental Satellite Service*, 1977–1978]. Gradients exceeding 1°C/100 km are black.

This longitude was chosen because fronts are well defined here and because of previous detailed hydrographic work in that area [*Roden*, 1972]. Gradients in excess of 1°C/100 km (black) are considered to be significant for locating the major fronts.

At any one time, one to four peaks stand out, where the meridional temperature gradient exceeds 1°C/100 km. The northernmost peak, between latitudes 41°N and 44°N, is associated with the subarctic front and is present throughout the year. Maximum frontal intensities occur in winter, when temperature gradients reach 5°C/100 km. Minimum intensities are found in summer, when temperature gradients rarely exceed 2°C/100 km. There is comparatively little latitudinal movement of the subarctic front during the course of a year; it is centered near 42°N and does not appear to move more than 150 km from its mean position.

The meridional temperature gradient peaks between 34°N and 38°N are associated with the Kuroshio intrusion. At intermittent times, one or two peaks with temperature gradients up to 3°C/100 km are seen. The existence of double peaks (such as those on May 10, 1977) indicates meandering of the Kuroshio intrusion front. The sporadic occurrence of double peaks suggests that the meanders are not fully resolved on the 100 km by 100 km grid scale used here. (The meanders are better seen on very high resolution infrared imagery where a 1 km by 1 km grid is used [*Legeckis*, 1978], for which, however, no time series exist.)

The subtropical front is encountered between latitudes 28°

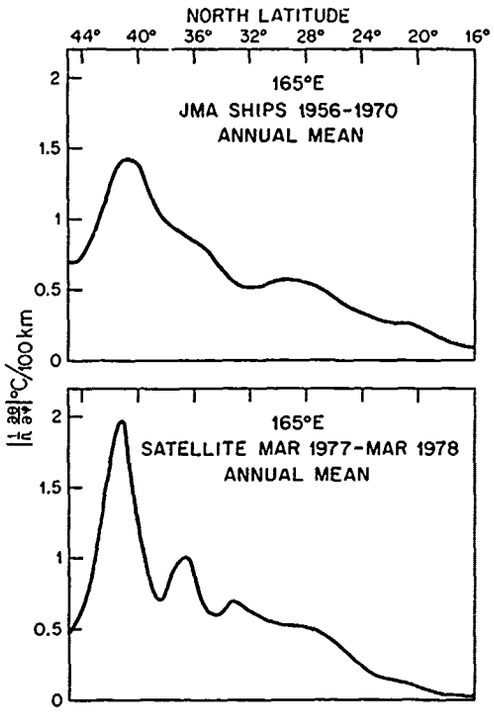

Fig. 4. Comparison of the magnitudes of meridional temperature gradients based on data collected (top) in presatellite days and (bottom) by NOAA satellites.

and 33°N. The front is strictly seasonal in character. It is best developed between March and July, when temperature gradients are about 2°C/100 km. It is not found at the sea surface in summer and early fall, and it starts to re-form with the approach of winter. The position of the subtropical front varies widely within the above stated latitude interval.

Comparison Between Satellite and Shipboard Results

To make a valid comparison, it is necessary to employ a similar sampling grid and to sample at approximately the same time intervals. The 10-day mean charts of sea surface temperature sampled at 1° latitude-longitude intersections [*Japan Meterological Agency*, 1956–1979] are the closest data set compatible with the Gosstcomp satellite-derived sea surface temperatures.

A comparison of the annual mean meridional sea surface temperature gradients along longitude 165°E is shown in Figure 4. There is agreement between the two independent data sets. The strongest gradients are associated with the subarctic front, which in both cases is centered near latitude 42°N. The ship observations give 1.5°C/100 km for the maximum gradient, while the satellite observations give a slightly higher gradient, namely, 2°C/100 km. The Kuroshio front is not resolved in the ship observations, but it appears as a small peak at latitude 37°N in the satellite observations. The temperature gradient associated with this peak is 1°C/100 km. South of latitude 32°N the magnitude of the meridional temperature gradient decreases gradually with decreasing latitude, at approximately the same rate in both data sets. The conclusion is that on time scales of 1 year and longer the gradients derived by satellite are compatible with those derived from shipboard observations in presatellite days.

To see whether such an agreement also exists at shorter time intervals, a comparison was made of the meridional temperature gradients at 165°E on weekly time scales. The results are shown in Figure 5. Both the satellite data and the ship data clearly indicate the subarctic front at latitude 42°N and the subtropical front at 31°N. The shapes of the curves are similar, though the peaks in the satellite data are slightly higher than those in the ships data. Disagreement exists, however, in regions of weak meridional temperature gradients, such as near 20°N, which may result from satellite errors (about 0.5°C/100 km), insufficient ship observations in low latitudes, or both.

Aspects of the Formation of Large-Scale Oceanic Fronts

An initially inhomogeneous medium is necessary for fronts to occur. The ocean is rendered horizontally inhomogeneous by large-scale geographical variations of radiative and evaporative heat fluxes that set up primary temperature gradients. These primary gradients are subsequently concentrated into frontal zones by convergence and deformation in the oceanic flow field [*Newton*, 1978]. Oceanic frontogenesis is dependent thus on both the configuration of the flow field and upon the initial temperature stratification. The dependence upon both of these factors cannot be overemphasized. A given favorable configuration of the flow field (for example, a convergence zone) will lead to strong frontogenesis in some geographical areas and weak or no frontogenesis in others, depending upon the primary thermal gradients in the area. The annual appearance and disappearance of the subtropical surface temperature front can be understood in these terms. In spring, when significant primary thermal gradients exist in the latitude belt between 25°N and 35°N (primarily as a result of gradients in radiative heat flux that have persisted through the previous fall and winter), surface temperature fronts are well defined in satellite views (Figure 3). In late summer and early fall, well defined in satellite views (Figure 3). In late summer and early fall, when primary thermal gradients are small (because the radiative heat flux field is flat), no distinct fronts are seen in this latitude range. Because of the seasonal variation of the primary thermal gradients, atmospheric disturbances during

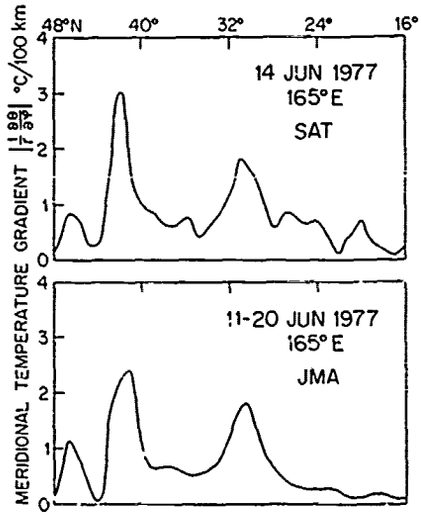

Fig. 5. Comparison of the magnitudes of meridional temperature gradients as seen by (top) satellite and (bottom) ships in mid-June 1977.

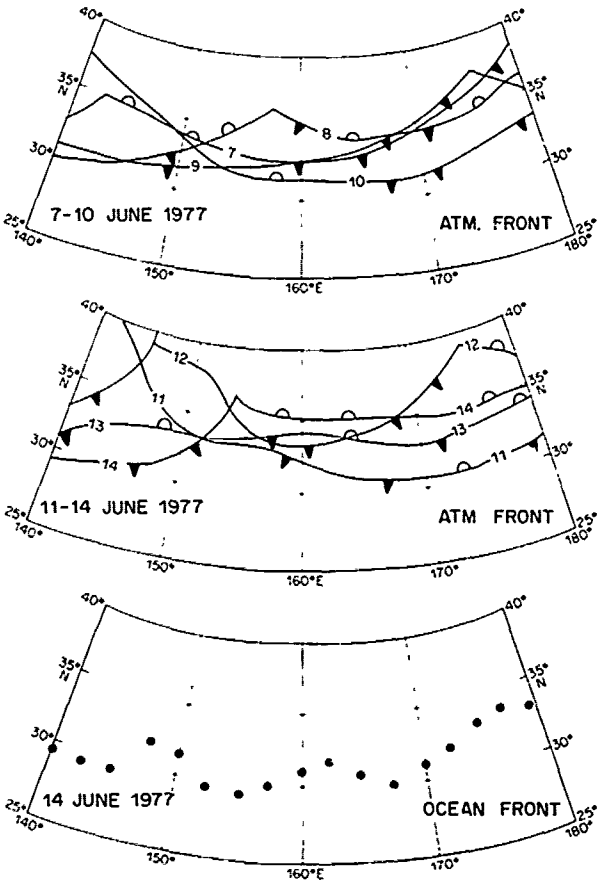

Fig. 6. Location of the sea surface temperature front (bottom) in relation to atmospheric fronts (top and middle) in mid-June 1977.

winter and spring have a greater potential for creating strong fronts than those in summer and fall.

Oceanic Fronts in Relation to Atmospheric Fronts and the Wind Stress Field

A definite relationship between surface temperature fronts and the wind stress field can be expected only where Ekman dynamics dominates the oceanic flow field and where a primary horizontal temperature gradient exists. The relationship can be expected to be most clear-cut in regions of a shallow pycnocline so that the wind effect is concentrated in a shallow upper layer. Much less energy is then required to move the water and deform the velocity field than is required in the case of a deep pycnocline. Such conditions are encountered in the subtropics during early summer. Consider the period June 7–14, 1977. During that period, persistent atmospheric fronts were encountered in the latitude range between 30°N and 35°N, as is shown in Figure 6. Long-lasting fronts in the atmosphere have been known to leave a signature in the ocean [*Shapiro*, 1978], and it comes therefore as no surprise that an oceanic front (dotted) is found near the atmospheric frontal zone.

Atmospheric fronts are regions of concentrated wind stress gradients, and because of the importance of such gradients in Ekman dynamics it is of interest to study briefly the configuration of the wind stress field during the period June 7–14, 1977. The gradients of the wind stress are best expressed in terms of the kinematic quantities of divergence, vorticity, shear deformation, and normal deformation [*Kirwan*, 1975]. These quantities are shown in Figure 7, which is based on the stress of the quasi-geostrophic wind evaluated on a 1° latitude-longitude grid and computed from

$$\tau = \gamma \rho_a \mathbf{v}_a |\mathbf{v}_a| \tag{1}$$

$$\mathbf{v}_a = -\frac{f \nabla_H p_a \times \mathbf{i}_z + k \nabla_H p_a}{\rho_a (f^2 + k^2)}$$

where τ and $\mathbf{v}_a$ are the wind stress and wind velocity vectors at the sea surface, respectively, γ is the drag coefficient ($1.5 \cdot 10^{-3}$), f is the Coriolis parameter, p_a is atmospheric pressure, ρ_a is air density, $\mathbf{i}_z$ is a vertical unit vector, and k is the surface friction coefficient for the wind ($2.5 \cdot 10^{-5}$ s^{-1}), which allows for cross-isobar flow (12°–18° in mid-latitudes) toward lower pressures.

The outstanding feature in Figure 7 is the bandlike structure of the wind stress field. Bands of opposite sign occur pairwise and in close proximity to each other. The atmospheric frontal zone between latitudes 30°N and 35°N is characterized by positive vorticity and negative shear deformation, of about equal magnitude, as well as by weaker convergence and positive normal deformation. South of the atmospheric frontal

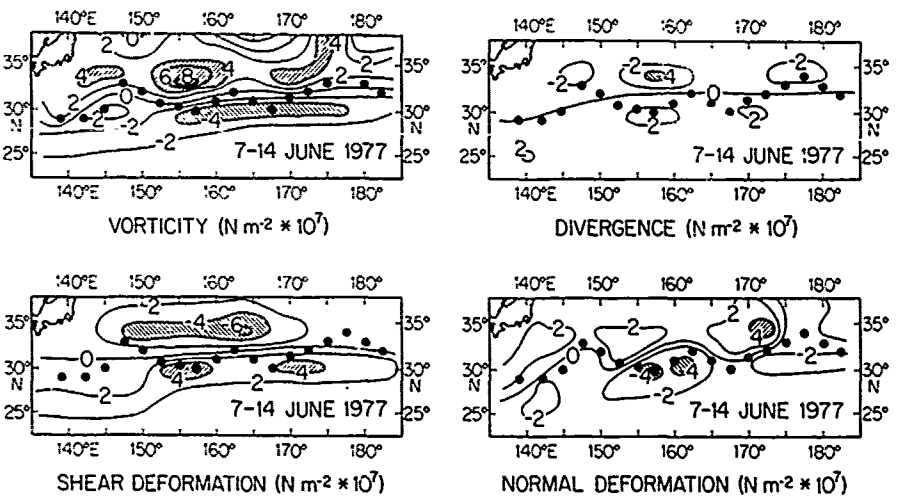

Fig. 7. Location of the sea surface temperature front (dotted) in relation to the configuration of the wind stress field, expressed in terms of vorticity, divergence, shear deformation, and normal deformation.

zone, between latitudes 25°N and 30°N, the opposite is found. The vorticity and normal deformation are negative, the shear deformation is positive, and there is divergence instead of convergence.

The oceanic front (dotted) occurs where the wind stress vorticity, deformation, and divergence change sign, that is, at the boundary of atmospheric circulation systems. Because positive vorticity implies upward motion and negative vorticity downward motion, the oceanic front is positioned between upwelling and downwelling regions.

To investigate how a wind stress field such as that presented in Figure 7 would change the intensity of an existing temperature gradient, consider the following simple but illustrative case. Assume that the atmospheric forcing consists solely of a geographically variable wind stress acting upon an initially uniform temperature gradient. This can be expressed mathematically by [*Roden*, 1977]

$$\frac{\partial}{\partial t}|\nabla_H \theta| = \frac{\partial v_n}{\partial n}|\nabla_H \theta| \tag{2}$$

where t is time, $|\nabla_H \theta|$ is the magnitude of the horizontal temperature gradient, and v_n is the velocity component normal to the front, the normal being taken toward increasing temperatures. A simple integration leads to

$$\frac{|\nabla_H \theta|}{|\nabla_H \theta|_0} = \exp\left[-\int_0^T \frac{\partial v_n}{\partial n}\, dt\right] \tag{3}$$

where $|\nabla_H \theta|_0$ is the magnitude of the initial temperature gradient. Concentration of this gradient depends clearly upon the time history of the velocity gradient normal to the front. Concentration will occur when the integral in the exponent is negative, that is, when the velocity component normal to the front decreases in the direction of the front over a period of time. The intensity of an existing front will double when the integral reaches a value of $-\ln 2 = -0.693$. To relate the doubling time to the configuration of the wind stress field, it is necessary to parameterize the Ekman flow by

$$\mathbf{v}_H = \tau_H/\rho f D \times \mathbf{i}, \tag{4}$$

where $\mathbf{v}_H$ is the water velocity, ρ is the water density, and D is the mixed layer depth, and to express the normal gradient of the normal velocity component in terms of wind stress vorticity and deformation. (Pure rotation does not contribute toward the concentration of velocity gradients; hence a term proportional to the divergence of the wind stress does not appear in the equation below.)

$$\begin{aligned}-\frac{\partial v_n}{\partial n} = &-\frac{1}{2}\left[\frac{1}{r\cos\phi}\frac{\partial}{\partial\lambda}\left(\frac{\tau_\phi}{\rho f D}\right) - \frac{1}{r}\frac{\partial}{\partial\phi}\left(\frac{\tau_\lambda}{\rho f D}\right) + \frac{\tau_\lambda}{\rho f D}\frac{\tan\phi}{r}\right] \\ &+ \frac{1}{2}\left[\frac{1}{r\cos\phi}\frac{\partial}{\partial\lambda}\left(\frac{\tau_\phi}{\rho f D}\right) + \frac{1}{r}\frac{\partial}{\partial\phi}\left(\frac{\tau_\lambda}{\rho f D}\right) + \frac{\tau_\lambda}{\rho f D}\frac{\tan\phi}{r}\right]\cos 2\alpha \\ &- \frac{1}{2}\left[\frac{1}{r\cos\phi}\frac{\partial}{\partial\lambda}\left(\frac{\tau_\lambda}{\rho f D}\right) - \frac{1}{r}\frac{\partial}{\partial\phi}\left(\frac{\tau_\phi}{\rho f D}\right) - \frac{\tau_\phi}{\rho f D}\frac{\tan\phi}{r}\right]\sin 2\alpha\end{aligned} \tag{5}$$

where r is the earth's radius, λ is longitude, ϕ is latitude, and α is the angle between the tangent to the front and the east direction. The first right-hand term denotes the convergence of Ekman transports, the second indicates the normal deformation of Ekman transports, and the third describes the shear deformation of Ekman transports For predominantly zonally oriented fronts, such as the subtropical front, the last term is small. From (3) and (5) it can be concluded then that existing thermal gradients will intensify most rapidly where the wind stress vorticity is strongly negative and the shear deformation of the wind stress is strongly positive. For the case of June 1977 this occurs between latitudes 28°N and 30°N, slightly to the south of the existing temperature front (Figure 7). In this region both the vorticity and the shear deformation of the wind stress act frontogenetically, and each term is of the order of $4 \cdot 10^{-7}$ N m^{-2}, yielding for the normal derivative of Ekman flow $2.5 \cdot 10^{-7}$ s^{-1}, in view of (5). This horizontal velocity shear would have to be maintained for a month to double the intensity of the initial temperature gradient. Thus on 100-km scales, considered here, substantial time is required to change the intensity of a front by a factor of 2. This is to a certain degree also borne out in satellite observations, in which the weekly changes of the intensity of the subtropical front are much less than a factor of 2.

The above calculations are valid only for shallow fronts dominated by Ekman dynamics. Fronts that are deep and are related to deformation and convergence fields of inertial and geostrophic flow, such as the Kuroshio fronts, can be expected to have different time scales for doubling their intensity. At present, these time scales cannot be estimated reliably because of a lack of adequate field observations.

CONCLUSIONS

The following conclusions can be drawn from an analysis of sea surface temperature fronts derived by satellite and ship, utilizing a sampling grid of 100 km and a time step of about 1 week:

1. In the western North Pacific the satellite recognizes the subarctic front, the subtropical front, and, occasionally, the Kuroshio front.
2. The annual mean position of the subarctic front at 165°E is near 42°N. Deviations from the mean position are small. The frontal gradients vary between 2°C/100 km and 5°/100 km, being weakest in summer and strongest in winter.
3. The subtropical front is defined clearly only from late fall to early summer, during which time it is found between latitudes 28°N and 33°N. Its intensity is strongest in spring, when the thermal gradients reach 3°C/100 km.
4. The Kuroshio front, when seen, occurs between 35°N and 37°N. One or two peaks, with gradients up to 3°C/100 km, are found at 165°E. Double peaks are probably associated with meanders of the Kuroshio, known to exist from previous hydrographic surveys.
5. On annual time scales, agreement exists between the fronts seen by satellite and those derived from shipboard observations.

The following conclusions can be drawn from a study of the atmospheric forcing of the subtropical front:

1. The subtropical oceanic front occurs near a persistent atmospheric front.
2. With respect to the configuration of the wind stress field the subtropical front is located where the vorticity, deformation, and divergence of the wind stress change sign.
3. A considerable amount of time is required to double the intensity of an existing thermal gradient by wind action. On 100-km scales, considered here, the doubling time is of the

order of 1 month for a typical horizontal Ekman velocity shear of $2.5 \cdot 10^{-7}$ s^{-1}.

Acknowledgments. I am indebted to C. Barnes and M. Rattray for advice. The research was supported by the Office of Naval Research under contract N-00014-75-C-502, NR 083-012. Contribution 1139 from the Department of Oceanography, University of Washington.

REFERENCES

Barnett, T. P., W. C. Patzert, S. C. Webb, and B. R. Bean, Climatological usefulness of satellite determined sea surface temperatures in the tropical Pacific, *Bull. Amer. Meteorol. Soc., 60,* 197–205, 1979.

Brower, R. L., H. S. Gohrband, W. G. Pichel, T. L. Signore, and C. C. Walton, Satellite derived sea surface temperatures from NOAA spacecraft, *Tech. Memo. NESS 78,* 74 pp., Nat. Oceanic and Atmos. Admin., Washington, D.C., 1976.

Chahine, M. T., H. H. Aumann, and F. W. Taylor, Remote sounding of cloudy atmospheres, III, Experimental verifications, *J. Atmos. Sci., 34,* 758–765, 1977.

Cheney, R. E., Synoptic observations of the oceanic frontal system of Japan, *J. Geophys. Res., 82,* 5459–5468, 1977.

Japan Meteorological Agency, Ten-day marine report, Tokyo, 1956–1979.

Japan Meteorological Agency, *Oceanographic Atlas of the Northwestern Pacific,* Vol. 1, 90 pp., Tokyo, 1975.

Japan Meteorological Agency, *Oceanographic Atlas of the Northwestern Pacific,* Vol. 2, no. 1, 112 pp., Tokyo, 1976*a*.

Japan Meteorological Agency, *Oceanographic Atlas of the Northwestern Pacific,* Vol. 2, no. 2, 122 pp., Tokyo, 1976*b*.

Kawai, H., Hydrography of the Kuroshio extension, in *Kuroshio: Physical Aspects of the Japan Current,* edited by H. Stommel and K. Yoshida, pp. 235–352, University of Washington Press, Seattle, 1972.

Kirwan, A. D., Oceanic velocity gradients, *J. Phys. Oceanogr., 5,* 729–735, 1975.

Legeckis, R., A survey of worldwide sea surface temperature fronts detected by environmental satellites, *J. Geophys. Res., 83,* 4501–4522, 1978.

National Environmental Satellite Service, Weekly maps of Gosstcomp sea surface temperature for the North Pacific Ocean, *Ser. MN 135 E,* Nat. Oceanic and Atmos. Admin., Washington, D.C., 1977–1978.

National Weather Service, Daily maps of northern hemisphere sea level atmospheric pressures, Nat. Meteorol. Center, Suitland, Md., 1977–1978.

Newton, C. W., Fronts and wave disturbances in the Gulf Stream and atmospheric jet stream, *J. Geophys. Res., 83,* 4697–4706, 1978.

Roden, G. I., Temperature and salinity fronts at the boundaries of the subarctic-subtropical transition zone in the western Pacific, *J. Geophys. Res., 77,* 7175–7187, 1972.

Roden, G. I., On North Pacific temperature, salinity, sound velocity and density fronts, and their relation to the wind and energy flux fields, *J. Phys. Oceanogr., 5,* 557–571, 1975.

Roden, G. I., On the subarctic fronts of the central Pacific: Structure of and response to atmospheric forcing, *J. Phys. Oceanogr., 7,* 761–778, 1977.

Shapiro, M., Oceanic fronts: A summary of a Chapman Conference, *Eos Trans. AGU, 59,* 490, 1978.

Uda, M., Researches on "siome" or current rip in the seas and oceans, *Geophys. Mag., 11,* 307–372, 1938.

(Received October 3, 1979;
revised December 11, 1979;
accepted December 17, 1979.)

UNCLASSIFIED

SECURITY CLASSIFICATION OF THIS PAGE (When Data Entered)

REPORT DOCUMENTATION PAGE		READ INSTRUCTIONS BEFORE COMPLETING FORM
1 REPORT NUMBER 378	2 GOVT ACCESSION NO.	3. RECIPIENT'S CATALOG NUMBER
4. TITLE (and Subtitle) The Depth Variability of Meridional Gradients of Temperature, Salinity and Sound Velocity in the Western North Pacific		5 TYPE OF REPORT & PERIOD COVERED TECHNICAL REPORT 6. PERFORMING ORG. REPORT NUMBER
7. AUTHOR(s) G. I. Roden		8. CONTRACT OR GRANT NUMBER(s) N-00014-75-C-0502
9. PERFORMING ORGANIZATION NAME AND ADDRESS UNIVERSITY OF WASHINGTON DEPARTMENT OF OCEANOGRAPHY SEATTLE, WASHINGTON 98195		10. PROGRAM ELEMENT, PROJECT, TASK AREA & WORK UNIT NUMBERS PROJECT NR 083-012
11. CONTROLLING OFFICE NAME AND ADDRESS ONR BRANCH OFFICE 1030 EAST GREEN STREET PASADENA, CALIFORNIA 91106		12. REPORT DATE 1980 13. NUMBER OF PAGES
14 MONITORING AGENCY NAME & ADDRESS(if different from Controlling Office)		15. SECURITY CLASS. (of this report) UNCLASSIFIED 15a. DECLASSIFICATION/DOWNGRADING SCHEDULE

16. DISTRIBUTION STATEMENT (of this Report)

APPROVED FOR PUBLIC RELEASE; DISTRIBUTION UNLIMITED

17. DISTRIBUTION STATEMENT (of the abstract entered in Block 20, if different from Report)

18 SUPPLEMENTARY NOTES

REPRINT FROM: Journal of Physical Oceanography, Vol. 9, No. 4, 1979

19. KEY WORDS (Continue on reverse side if necessary and identify by block number)

Meridian gradients
Temperature
Salinity
Western North Pacific
Sound velocity

20. ABSTRACT (Continue on reverse side if necessary and identify by block number)

In the western North Pacific, meridional gradients of temperature, salinity and sound velocity show considerable variation with depth. Gradients of frontal intensity (more than three times the rms value) occur in the upper 600 m of the ocean. Fronts in the surface layer are spaced at irregular intervals. Many deep fronts have no surface manifestation and are spaced at intervals between 300 and 600 km. A spectral analysis of the meridional gradients as functions of depth and longitude was carried out for the wavenumber range between 0 and 13.4 cycles per 1000 km (c.p. 1000 km). The shape of the power density spectra strongly depends on depth. In the upper 150 m the shape is irregular. Between 300 and 600 m, the spectra show a well-defined peak between 1.5 and 3.3 c.p. 1000 km and a sharp decrease in power beyond 10 c.p. 1000 km.

DD FORM 1 JAN 73 1473 EDITION OF 1 NOV 65 IS OBSOLETE
S/N 0102-014-6601

UNCLASSIFIED

SECURITY CLASSIFICATION OF THIS PAGE (When Data Entered)

UNCLASSIFIED

SECURITY CLASSIFICATION OF THIS PAGE (When Data Entered)

REPORT DOCUMENTATION PAGE		READ INSTRUCTIONS BEFORE COMPLETING FORM
1 REPORT NUMBER: 379	2 GOVT ACCESSION NO.	3 RECIPIENT'S CATALOG NUMBER
4. TITLE (and Subtitle): On the Subtropical Frontal Zone North Of Hawaii During Winter		5 TYPE OF REPORT & PERIOD COVERED: TECHNICAL REPORT
		6. PERFORMING ORG. REPORT NUMBER
7. AUTHOR(s): G. I. Roden		8. CONTRACT OR GRANT NUMBER(s): N-00014-75-C-0502
9 PERFORMING ORGANIZATION NAME AND ADDRESS: UNIVERSITY OF WASHINGTON DEPARTMENT OF OCEANOGRAPHY SEATTLE, WASHINGTON 98195		10. PROGRAM ELEMENT, PROJECT, TASK AREA & WORK UNIT NUMBERS: PROJECT NR 083-012
11. CONTROLLING OFFICE NAME AND ADDRESS: ONR BRANCH OFFICE 1030 EAST GREEN STREET PASADENA, CALIFORNIA 91106		12. REPORT DATE: 1980
		13. NUMBER OF PAGES
14 MONITORING AGENCY NAME & ADDRESS(if different from Controlling Office)		15. SECURITY CLASS. (of this report): UNCLASSIFIED
		15a. DECLASSIFICATION/DOWNGRADING SCHEDULE

16 DISTRIBUTION STATEMENT (of this Report)

APPROVED FOR PUBLIC RELEASE; DISTRIBUTION UNLIMITED

17. DISTRIBUTION STATEMENT (of the abstract entered in Block 20, if different from Report)

18 SUPPLEMENTARY NOTES

REPRINT FROM: Journal of Physical Oceanography, Vol. 10, 1979

19. KEY WORDS (Continue on reverse side if necessary and identify by block number)

Oceanic fronts
Subtropical frontal zone
Hawaii

20 ABSTRACT (Continue on reverse side if necessary and identify by block number)

Oceanic fronts in the subtropical frontal zone north of Hawaii are investigated and related to atmospheric forcing. Particular attention is paid to the winter of 1974 when a detailed study was made of the thermohaline structure aboard the R. V *Thomas G. Thompson*. In that winter, well defined fronts occurred at 34, 31 and 28°N. In the upper 100 m, these fronts are nearly vertical and are characterized by temperature, salinity and sound velocity gradients of up to 2°C (27 km)$^{-1}$, 0.3‰ (27 km)$^{-1}$ and 12 m s^{-1} (27 km)$^{-1}$, respectively. Horizontal density gradients across the northern two fronts are small because of compensating horizontal temperature and salinity gradients. A thin layer of increased stability is encountered between 100 and 125 m. Below this layer, there are prominent lateral intrusions of cool and low-salinity subsurface water under warmer and higher salinity surface water, at latitudes north of 31°N and longitudes east of 155°W.

DD FORM 1 JAN 73 1473 EDITION OF 1 NOV 65 IS OBSOLETE

S/N 0 02-014-6601

UNCLASSIFIED

SECURITY CLASSIFICATION OF THIS PAGE (When Data Entered)

UNCLASSIFIED

SECURITY CLASSIFICATION OF THIS PAGE (When Data Entered)

REPORT DOCUMENTATION PAGE		READ INSTRUCTIONS BEFORE COMPLETING FORM
1 REPORT NUMBER 380	2 GOVT ACCESSION NO.	3 RECIPIENT'S CATALOG NUMBER
4 TITLE (and Subtitle) Upper Ocean Workshop, Summary Report		5 TYPE OF REPORT & PERIOD COVERED TECHNICAL REPORT 6. PERFORMING ORG. REPORT NUMBER
7. AUTHOR(s) M. C. Gregg		8. CONTRACT OR GRANT NUMBER(s) N-00014-75-C-0502
9. PERFORMING ORGANIZATION NAME AND ADDRESS UNIVERSITY OF WASHINGTON DEPARTMENT OF OCEANOGRAPHY SEATTLE, WASHINGTON 98195		10. PROGRAM ELEMENT, PROJECT, TASK AREA & WORK UNIT NUMBERS PROJECT NR 083-012
11. CONTROLLING OFFICE NAME AND ADDRESS ONR BRANCH OFFICE 1030 EAST GREEN STREET PASADENA, CALIFORNIA 91106		12. REPORT DATE 1980 13. NUMBER OF PAGES
14 MONITORING AGENCY NAME & ADDRESS(if different from Controlling Office)		15. SECURITY CLASS. (of this report) UNCLASSIFIED 15a. DECLASSIFICATION/DOWNGRADING SCHEDULE

16. DISTRIBUTION STATEMENT (of this Report)

APPROVED FOR PUBLIC RELEASE; DISTRIBUTION UNLIMITED

17. DISTRIBUTION STATEMENT (of the abstract entered in Block 20, if different from Report)

18 SUPPLEMENTARY NOTES

19. KEY WORDS (Continue on reverse side if necessary and identify by block number)

Upper ocean
Atmospheric forcing

20. ABSTRACT (Continue on reverse side if necessary and identify by block number)

Approximately 30 academic physical oceanographers interested in observational programs in the upper ocean met for informal discussions from 3-5 March 1980 at Timberline Lodge, Oregon. The emphasis was on ideas for future research, including that work concerned with the direct response of the upper ocean to atmospheric forcing.

DD FORM 1 JAN 73 1473 EDITION OF 1 NOV 65 IS OBSOLETE
S/N 0102-014-6601

UNCLASSIFIED
SECURITY CLASSIFICATION OF THIS PAGE (When Data Entered)

UNCLASSIFIED

SECURITY CLASSIFICATION OF THIS PAGE (When Data Entered)

REPORT DOCUMENTATION PAGE		READ INSTRUCTIONS BEFORE COMPLETING FORM
1 REPORT NUMBER: 381	2 GOVT ACCESSION NO.	3 RECIPIENT'S CATALOG NUMBER
4 TITLE (and Subtitle): Signatures of Mixing from the Bermuda Slope, the Sargasso Sea and the Gulf Stream		5 TYPE OF REPORT & PERIOD COVERED: TECHNICAL REPORT 6. PERFORMING ORG. REPORT NUMBER
7. AUTHOR(s): M. C. Gregg and T. B. Sanford		8. CONTRACT OR GRANT NUMBER(s): N-00014-75-C-0502
9. PERFORMING ORGANIZATION NAME AND ADDRESS: UNIVERSITY OF WASHINGTON DEPARTMENT OF OCEANOGRAPHY SEATTLE, WASHINGTON 98195		10. PROGRAM ELEMENT, PROJECT, TASK AREA & WORK UNIT NUMBERS: PROJECT NR 083-012
11. CONTROLLING OFFICE NAME AND ADDRESS: ONR BRANCH OFFICE 1030 EAST GREEN STREET PASADENA, CALIFORNIA 91106		12. REPORT DATE 13. NUMBER OF PAGES
14 MONITORING AGENCY NAME & ADDRESS(if different from Controlling Office)		15. SECURITY CLASS. (of this report): UNCLASSIFIED 15a. DECLASSIFICATION/DOWNGRADING SCHEDULE

16. DISTRIBUTION STATEMENT (of this Report)

APPROVED FOR PUBLIC RELEASE; DISTRIBUTION UNLIMITED

17. DISTRIBUTION STATEMENT (of the abstract entered in Block 20, if different from Report)

18. SUPPLEMENTARY NOTES

REPRINT FROM: Journal of Physical Oceanography, Vol. 10, No. 1, 1980

19. KEY WORDS (Continue on reverse side if necessary and identify by block number)

Mixing
Bermuda Slope
Sargasso Sea
Gulf Stream

20. ABSTRACT (Continue on reverse side if necessary and identify by block number)

Nearly simultaneous profiles of temperature microstructure and velocity shear were made adjacent to the island of Bermuda. Profiles with elevated microstructure levels were found in close association with regions of pronounced steplike finestructure, which contained nearly adiabatic regions from 2 to 10 m thick. The temperature spectra and the presence of numerous centimeter-scale temperature inversions gave evidence that active turbulent mixing was occurring in some of these regions. These were the locations in which large-scale surveys, reported by Hogg *et al.* (1978), found that eddies impinging on the island were forcing alongshore flow.

Although the mixing was intense by comparison with profiles in the thermocline, the limited geographical extent of the affected areas and the moderate levels indicate that mixing adjacent to islands is of minor importance on a global basis.

DD FORM 1 JAN 73 1473 EDITION OF 1 NOV 65 IS OBSOLETE
S/N 0102-014-6601

UNCLASSIFIED
SECURITY CLASSIFICATION OF THIS PAGE (When Data Entered)

UNCLASSIFIED

SECURITY CLASSIFICATION OF THIS PAGE (When Data Entered)

REPORT DOCUMENTATION PAGE		READ INSTRUCTIONS BEFORE COMPLETING FORM
1 REPORT NUMBER: 382	2 GOVT ACCESSION NO.	3 RECIPIENT'S CATALOG NUMBER
4 TITLE (and Subtitle): On the Variability of Surface Temperature Fronts in the Western Pacific, as Detected by Satellite		5 TYPE OF REPORT & PERIOD COVERED: TECHNICAL REPORT 6 PERFORMING ORG. REPORT NUMBER
7 AUTHOR(s): G. I. Roden		8 CONTRACT OR GRANT NUMBER(s): N-00014-75-C-0502
9 PERFORMING ORGANIZATION NAME AND ADDRESS: UNIVERSITY OF WASHINGTON DEPARTMENT OF OCEANOGRAPHY SEATTLE, WASHINGTON 98195		10 PROGRAM ELEMENT, PROJECT, TASK AREA & WORK UNIT NUMBERS: PROJECT NR 083-012
11 CONTROLLING OFFICE NAME AND ADDRESS: ONR BRANCH OFFICE 1030 EAST GREEN STREET PASADENA, CALIFORNIA 91106		12 REPORT DATE: 1980 13 NUMBER OF PAGES
14 MONITORING AGENCY NAME & ADDRESS (if different from Controlling Office)		15 SECURITY CLASS. (of this report): UNCLASSIFIED 15a DECLASSIFICATION/DOWNGRADING SCHEDULE

16 DISTRIBUTION STATEMENT (of this Report)

APPROVED FOR PUBLIC RELEASE; DISTRIBUTION UNLIMITED

17 DISTRIBUTION STATEMENT (of the abstract entered in Block 20, if different from Report)

18 SUPPLEMENTARY NOTES

REPRINT FROM: Journal of Geophysical Research, Vol. 85, No. C5, 1980

19 KEY WORDS (Continue on reverse side if necessary and identify by block number)

Temperature fronts
Satellite
Western Pacific

20 ABSTRACT (Continue on reverse side if necessary and identify by block number)

The variability of sea surface temperature fronts in the western North Pacific is investigated by using satellite and shipboard data. On a 100 km by 100 km grid and on a time step of 1 week the satellite recognizes the subarctic front, the subtropical fronts, and one to two fronts associated with the Kuroshio intrusion. The subarctic front is centered near 42°N and can be seen throughout the year. Frontal gradients vary from 5°C/100 km in winter to 2°C/100 km in summer, and deviations from the mean latitude are small. The subtropical front is seen only from late fall to early summer in the latitude range between 28°N and 33°N. Maximum frontal gradients are of the order of 3°C/100 km and occur in late spring. Kuroshio fronts occur sporadically in the latitude range between 35°N and 37°N.

DD FORM 1 JAN 73 1473 EDITION OF 1 NOV 65 IS OBSOLETE
S/N 0102-014-6601

UNCLASSIFIED
SECURITY CLASSIFICATION OF THIS PAGE (When Data Entered)

FOR UNCLASSIFIED TECHNICAL REPORTS, REPRINTS & FINAL REPORTS

PUBLISHED BY OCEANOGRAPHIC CONTRACTORS

OF THE OCEAN SCIENCE & TECHNOLOGY DIVISION

OF THE OFFICE OF NAVAL RESEARCH

12 Defense Documentation Center
Cameron Station
Alexandria, Virginia 22314

Office of Naval Research
Department of the Navy
Arlington, Virginia 22217

6 ATTN: Code 102-IP

1 Cognizant ONR Branch Office
1030 East Green Street
Pasadena, California 91106

1 ONR Resident Representative

Director
Naval Research Laboratory
Washington, D.C. 20375

6 ATTN: Library, Code 2627

Scientific Officer
NORDA
Bay St. Louis, Mississippi 39520

1 ATTN: Code 461

END